UNIVERSITY OF INSUBRIA
DEPARTMENT OF MEDICINE AND SURGERY
PHD in EXPERIMENTAL AND TRANSLATIONAL MEDICINE
COORDINATOR: PROF. DANIELA NEGRINI

DEVELOPMENT OF SAPORIN-BASED THERAPEUTIC OPTIONS FOR THE TREATMENT OF SOLID TUMORS

PhD candidate: STEFANIA ZUPPONE

Tutor: PROF. FAUSTO SESSA

Co-tutor: DR. RICCARDO VAGO

Academic year: 2017-2018

Index:

Summary

Up to now, cancer represents one of the most challenging disease to treat, mostly due to its ability to adapt and negatively respond to current available therapies. Over the past 30 years, Ribosome Inactivating Proteins (RIPs) have attracted great interest in the scientific community for their therapeutic potential. Indeed, such toxins have been extensively used as potent and versatile therapeutic weapons due to important advantages compared to chemotherapeutics: for instance, they act independently form cell cycle, killing both quiescent and dividing cells, limiting the development of cancer resistance. However, the successful application of toxins-based therapeutics to solid tumors remains to be demonstrated. In this study, we explored the potential use of the plant-RIP saporin (SAP) for the treatment of solid tumors. In particular, we propose two different strategies, in which SAP is selectively and safely conveyed to malignant cells either in the form of recombinant protein through genetically fused targeting moieties, or throughout cell-derived extracellular vesicles as vehicles. Previous studies have shown that the urokinase receptor (uPAR)- targeting ATF-SAP chimera improved the therapeutic index of the toxin *in vitro* on uPAR expressing cells. To explore SAP therapeutic applicability, in this study we compare and combine ATF-SAP toxic activity to a new αv-integrins-targeting recombinant protein (RGD-SAP) with the aim to cope with tumor heterogeneity, targeting both tumor epithelial and endothelial cells. The recombinant proteins resulted in a safe and cancer specific toxicity in plenty tumor cell models, which was proportional to the receptors expression levels on cells surface. Receptor recognition by targeting moieties was not impaired by the presence of the toxin, as, in case of RGD-SAP, competitive binding experiments induced a partial rescue of cell viability. In addition, *in vivo* results showed that recombinant proteins are able to induce potent antitumor effects in bladder tumor-bearing mice, either when used as single treatment or in combination. Eventually, we demonstrate that SAP delivery can be improved by the use of extracellular vesicles (exosomes) as drug nanocarriers. Specifically, we propose a “genetic” method, in which we genetically engineered cells to produce targeted therapeutic exosomes, using Lamp2b as exosomal resident protein, or a “chemical” method,

based on a pH shock exposition, to achieve SAP incorporation. We show that, in contrast to previous studies, the expression of Lamp2b fusion proteins is not a suitable method to achieve a sustained production of engineered exosomes, in contrast to tetraspanins, that are massively incorporated into the vesicles. In addition, we demonstrate that a protease-dependent smart prodrug system is promising for the selective release of the cargo in target cancer cells. On the other hand, a highly alkaline solvent is able to induce a massive SAP encapsulation in exosomes compared to commonly used techniques, preserving exosomal size, structure and integrity and mediating a higher toxicity compared to SAP alone. Overall our data indicate that SAP-based recombinant proteins are promising anti-tumoral therapeutic options. Applied as single or combined treatment, as well as used together with traditional therapeutics, they appropriately address both intra- and inter- tumor heterogeneity. In addition, the use of exosomes as SAP nanocarriers is a promising strategy to improve safety and drug delivery to tumor cells.

1. Introduction

1.1 State of the art therapies against cancer and their limitations

Cancer is one the major causes of death worldwide. Current clinical protocols are mostly based on the combination of surgical resection to debulk, followed by radiation and chemotherapy. However, not all tumors can be completely eradicated by surgery as they might have spread to nearby organ/tissues or metastasized throughout the body. The drugs used in the classical chemotherapy, approved for the treatment of a variety of tumor types include predominantly small molecules like cisplatin, taxol, doxorubicin and anthracyclines, which target the rapidly growing cells, blocking cell proliferation and DNA replication. Albeit in some cases efficient in reducing or completely eradicating tumor mass, these kinds of therapies suffer from two big limitations: lack of a specificity and poor solubility in water. They kill cells in a cell cycle dependent manner, causing an increased toxicity against normal tissues, like bone marrow, intestinal epithelial cells and hair follicles besides rapidly dividing cancer cells. Moreover, most of the chemotherapeutics are chemically synthetized, highly hydrophobic compounds and minimally hydro-soluble, requiring oily moistures or lipophilic solutions to solubilize the formulation, thus contributing to their toxic effect on patients' body. Therefore, the ability of the patients to tolerate and afford the side effects have to be considered when the appropriate treatment is decided.

Targeted therapies have gained great attention in the last decades as they opened up the possibility to specifically deliver drugs to diseased tissues and kill cancer cells without or minimally affecting healthy organs. The target specificity is addressed by the interaction of drugs with molecules, mainly proteins, exclusively expressed or overexpressed in cancer cells. In fact, progression and dissemination of malignant cells is characterized by the acquisition of novel functional competences, including self-sufficiency in growth signals, insensitivity to anti-growth signals, evasion of apoptosis, limitless replicative potential, sustained angiogenesis and tissue invasion. Several of those novel functions are linked to the massive-expression of surface receptors, usually growth factors, whose identification could

lead to the development of effective and personalized treatments. Recently, the molecular diagnostics is rapidly developing, and more and more targeted therapeutic agents have been approved by the US Food and Drug Administration (FDA) across many cancer subtypes, providing new treatment options to patients who cannot receive chemotherapy. These therapies include hormone therapies, signal transduction inhibitors, gene expression modulators, apoptosis inducers, angiogenesis inhibitors, immunotherapies and toxin-based drugs (www.cancer.gov). Even if safer, these approaches are not free from drawbacks. In fact, patients can stop responding to the treatment throughout complicate, tumor specific mechanisms that result in alterations of the drug target, activation of pro-survival pathways and ineffective induction of cell death, that can be collectively defined as multidrug resistance [1]. Furthermore, the high intra- (within a tumor) and inter- (tumor by tumor) tumor heterogeneity remarkably limit their use to be applied to different cancer subtypes. Other problems that hinder the widespread use of targeted therapies are related to their size and, thus, poor penetration into the tumor mass. Monoclonal antibodies, for instance, nowadays represent one of the most successful strategies adopted for both hematological and solid tumors but have a high molecular mass (around 150 kDa), generally causing an inadequate pharmacokinetics and tissue accessibility. Even if fragmented derivatives have been developed (using just the small chain variable fragment -ScFv-), high dosage administrations are still required to achieve clinical efficacy, due to the limited duration of action, contributing to undesired immunogenicity and toxicity [2].

1.2 Tumor microenvironment and its associated therapeutic targets

As a pathologic condition, solid tumors microenvironment is extremely abnormal: blood flow is low with low perfusion, due to a vascular hyper-permeability and the lack of functional lymphatic vessels results in an elevated interstitial fluid pressure (IFP). A large number of active stromal cells and extracellular matrix (ECM) are often dense and stiff, compressing the blood vessels, which represent one to 10% of the volume of the tumor mass. The remaining space is filled primarily by an abundant collagen-rich matrix, the interstitium. [3, 4]. Due to this complex and

hostile architecture, systemically administered small-sized anticancer drugs preferentially leak and passively accumulate in the tumor tissue (enhanced permeability and retention -EPR- effect). However, even if widely exploited to improve treatment efficacy, this "passive targeting" process is not sufficient to guarantee the delivery of appropriate concentrations of drugs to tumor environment just by itself. Anticancer drugs, in fact, need to undergo and accomplish a three-step process to exert their therapeutic effect, including: 1- vascular transportation to different areas of the tumor; 2- trans-vascular transport across the vessel wall: 3- interstitial transport to reach the tumor cells [5]. Therefore, drugs able to either passively accumulate into the tumor throughout the EPR effect and actively target malignant cells would be a smart strategy to improve the therapeutic index. Endothelial cells are the first cell type directly exposed to the circulating drugs and, thus, more accessible to them. The elimination of a single endothelial cell leads to the indirect killing of tumor cells due to the lack of oxygen and nutrients [6]. In this contest, αv- integrins represent one of most suitable class of molecules to be targeted, owing to their augmented expression in several human malignancies. In cancer, their presence on both endothelial and epithelial cancer cells compared to normal cells regulate many steps of tumor progression, including angiogenesis, spreading, migration, growth signaling, survival signaling, secretion of proteases and invasion [7, 8, 9]. They are heterodimeric membrane glycoproteins composed by non-covalently associated α- and β-subunits that act as adhesion receptors for extracellular matrix (ECM) proteins, immunoglobulin, growth factors, cytokines, and matrix-degrading proteases, by binding their ligands often through recognition of short amino-acid sequences. A subset of integrins, for instance, recognize the arginine-glycine-aspartic acid (RGD) motif within their ligands (i.e. fibronectin, vitronectin, laminin). This binding results in the transduction of the information from the extracellular environment to modulate cell response [10, 11]. Among integrins, $\alpha v\beta 3$ is probably the most strongly involved in the regulation of angiogenesis. It localizes with proteolytically active metalloprotease (MMP)-2 on the surface of angiogenic blood vessels, playing an important role in cell-mediated collagen degradation and consequently rearrangement of the ECM [12]. About 480 drugs targeting integrins have been developed and tested so far in clinical trials with

multiple indications, but unfortunately, only few inhibitory antibodies (abciximab; tirofiban; eptifibatibe; natalizumab; vedolizumab; and lifitegrast; with efalizumab) reached the clinical market, because of integrins complexity and different regulation in human cancers with respect to preclinical mouse model [13].

Besides integrins, the urokinase plasminogen activator receptor (uPAR) represent a good candidate as a target for innovative cancer therapies. It is a glycoprotein of 55-60 kDa, associated to the external surface of the plasma membrane by a glycosyl-phosphatidylinositol (GPI) anchor and an important regulator of the plasminogen activation system (PAS), an extracellular proteolytic cascade responsible for the extracellular matrix (ECM) degradation. Upon binding its natural ligand, the urokinase plasminogen activator (uPA), uPAR allows the conversion of plasminogen into the serin-protease plasmin, which reciprocally cleaves and activates pro-uPA and matrix MMPs, thereby facilitating cell migration by tissue remodeling. Thus, uPAR plays a pivotal role in microenvironment modification, promoting ECM proteolysis and ECM interaction. It participates in a number of transitory physiological processes that require blood vessels formation and degradation of the ECM (menstrual cycle and trophoblast implantation, embryonic development, inflammation and wound healing), being expressed by cells that are in motion, such as activated leukocytes, endothelial cells and fibroblasts [14]. However, uPAR expression is significantly upregulated in cancer under particular stimuli (such as hypoxia), where the reorganization of tumor microenvironment leads to cancer cells to migration, angiogenesis, vascular invasion and propagation to distant sites. Furthermore, uPAR activation is also involved in intracellular signaling pathways of migrating cells, mainly through interactions with co-localized integrins (β1, β2, and β3 integrin receptor families) [15] and tyrosine kinase receptors (EGFR), that result in the activation of cell survival and proliferation pathways [16]. In agreement with its roles in cancer progression, the importance of uPAR is widely strengthened by a positive correlation between its levels and patient outcome/low overall survival in most human solid and hematological malignancies, among which breast [17] and bladder cancers [18]. The only therapeutic monoclonal antibodies that specifically target uPAR developed so far are HuATN-658 (Cancer Research UK's Centre for Drug

Development) and ATN-658, shown reliable preclinical anti-tumors effects across a variety of tumor models, blocking the interaction between uPA and uPAR [19] and, thus, inhibiting invasion, metastasis and tumor proliferation as well as inducing apoptosis.

1.3 αv-integrins and uPAR targeting peptides

In the last years, many investigators have explored the potential of targeting peptides, a promising class of molecules that, owing to their small size, low immunogenicity, ease of manufacture at reasonable costs, can overcome many monoclonal antibodies-associated limitations. They are usually obtained from the binding region of the main ligand of the protein of interest or selected from combinatorial phage display libraries (∼1011 different sequences) to identify the sequences with the higher affinity that may improve tumor homing property. For instance, most integrins recognize their respective ECM proteins through short peptide sequences such as Arg- Gly-Asp (RGD), Glu-Ile-Leu-Asp-Val (EILDV), or Arg-Glu-Asp-Val (REDV). Therefore, these sequences have been exploited to synthetize integrins-specific peptides and shown to be endowed with a high therapeutic activity. One of the first RGD-based integrins targeting peptide developed was Cilengitide (EMD121974), from Merck KGaA, a cyclic pentapeptide that specifically inhibits αvβ3 and αvβ5 [20]. Preclinical studies have demonstrated its efficacy as anti-angiogenic and anti-tumor agent, suppressing breast metastasis to bone and favoring radiotherapy efficacy in orthotopic brain tumors models [21, 22]. However, it has been observed that if, on one hand, this cyclic peptide is able to enhance intra-tumoral vascular permeability and increase drug delivery [23], on the other, nanomolar concentrations of cilengitide activate αvβ3 and enhance angiogenesis and tumor growth [24]. Furthermore, as for many inhibitory targeting peptides, unsuccessful early trials revealed its rapid clearance from serum ($t_{1/2}$ = 3–5 h) [25]. Therefore, other strategies have been adopted in order to exploit RGD-based targeting peptides to achieve drug delivery to tumors other than as therapeutics themselves. ACDCRGDCFC peptide, in particular, has been proven to enhance the selective delivery of antitumor compounds to tumor

vessels, binding to integrins, such as αvβ3, αvβ5, αvβ6, αvβ8 and α5β1, with different affinity and selectivity and allowing the "active targeting" of both endothelial and epithelial tumor cells [12, 26, 27, 28]. Importantly, RGD-targeted compounds have been demonstrated to be internalized via receptor-mediated endocytosis, particularly interesting aspect for the intracellular delivery of drugs to cancer cells [12]. As for integrins, uPAR targeting peptides have also been developed to overcome antibodies limitations. In this case, they were not used as such to inhibit uPAR signaling activity, but mostly in conjugation to cytotoxic moieties or nanoparticles to address uPAR expressing cancer cells in *in vitro* studies. The first peptide was created by isolating the amino-terminal fragment (ATF) of uPAR natural ligand, uPA, containing the initial 135 amino acids including the growth factor domain [29, 30]. The ATF peptide was shown to be highly efficient in the *in vitro* specific delivery of a biological toxic compound to uPAR overexpressing hematological tumors (30, 31). Since then, two more uPAR targeting peptides have been derived from the uPAR binding sequence of ATF, consisting of 7 or 11 amino acids, named U7 and U11. They were proven to be uPAR-specific in cellular model of breast and prostate cancer [29, 32, 33]

1.4 Urothelial bladder cancer

Urothelial bladder cancer (UBC) is one of the leading causes of death in developed counties, three to four times more prevalent in males than in females. The prognosis and treatment of bladder cancer have improved little in the past 20 years and it remains among the most expensive cancer to treat (life-long clinical management of patients with non-muscle invasive disease as well as costs associated with caring for patients after radical cystectomy, surgical removal of the bladder). A staging system (TNM system), ranging from stage 0 (carcinoma in situ) to stage 4 (the most advanced one) is a standard way to describe the extent of cancer spread and it is based on three specific parameters: T describes how far the main (primary) tumor has grown through the bladder wall and whether it has grown into nearby tissues; N indicates if cancer cells have spread to lymph nodes near the bladder; M describes if the cancer has metastasized to distant organs or lymph nodes. Although

characterized by heterogeneous further subtypes that have a range of disease outcomes, the broad subgroup (70-75%) is represented by non-muscle invasive bladder cancer (T0 and T1), which is more common and usually associated with a favorable prognosis. The remaining 25-30% of bladder cancer is muscle invasive (T2, T3 and T4), less prevalent, but typically associated with poor prognosis. The optimal treatment for UBC depends on the cancer's stage, reflecting the depth of invasion of the primary tumor through the bladder wall and nearby tissues [http://www.cancer.net/cancer-types/bladder-cancer/stages-and-grades/trackback]. The prognosis of the tumor in the initial phase is generally favorable and finds an easy resolution through the endoscopic removal of the lesion. However, more than 50% of patients undergoing primary tumor resection face further problems due to cancer relapse [34]. In patients with superficial or non-muscle invasive tumors, pre- (neoadjuvant chemo) or post-surgical (adjuvant chemo) endovesical chemotherapy is a first line of intervention aimed at reducing the number of relapses but has limited efficacy and non-negligible side effects at the local level [35]. The second line of intervention is instead constituted by the immunotherapy which involves the endo-vesical use of Bacillus Calmette-Guerin (BCG) or the chemotherapeutic mitomycin. In the case of infiltration of the bladder wall by the tumor (which is therefore defined as muscle invasive), cystectomy represents the standard intervention. Following cystectomy, 5-year survival is below 50%, depending on the degree of infiltration of the bladder wall, the presence of extra-vesical extension and the presence or absence of metastases in the lymph nodes [36]. However, cystectomy is not a valid treatment for patients presenting metastases. In this case, the preferential intervention line is represented by a systemic chemotherapy regimen consisting of methotrexate, vinblastine, adriamycin and cisplatin (MVAC) or, alternatively, gemcitabine associated with cisplatin (GC), both with a low response rate (~ 40-50%) and a limited increase in survival (12-15 months) [37]. Although these drugs have a broad spectrum of activity and are partially effective in the treatment of bladder cancer, severe side effects limit their use. In fact, they totally lack specificity and need to be administered in very high doses to reach the active concentration at the tumor sites. Patients who cannot tolerate chemotherapy (because of other health problems) are treated with radiation therapy or with

immunotherapy, such as atezolizumab (anti PD-L1) or pembrolizumab (anti PD1) [www.fda.gov]) [38]. In this context, many efforts are focused on the development of a targeted therapy, aimed at inhibiting or exploiting specific tumor pathways and receptors to selectively kill the neoplastic cells [39].

1.5 Breast cancer

Breast cancer is a highly genetically and clinically heterogeneous disease that represents the second leading cause of death among women in the world. Every year, in fact, the number of diagnosed breast cancer cases have been estimated to be 1 to 1.3 million. Of these, approximately 15- 20% belong to the triple-negative subtype (TNBC). TNBC is the most biologically aggressive breast cancer subtype, with an increased likelihood of distant recurrence and of death compared to the others. Its phenotype is defined by the lack of expression of estrogen receptor (ER), progesterone receptor (PR) and human epidermal growth factor receptor 2 (HER2), therefore hormone therapies and anti-HER2 targeted therapies are not effective [40]. Due to the current absence of a recognized therapeutic target and the high inter and intra-tumoral heterogeneity, the primary line of intervention is represented by a combination of surgery, chemotherapy (with international guidelines supporting the use of single-agent taxanes or anthracyclines [41]) and radiation therapy. In some cases, a neoadjuvant chemotherapy is given to shrink tumor before surgery. Despite initial good response, only 20% of patients respond well to standard chemotherapy and their prognosis remains poor as compared to non-TNBCs [42]. At present, PARP inhibitor Olaparib is the only molecular-based targeted therapy for BRCA1-mutation presenting patients with TNBC, but only approximately 10-20% of them positively respond to the treatment [43, 44]. Thus, developing improved treatments for TNBC is one of the highest priorities of current breast cancer research.

As no effective specific targeted therapies for both bladder and triple negative breast cancers are readily available, the exploration of novel therapeutic markers

and the development of new agents with therapeutic potential need in-depth investigations.

1.6 Toxins therapeutic potential

Toxins are natural dangerous molecules produced by bacterial or plant that have been structurally and functionally optimized under evolutionary pressure as defensive strategy against predators. Many research groups turned to explore their pharmaceutical potential when used to efficiently impair essential cellular processes and induce cell death. Indeed, acting in a cell cycle independent manner, they can kill both quiescent and rapidly dividing cells, resulting suitable to fight both tumors with a slower progression and aggressive cancers. Toxins use as effectors in cancer therapy has been studied for decades with promising results. Pseudomonas exotoxin A (PEA) and diphtheria toxin (DT) from bacterial origin, for instance, have been employed for diverse therapeutic purposes [45] mainly in the form of immuno-conjugates. The presence of an antibody portion or ligand domain confer target specificity, providing an antigen-specific binding affinity to molecules over-expressed on the surface of malignant cells. The most successful developed toxin-based drug is Denileukin diftitox, the first recombinant protein formed by a truncated form of DT and human cytokine interleukin-2, approved by the US Federal Drug Administration (FDA), for the treatment of cutaneous T-cell lymphomas. Numerous other toxin-based conjugates are under investigations in pre-clinical and clinical trials against hematological as well as solid tumors with encouraging results [46]. However, as mentioned before, the major obstacles to successful treatment of solid tumors using immunotoxins (Its) include multiple factors, among which the poor penetration into tumor masses. Solid tumor core is not easily accessible, and the drug effect is often confined to the surface of the tumor mass. Moreover, the other limiting factors are represented by the dimensions of the antibody portion and the activation of the immune response against the antibody component, which limits the number of treatment cycles. Furthermore, even if the dimension problem has been overcome by using only the small variable fragment of the antibody, the cost and scaling of production of these compounds

remain constraining. Another promising way to exploit toxins as a pharmacological weapon is to design recombinant chimeras/recombinant proteins consisting of a fusion between the catalytic domain of the toxin and a tumor targeting ligand domain, usually a growth factor [47]. The advantages of these compounds are related to the reduced dimensions (the targeting moiety is generally a small peptide composed by a small number of amino acids), which ameliorate the penetration capacity into the tumor environment (EPR effect), and immunogenicity, thus prolonging the half-life of the therapeutic protein. In 2002 Vallera et al. [48] produced a recombinant protein fusing diphtheria toxin (DTAT) to the amino terminal fragment (ATF) of uPA, demonstrating its *in vitro* biological activity on human uPAR positive glioblastoma cells (U118MG) (IC_{50} <1 nM). They also showed that DTAT was able to regress U118MG tumours in mice. A recombinant protein consisting in ATF fused to a truncated form of *Pseudomonas* exotoxin has similarly been prepared and shown to be highly active on breast cancer cell line MCF7(IC_{50} = 2.8 pM) [49].

Plant derived Ribosome-Inactivating Proteins (RIPs), are suitable candidates to pursue this latter strategy. They belong to the N-glycosidase family of toxins able to depurinate a specific adenine base located in the universally conserved GAGA tetraloop in the 23/26/28S rRNA. This activity results in the inability of the ribosome to bind the elongation factor 2 and, thus, in the irreversible inactivation of protein translation, causing apoptotic cell death [46, 50]. Plant RIPs have been classified into three main groups: type I RIPs are composed of a single polypeptide chain with catalytic activity; type II RIPs are heterodimer consisting of an A chain, functionally equivalent to the type I polypeptide, linked to a B subunit, which is endowed with lectin-binding properties; type III RIPs are polypeptides synthesized as inactive precursors (ProRIPs) that require proteolytic processing to form an active RIP [50]. The lack of a specific binding domain in types I RIPs natural structure have allowed their direct exploitation as catalytic moiety of recombinant chimeras. In this class of molecules, saporin (SAP) is one of the most studied because of its strong intrinsic activity both in cell-free systems and in cell lines and its unusual resistance to high temperature, denaturation and attacks by proteolytic enzymes, making it a suitable candidate for therapeutic intervention. Its

internalization pathway has been demonstrated to involve the low-density lipoprotein receptor (LDLR) family that includes seven closely related family members: the very-low-density lipoprotein (VLDL) receptor, apoE receptor 2, multiple epidermal growth factor-like domains 7 (MEGF7), glycoprotein 330 (gp330/megalin/LRP2), lipoprotein receptor-related protein 1 (LRP1), and LRP1B [50]. Among these, the α2-macroglobulin receptor/low-density lipoprotein receptor-related protein 1 (LRP1) in particular was shown to bind saporin *in vitro* [51, 31], mediating saporin internalization in human monocytes and fibroblasts [52, 53]. Furthermore, downregulation of LRP in human U937 lymphoma cells as well as its knock out in mouse embryonic fibroblasts (MEF) resulted in an increased resistance to saporin [52, 54]. Saporin-based uPAR targeting conjugate, carrying the entire pro-uPA sequence [55] and a saporin-based recombinant chimera, in which saporin was fused to the amino terminal fragment (ATF) of uPA [29, 31, 32] were found to specifically recognize and bind uPAR overexpressing cells in *in vitro* studies, therefore modifying the internalization pathway of the toxin and making it dependent on the expression of the target molecule, paving the way for the use of targeting toxins as anti-cancer therapeutic strategies.

1.7 Nanotechnology to improve drug delivery

In recent years, outstanding progresses have been achieved by using nanotechnology to increase the targeted delivery of drugs. Among them, drugs-encapsulating nano-vectors, such as liposomes, currently represent a preferred system, offering several advantages compared to the use of drugs themselves. In fact, they enable a reduced systemic toxicity, enhanced drug solubility and improved homing in diseased tissues, as the drug is "protected" inside the carrier, it is not subjected to degradation by serum components and could be better retained in the tumor mass through both an active (surface customization) or passive targeting (EPR effect) mechanism. However, the ability of an ideal liposome to evade the host immune system and achieve a longer circulating capability and stability still remains elusive [56]. In this contest, naturally secreted nano-sized extracellular vesicles (exosomes) appear to be a preferable choice, offering

important advantages compared to synthetic liposomes, among which: 1) lack of immunogenicity and cytotoxicity, due to their composition, which resembles body's own cells; 2) improved circulation time, decelerating mononuclear phagocyte system-mediated clearance; 3) innate stability in biological fluids. These features, together with the average nano-scaled size (50-200 nm) that allows them to easily penetrate in almost all body districts and cross biological barriers, the cargo protection and the customizable surface, make them ideal nanocarriers for targeted drug delivery [57].

1.7.1 Exosomes biogenesis, isolation and characterization

Exosomes are small extracellular vesicles that originate from the inward budding of the membrane of late endosomes that results in the formation of vesicles inside the lumen. The neo-formed structure, called multi-vesicular body (MVB), can either fuse with lysosome for degradation or with the plasma membrane of the cell, releasing its exosomes content in the extracellular environment. Therefore, exosomes molecular composition is associated with MVB biogenesis and includes nucleic acids, transport proteins, heat shock proteins, soluble proteins and membrane proteins such as tetraspanins. In addition to proteins, exosomes are characterized by different types of lipids, such as cholesterol, sphingolipids, phosphoglycerides, ceramides and saturated fatty acid chains [58], present in highly abundant amount. This peculiar lipid composition allows the use of fluorescent lipophilic dyes to stain their membrane and trace their intracellular fate. Importantly, exosomes molecular composition is critical, since they provide an indication of their functions in biological processes. Therefore, it is very important to select the proper cell type as origin of exosomes to be used for a therapeutic purpose. Different exosomes isolation methods have been optimized over the years [59]. The most common one consists in differential centrifugation steps, whereby cell debris and large particles (microvesicles and apoptotic bodies) in the culture medium are eliminated using low centrifugal force and exosomes are collected from supernatant by high speed ultracentrifugation. Other isolation techniques include the use of flotation density gradient centrifugation with sucrose or Optiprep,

ultrafiltration, high performance liquid chromatography, capturing by monoclonal antibodies against exosome-associated membrane proteins, such as tetraspannins CD9, CD63, CD81, CD82, epithelial cell adhesion molecule (EpCAM), and Ras-related protein 5 (Rab5). The antibodies can be combined with magnetic beads, chromatographic matrix, plates and microfluidic devices for separation [59]. Most the above-mentioned isolation methods provide a highly selective purification of exosomes. Furthermore, several techniques can then be used to characterize exosomes, including flow cytometry, nanoparticle tracking analysis, dynamic light scattering (DLS), western blot, mass spectrometry, and microscopy [60]. Exosomes can also be characterized on the basis of their protein compositions: typical exosomal markers are tetraspanins, TSG101, ALG-2 interacting protein X (ALIX), flotillin 1, and Lysosomes associated membrane glycoprotein 2 (Lamp2). According to ExoCarta, a wide exosome database, there are currently around 8000 proteins and 194 lipids known to be associated with exosomes [61] (www.exocarta.org).

1.7.2 Methods of drug encapsulation into exosomes

The approaches investigated so far to incorporate drugs into exosomes can be classified into active and passive loading strategies. The formers include the use of mechanical (extrusion), chemical (incubation with or without permeabilization agents, like saponin or other detergents) or physical stimuli (sonication, electroporation, freeze and thaw cycles) to incorporate either small molecules (curcumin, paclitaxel, doxorubicin), RNAs or proteins (catalase, saporin) into purified exosomes [62, 63, 64, 65, 66, 67]. Even if demonstrated to be successful, these methods suffer from the great limitation of affecting vesicles structural composition and achieving very low drug encapsulation efficiency. Electroporation, in particular, acts by perturbing the exosomal membrane throughout the application of an electrical current, that results in the temporary formation of pores, allowing the diffusion of the drug in the vesicle. It is widely used to incorporate a broad spectrum of drugs into isolated exosomes, among which siRNA, miRNA, proteins and small molecules, leading to an increased loading

efficiency over the other methods. Nakase et al. have demonstrated that electroporation is highly effective in enhancing saporin encapsulation, as shown by *in vitro* cytotoxic assays, but the amount of exogenous protein loaded was calculated to be around only 0.1% [66, 68]. The passive loading strategies, on the other hand, are modeled on the incubation of exosomes/cells with free drugs, that do not compromise the vesicles membrane integrity but, similarly, enhance a very low cargo-incorporation [69, 70].

1.7.3 Methods to confer targeting properties to exosomes

As for cargo loading, surface decoration of exosomes with targeting moieties can be achieved through genetic engineering of donor cells. The first proof of concept of the applicability of this strategy was obtained by Alvarez-Ervitii et al., who used Lamp2b, a well characterized exosomal membrane protein, as anchor and fusion partner for targeting domain of interest. They demonstrated that acetylcholine receptor binding rabies viral glycoprotein (RVG) peptide could be displayed onto exosomes from dendritic cells and improve their delivery to target cells [65]. This seemingly simple yet effective engineering technique was also applied to other targeting ligands, such as iRGD peptide, that showed highly efficient drug delivery to αv integrin-positive breast cancer cells *in vivo* [71, 72], and for exosomes incorporation of tags and reporter proteins [73, 74]. However, despite the clear advantages that this method would achieve, such as an increased homogeneity of vesicles batches, surface structure preservation and reduced time-consuming work, a recent report demonstrated that, instead of sorting into exosomes, degradation of fusion proteins may occur when this approach is employed [73]. As an alternative, stable conjugation of targeting ligands to the surface of isolated exosomes can be realized using chemical linkers, with similar methods employed to functionalize synthetic particles and liposomes. Smyth et al., for instance, have reported that N-hydroxy succinimidyl ester reactive groups on exosomes, mostly comprising available N-termini and lysine residues of membrane proteins, can be stably linked to targeting ligands under biocompatible reaction conditions [75]. This conjugation has been shown to not change the physical characteristics of

exosomes nor their interaction with recipient cells. In addition, stearyl anchoring moieties have also been proposed and demonstrated to be effective in improving exosomes surface decoration with cell penetrating peptides [76]. However, the successful and stable modification of exosomes surface with targeting moieties is nontrivial. The reaction conditions must be strictly limited to avoid exosome disruption, aggregation and alteration of uptake properties due to inappropriate conditions.

Aim of the study

Surgery represents the primary choice in the treatment of solid tumors, usually in combination with chemotherapy or radiotherapy cycles. Although conventional radio-chemotherapeutics have a broad spectrum of action and are partially effective in the treatment of many cancers, serious side effects severely limit their use, pharmacological dosage and number of cycles that can be given. In fact, they totally lack specificity and, as a result, patients are treated with levels of drug that are often sub-lethal to the cancer. These limitations have been partially overcome by the use of immunotherapies as combination therapies, that are certainly more specific in targeting cancer cells but can poorly penetrate into the tumor mass due to their dimensions and can induce cancer cells to develop drug resistance. In this context, many efforts are focused on the development of targeted and personalized therapies aimed at exploiting specific tumor pathways and receptors to selectively kill neoplastic cells. Compared to monoclonal antibodies, RIP toxins have many incremental advantages, such as the small dimensions and globular structure, the lack of a specific ligand domain and the direct cells killing property. The aim of this project is to develop two different therapeutic options, based on the plant toxin SAP, for the treatment of bladder cancer, whose application could also be extended to a broader range of solid tumors. In fact, we have selected targets expressed in multiple-tumor types that would widen disease indications and prevent tumor resistance caused by the emergence of antigen-loss variants. In particular, as a first approach we explore the therapeutic potential of a targeted protein-based strategy, in which small peptides are employed to specifically deliver SAP to cancer cells and tumor microenvironment. In parallel, we propose to couple the features of exosomes as drug delivery system with SAP activity. The biocompatible characteristics of exosomes, with suitable modifications, can increase the stability and efficacy of SAP therapeutics while enhancing cellular uptake and reducing potential in vivo immunogenicity. Overall, we expect to prepare a number of therapeutic options as large as possible to cope with intra- and inter- tumor heterogeneity. Synergistic coupling of high toxin activity to targeting peptides or

nanovesicles would provide novel strategies and useful tools to achieve major advancements for the treatment of heterogeneous diseases such as cancer.

2. Materials and methods

2.1 Cells culture

Human bladder (RT4, RT112, 5637, HT1376), breast (MDA-MB 231, MDA-MB 468, BT549, SKBR3) and glioblastoma (U87) cancer cell lines were obtained from American Type Culture Collection (ATCC) and maintained respectively in RPMI 1640 (bladder) or DMEM medium (breast and glioblastoma) supplemented with 10% FCS, 2 mM L-Glutamine and antibiotics (100 U/mL penicillin and 100 μg/mL streptomycine-sulphate). Human ECV304 bladder cancer cells were maintained in medium 199 supplemented with 10% FCS, 2 mM L-Glutamine and antibiotics (100 U/mL penicillin and 100 μg/mL streptomycine-sulphate). Human SUM149 and SUM159 triple negative breast cancer cells were cultured in HAM-F12 medium, supplemented with 5% FCS, 2 mM L-Glutamine, antibiotics (100 U/mL penicillin and 100 μg/mL streptomycine-sulphate), insulin (2 μg/ml) and hydrocortisone (1 μg/ml), 10 mM HEPES. Murine MB49 bladder cancer cells were cultured in DMEM medium, supplemented with 10% FCS, 2 mM L-Glutamine, antibiotics (100 U/mL penicillin and 100 μg/mL streptomycine-sulphate) and Sodium Pyruvate (1 mM).

MB49 Luc cells stably expressing luciferase were generated by transduction with a 3rd generation lentiviral vector carrying the luciferase gene. pLenti PGK V5-LUC Neo (w623-2) was a gift from Eric Campeau (Addgene plasmid # 21471). For lentivirus production, HEK293T cells were transfected with the $CaCl_2$ method. To this end, a mix containing 10 μg of transfer vector, 6.5 μg of packaging vector Δr 8.74, 3.5 μg of Env VSV-G, 2.5 μg of REV, ddH2O to 450 μl, 50 μl of 2.5 M $CaCl_2$ and 500 μl of 2X HBS was added dropwise over a monolayer of HEK293T cells seeded on a 10 cm^2 dish. After 16 hours, the medium was replaced; 24 hours later the medium containing virus particles was collected, filtered on a 0.22 μm filter and used to transduce cells. Infected cells were selected by G418 for fifteen days.

2.2 Flow cytometry analysis

Cultured cell lines were detached by TripLE Express (Gibco) to preserve receptor integrity, washed with PBS containing 1% FCS and incubated with primary antibody (Ab) specific for human uPAR (Sekisui), PE-conjugated Ab specific for human αvβ3 (R&D System) and FITC-conjugated Ab specific for human αvβ6 integrins (NovusBio). For uPAR detection, cells were incubated with the primary Ab at 4° C for 1 h, followed by secondary antibodies conjugated to FITC for 30 min. For integrins detection, cells were incubated with the fluorescently labelled Ab at 4° C for 30 min. Stained cells were resuspended in 100 µL of PBS containing 1 % FCS. Secondary FITC-conjugated antibody only or isotype control stained cells were used as negative controls. Samples were run through an Accuri™ flow cytometer (BD Biosciences). All data were analysed by FCS Express and expressed as relative fluorescence intensity (RFI), calculated as follows: mean fluorescence intensity after mAb staining/mean fluorescence intensity after isotype-negative control staining. 5637 and RT112 cells were cultured in 24-well microplates until 60% confluence. 24 hours later, the cells were treated with labelled exosomes (15 µg/well) and incubated at 37° C, 5% CO_2 for 48 hours. Then, cells were detached by incubation with 0.01% trypsin for 5 min at 37° C, collected, washed with 1% FBS (in PBS) and subjected to flow cytometry analysis using Accuri™ flow cytometer. Analysis was done on 10,000 gated events per sample.

2.3 Cell viability assay

Cultured cell lines were seeded in 96 wells plates and incubated for 72 hours with scalar logarithmic concentrations of ATF-SAP WT, ATF-SAP KQ, pro-uPA-SAP, RGD-SAP, CYS-SAP or saporin alone (seed SAP). After 72 hours of incubation at 37° C, 3-(4,5-dimethylthiazol-2-yl)-2,5-diphenyltetrazolium bromide (MTT) (5 mg/ml in PBS) was added (0.5 mg/ml working concentration). After 1 hour incubation at 37° C, supernatants were removed and 100 µl/well of dimethyl sulfoxide were added to dissolve formazan crystals. Cell viability was assessed by measuring the absorbance at 570 nm and expressed as percentage to untreated

control. The toxic activity of the recombinant proteins was evaluated as IC_{50}, shown as mean ± SD from three independent experiments. For the competition experiments, MDA-MB-468 cells were seeded in 96 well plates, exposed to 20 nM ATF-SAP in the absence or presence of increasing concentrations of uPA (4, 20, 100 nM), PAI (4, 20, 100 nM) or uPA+PAI (100 nM + 100 nM), for 72 h. RGD-SAP binding to αν integrins was competed by exposing 5637 cells to 100 nM RGD-SAP or 1 μM CYS-SAP in the presence of 5 μg/ml ACDCRGDCFCG peptide for 24 and 48 hours. Residual cells viability was evaluated by MTT assay.

2.4 Establishment of primary human bladder-derived fibroblasts culture

Human bladder biopsies were obtained from men undergoing bladder surgery in agreement with informed consent. Cells were obtained through a primary explant technique. Briefly, the tissue was minced with a scalpel into small pieces (1–2 mm^3) and washed in fresh medium to eliminate the excess of mucus or blood proteins. Tissue pieces were then placed on a dish for primary culture and incubated in MEM-Non-essential amino acids (100x, without L-Glutamine) (Lonza), supplemented with 1% FCS, antibiotics (100 U/mL penicillin and 100 μg/mL streptomycine-sulphate), 200 nM Hydrocortisone (Sigma), 10 nM Triiodothyronine (Sigma), 5 ng/ml Epidermal growth factor (Gibco, Life Technologies). The incubation was carried out for 3-5 days. Then the medium was changed at weekly intervals until a substantial outgrowth of cells was observed. The explants were thus removed and the cells transferred to a fresh dish. Cells were cultured for a maximum of 20 days.

2.5 Immunofluorescence analysis

ECV304 epithelial bladder cancer cells, skin and bladder-derived fibroblasts were seeded in sub-confluent conditions and grown overnight on glass coverslips. After 24 hours, cells were quickly washed in PBS and fixed in 4% paraformaldehyde in PBS at room temperature for 30 min. After extensive PBS washing to remove the excess of paraformaldehyde, cells were permeabilized in 0.2% Triton and incubated

in 10% donkey serum in PBS for 1 hour. Primary antibody incubation was performed for 1 hour at room temperature using: anti-human Fibroblasts Surface Protein (Abcam, working dilution 1:100 in 1% donkey serum, 0.1% Triton in PBS) or anti- human Actin α–Smooth Muscle (Sigma-Aldrich, working dilution 1:500 in 1% donkey serum, 0.1% Triton in PBS). Fluorescent signal was detected by the use of Alexa488-conjugated secondary antibody (working dilution 1:500 in 1 % donkey serum, 0.1% Triton in PBS). Then, coverslips with stained cells were mounted on a microscope slide with VECTASHIELD Antifade Mounting Medium with DAPI (Vector Laboratories, Burlingame, CA, USA), carefully avoiding the formation of air bubbles. Fluorescent images were taken by using Axio Vision Imaging Software (Axiovision Rel 4.8®) on an Axio Imager M2 microscope (Carl Zeiss, Oberkochen, Germany).

2.6 RNA extraction and quantitative analysis

Total RNA from bladder and breast cancer cell lines was extracted using TRIzol LS Reagent (Invitrogen) according to the manufacturer's recommended protocols. RNA was then retrotranscribed with High Capacity cDNA Reverse Transcription Kit (Applied Biosystems). A calibration curve was performed for each gene of interest to test primers and to determine the correct concentration of cDNA to use for quantitative Real Time. For primers used, see Table 1. Each cDNA sample was diluted with nuclease free water to obtain the correct amount (0.5 ng) in a volume of 12.5 μl. The mix for the primers was prepared as follows: 12 μl of SYBR green PCR master mix and 0.5 μl of primers (forward and reverse). The total reaction was set for 25 μl/well. Two complementary primers for each gene of interest were purchased from Eurofins. uPAR, uPA and LRP1 expression levels (indicated as "fold change" compared to healthy fibroblasts, used as a reference) were analyzed in triplicate, normalized to HPRT1 and calculated according to the CT method.

2.7 Preparation of RGD-SAP and CYS-SAP

SAP fused with the C-terminus of respectively ACDCRGDCFCG or CGGSGG were prepared by recombinant DNA technology. For primers used, see Table 1. To place the ACDCRGDCFCG sequence upstream the SAP sequence, two complementary single strand oligonucleotides encoding the ACDCRGDCFCG sequence, flanked by NdeI and BamHI restriction sites at the 5′ and 3′ ends, respectively, were designed. They were annealed by heating to 95° C for 10 min in nuclease free water and slowly cooled to 25° C. The procedure produced a double-strand DNA fragment with NdeI and BamHI cohesive ends ready for ligation. No further purification was used. A GGSSRSS sequence containing a BamHI restriction site was interposed between ACDCRGDCFC and SAP as a spacer and introduced to the N-term of the SAP encoding sequence by PCR amplification. This PCR product was digested with BamHI and EcoRI. To position the CGGSGG sequence, standard PCR was performed on SAP encoding gene with a forward primer including the CGGSGG sequence flanked by NdeI restriction site and a reverse primer including an EcoRI site. The NdeI site contains also the translation starting codon. The pET22b (+) vector (Novagen) was linearized with NdeI and EcoRI to clone the CYS-SAP sequence or with BamHI and EcoRI to clone SAP encoding sequence containing the spacer. The oligonucleotide encoding for the ACDCRGDCFCG sequence was then sub-cloned by linearizing the plasmid with NdeI and BamHI. The inserts were ligated into the linearized vectors overnight at 16° C, forming the pET22b (+)-RGD-SAP (5′-NdeI-RGD-BamHI-GGSSRSS-SAP-EcoRI-3′) and the pET22b (+)-CYS-SAP (5′-NdeI-CYS-SAP-EcoRI-3′) expression vectors. The 6xHis tag at C-terminus of each recombinant protein was maintained in order to allow the purification by affinity chromatography. Ligation products were used to transformed the *E.coli* strain DH5alpha (Invitrogen). The plasmid sequence was checked through analytical digestion and sequencing.

The expression of RGD-SAP and CYS-SAP in transformed BL21(DE3) *E.coli* cells (Novagen) was induced for 3 hours at 37° C with IPTG 0.1 mM. Bacterial pellet from 1 L culture was resuspended in 15 ml of lysis buffer (Tris-HCl, 50 mM pH 7.5 supplemented with a cocktail of protease inhibitor (Sigma-Aldrich). Soon after,

10 mM of imidazole, lysozyme 250 μg/ml and DNAse 20 μg/ml were added. The resuspended bacterial lysate was then incubated for 45 min on ice, sonicated on ice with the UW3100 Bandelin sonicator with 60% power for 2 min (1 second pulse / 1 second pause) for 3 cycles and centrifuged at 4° C for 25 min at 11,000 rpm. The supernatant (total cell extract) was stored at -80° C before purification.

2.8 Preparation of Lamp2b, CD9 and CD81-based constructs

Lamp2b signal peptide (SP) and gene sequence, CD9 and CD81 cDNA sequences were amplified from HEK293-derived cDNA. To place the ACDCRGDCFCG peptide between SP and Lamp2b sequences, standard PCR was performed, using a forward primer specific for Lamp2b including a half of the peptide sequence, flanked by SpeI restriction site, and a reverse primer specific for the SP including the other half of the peptide, flanked by SpeI restriction site. The two fragments carrying the SpeI restriction sites were digested and ligated together to obtain SP-RGD-Lamp2b product. NheI and SalI restriction sites were inserted respectively at N-terminus and C-terminus of the full construct (5′-NheI-SP-RGD-Lamp2b-SalI-3′). The same restriction sites were also inserted at the N-terminus and C-terminus of CD9 and CD81 encoding genes by PCR amplification. PCR amplification was also performed to position the RFP or SAP encoding genes downstream the Lamp2b or tetraspanins sequences. Cathepsin B specific Phe-Leu dipeptide (cleavage site, CS) or its non-specific variant Gly-Ser (nonactive cleavage site, NACS), flanked by two glycine as a spacer and SalI restriction site were included in RFP or SAP forward primers, flanked by the SalI restriction site. A NotI containing primer was used as reverse. The sequences contain: 5′-NheI-SP-RGD-Lamp2b-SalI-GFLG/GGSG-RFP/SAP-NotI-3′; 5′-NheI-CD9-SalI-GFLG/GGSG-RFP-NotI-3′; 5′-NheI-CD81-SalI-GFLG/GGSG-RFP-NotI-3′. All the linearized constructs were sub-cloned downstream the CMV promoter into a pcDNA 3.1(+) vector.

2.9 Stable transgene expression

5637 or HEK293 cells (2 x 10^6) were plated in a 10 cm^2 dishes and incubated for 24 hours. Plasmid DNA (total 8 μg/dish) and TransIT-X2 transfection reagent (Mirus) were diluted separately in serum- and antibiotic free medium and then mixed together in a 1:2 ratio. After 20 min incubation, the mixture was added dropwise over the cells monolayer. After 16 hours the medium was replaced and transfected cells were selected by G418 for fifteen days

2.10 RGD-SAP and CYS-SAP purification

Soluble RGD-SAP and CYS-SAP were purified from bacterial lysates by affinity chromatography using a HisPur™ NiNTA resin (TermoFisher Scientific) equilibrated in Tris-HCl 50 mM pH 7.5 supplemented with 10 mM imidazole. For recombinant protein elution 1 M imidazole was used. An ion exchange chromatography on SP-Sepharose XL column (HiPrepSP XL 16/10, GE Healthcare Life Sciences) was then performed for further purity achievement. 1 M NaCl was added to the product of ion exchange. The proteins were then concentrated using 10 kDa cut off Amicon centrifugal Filters (Millipore-Sigma). All solutions used in purification steps were prepared with sterile and endotoxin-free water (S.A.L.F. Laboratorio Farmacologico SpA, Bergamo, Italy). Protein concentration was measured using the BCA Protein Assay DC™ Kit (BioRad). Protein purity and identity was checked by SDS-PAGE and Coomassie blue staining and Western blotting.

2.11 Protein extraction, Coomassie blue staining and western blot analysis

Cells were washed twice with cold PBS, collected by scraping and centrifuged 5 min at 1200 rpm. Cells were lysed for 30 min on ice in ice-cold buffer (150 mM NaCl, 2 mM NaF, 1 mM EDTA, 1 mM EGTA, 1 mM Na_3VO_4, 1 mM PMSF, 75 mU/ml aprotinin -Sigma-, 50 mM Tris-HCl, pH 7.5) containing 1 % TX-100 and a cocktail of proteinase inhibitors (Sigma-Aldrich). Cell lysates were centrifuged at

10000 xg at 4° C for 10 min. Proteins contained in the supernatant were quantified, resuspended in sample buffer (62.5 mM Tris-HCl (pH = 6.8), 2% SDS, 10% glycerol, 0.002% bromophenol blue, 5% 2-mercaptoethanol) and boiled at 95°C for 5 minutes. Proteins were separated via SDS-PAGE. All the SDS-PAGE were run under reducing conditions unless stated otherwise. For Coomassie blue staining, acrylamide gels were incubated in a Coomassie blue solution (0.1% Coomassie Brilliant Blue R-250, 50% methanol and 10% glacial acetic acid) for 1 hour; then a 5% acetic acid solution and 45% of methanol incubation was used to detect the protein of interest. For western blot analysis, proteins were transferred onto a nitrocellulose membrane, incubated with 5% non-fat powdered milk in TBS-T (0.5% Tween-20) for 1 hour and then with the following antibodies: Saporin (1:5000), Caspase 3 (1:2000, Abcam), β-actin (1:10000, Sigma), Flotillin (1:5000, Sigma), Alix (1:800, Santa Cruz Biotechnology), CD63 (1:1000, BD Biosciences), CD9 (1:1000, BD Biosciences), CD81 (1:1000, BD Biosciences). Secondary horseradish peroxidase conjugated antibodies (anti-mouse/rabbit IgG HRP-linked whole antibody donkey, GE Healthcare) were used and immunoreactive bands were visualized by using the Enhanced Chemiluminescence (ECL) (Merck Millipore).

2.12 *Ex vivo* studies

A sub-confluent 5637 or RT112 bladder cancer cells were plated in 10mm dish, detached in exponentially growth conditions and resuspended in serum and antibiotics free RPMI. 7-week-old NSG mice were subcutaneously injected with $1x10^6$ cells in the left flank. Tumor growth was monitored with caliper. Animals were sacrificed when the tumor started to grow exponentially. The tumor mass was explanted, minced and dissociated with Trypsin (0.25 mg/ml in RPMI) at 37°C for 10 min to obtain single-cell suspension. Cells were then further mechanically disaggregated by pressing the pellet through a cell strainer (70 μm) and treated with DNAse (100 μg/ml, Sigma-Aldrich) and ACK lysing buffer (Lonza) to remove red blood cells. Single cells were finally washed extensively with medium supplemented with FCS 10%, 2 mM L-Glutamine and antibiotics (100 U/mL penicillin and 100 μg/mL streptomycine-sulphate) and dispersed into 10 mm

dishes. After 1 week of *in vitro* culture, cells were collected, counted and reinjected in the left flank of 7weeks old NSG mice (1 x 10^6 cells/mouse). After mice sacrifice and cells recovery from tumor mass dissociation, flow cytometry analysis to monitor uPAR expression and cell killing assay with ATF-SAP were performed as described above.

2.13 ***In vivo*** **studies**

Studies on animal models were approved by the the Institutional Animal Care and Use Committee (Institutional Animal Care and Use Committee, IACUC) and performed according to the prescribed guidelines. Subcutaneous syngeneic mouse model: 7 weeks old C57BL/6 female mice (Charles River, Calco, Italy) were injected in the left flank with 5 x 10^5 (experiment 1) or 3 x 10^5 (experiment 2) MB49 living cells; 5 days later, mice were treated with RGD-SAP or CYS-SAP solutions (200 μl). The treatment was repeated every 5 days for 3 times. Subcutaneous xenograft mouse model: 7-week-old CD1 nude female mice (Charles River, Calco, Italy) were injected in the left flank with 1 x 10^6 RT112 living cells; 10 days later, mice were treated with ATF-SAP, RGD-SAP or ATF-SAP + RGD-SAP solutions (200 μl). The treatment was repeated every 5 days for 3 times. All toxins, diluted with sodium chloride, were administered intravenously (i.v.). Orthotopic syngeneic mouse model: 7 weeks old C57BL/6 female mice (Charles River, Calco, Italy) were anesthetized with Ketamine/Xylazine (80/10 mg/kg) and catheterized with PE50 catheters (BD Biosciences). The catheters were lubricated with 2.5 % lidocaine-containing gel (Luan). To enhance tumor engraftment, bladder was pretreated with 100 μl of 0.1 mg/mL poly-L-lysine (PLL, mol. wt. 70,000–150,000) (Sigma Aldrich), which was injected transurethrally and kept into the bladder for 30 min, as described by Loskog et al. 2005. The bladder was then washed with PBS before the instillation of 100 μL of 5 x 10^4 MB49 Luc. Tumor cells were kept in the bladder for 30 min. After the final incubation the catheters were removed. On day 7 after injection, mice were treated with RGD-SAP (200 μl) every 5 days for 3 times (experiment 1) or with MMC in PBS (50 μg) every 4 days for 2 times and RGD-SAP every 5 days for 3 times. MMC treatment was given transurethrally in

anesthetic conditions (Ketamine/Xylazine) and kept in the bladder for 1 hour. Before MMC treatment, urine was squeezed out from the bladder and the bladder was washed with PBS. Subcutaneous tumor growth was monitored daily by measuring tumor volumes with calipers as described previously. Tumor volumes are shown as mean ± SD (4 animals/group experiment 1; 6 animals/group experiment 2) and calculated as follows: $r_1 \times r_2 \times r_3 \times 4/3\ \pi$, where r_1 and r_2 are the longitudinal and lateral radii, and r_3 is the thickness of tumors protruding from the surface of normal skin. Orthotopic tumor engraftment and growth was monitored once a week by *in vivo* bioluminescence imaging (IVIS). Tumor bioluminescence was calculated as total photon flux and shown as mean ± SD. Mice weight was recorded every 2 days and their health/behaviors monitored daily. Animals were euthanized when tumors reached 10 mm in diameter, became ulcerated or a 20% weight loss was detected. In the case of the orthotopic model, mice were euthanized when the bioluminescence intensity (BLI) reached 10^9 value, in case of a sudden drop of the BLI signal, in case of 20% weight loss or animal lethargy.

2.14 Blood sample collection and biochemical parameters analysis

Blood samples were collected from the retroorbital plexus of anesthetized mice. Anesthesia was induced by placing each mouse in an inhalation chamber with 4 % isoflurane regulated with a calibrated vaporizer. Blood samples were left at room temperature for at least 30 min before being processed, then centrifuged (3,000 rpm, 10 min) for serum separation. Serum Albumin, aspartate transaminase (AST), alanine transaminase (ALT), creatinine and urea were determined by using an automated analyzer (ScilVet ABC plus and Idexx Procyte analyzers) according to the manufacturers' instructions. Standard controls were run before each determination.

2.15 Exosomes and microvesicles isolation

Human embryonic kidney cell line HEK293T (5 x 10^6) were seeded on 150 mm dishes in DMEM medium supplemented with 10% FCS, 2 mM L-Glutamine and antibiotics. 72 hours after incubation, the cell culture medium was collected and centrifuged (1500 rpm) for 25 min to remove cell debris. For exosomes isolation, the obtained supernatant was filtered through 0.22 μm filter before ultracentrigugation at 150,000 xg for 2 hours at 4° C (Beckman Coulter). The exosomes containing pellet was resuspended in PBS. For microvesicles isolation, cell debris-free supernatant was centrifuged at 10,000 xg for 30 min at 4° C. The microvesicles containing pellet was resuspended in PBS. Concentration of isolated exosomes and microvesicles was calculated as protein concentration, which were determined using a Pierce BCA protein assay kit (Thermo Scientific).

2.16 Dynamic light scattering (DLS) analysis

DLS analysis was performed with a Zetasizer nanoseries instrument (Malvern Nano-Zetasizer = 532 nm laser wavelength). The exosome size data refers to the scattering intensity distribution (z-average). Exosomes were re-suspended in PBS at a concentration of 1 ng of protein/ml. Samples were manually injected into the sample chamber at room temperature. Each sample was measured in triplicate with an acquisition time of 30 s.

2.17 Nanoparticle tracking analysis (NTA)

NTA was performed by an expert EV laboratory (Exosomics Siena S.p.A, Siena) in order to provide a validation of the results. NTA was performed using a NanoSight LM10-HS microscope (NanoSight Ltd., Amesbury, UK). For the analysis, exosomes were diluted in 50 μl of PBS and concentrations adjusted, if necessary, in order to specifically fit the optimal working range (20–50 particles per frame) of the instrument. Three 60-s videos were recorded under the flow mode for each sample with camera level set at 16 and detection threshold set at 10. At

least 200 completed tracks per video were collected. The camera level and overall settings were selected as optimal for the accurate detection of exosome-sized nanoparticles following the manufacturer recommendations and as confirmed during instrument calibration. Videos were analyzed with NTA software version 2.3 to determine the mean, mode and estimated concentration of measured particles with corresponding standard error. The NanoSight system was calibrated with polystyrene latex microbeads of 50, 100, and 200 nm (Thermo Scientific Waltham, MA, USA) prior to analysis and auto settings were used for blur, minimum track length and minimum expected particle size.

2.18 Transmission electron microscopy (TEM) analysis

Preparation of samples for TEM analysis was performed using the method described by Théry *et al*. [59]. HEK293-derived exosomes were mixed with an equal volume of 4% PFA and deposited by airfuge onto Formvar/Carbon coated EM grids (Ted Pella, Redding, CA, USA). Samples were contrasted and embedded by treatment with uranyl-oxalate solution (Electron Microscopy Science, Hatfield, PA, USA), pH 7, for 5 min, followed by methyl-cellulose-uranyl-acetate (Sigma, Saint Louis, MO, USA) on ice for 10 min. LEO 912AB Omega electron microscope (Carl Zeiss NTS, Oberkochen, Germany) was used for image analysis.

2.19 Fluorescent labelling of exosomes and *in vitro* uptake tracing

Exosomes isolated from cell culture media were resuspended in PBS and then combined with a PBS solution containing Vybrant™ DiO (1 µl for 100 µg exosomes, Molecular Probes, Eugene, OR, USA). The sample were incubated at 37° C for 30 min (protected from light) in stirring conditions and then passed through Exosome spin colums MW 3000 (Invitrogen) to remove any incorporated dye. PBS containing dye only was used as negative control. The samples were then ultracentrifuged (150,000 xg, 2 hours at 4° C) and the pellet resuspended in PBS. For the *in vitro* tracing assay, fibroblasts were seeded (up to 50-60% confluence) in a 24 multiwell plate and incubated at 37° C with 5 % CO_2. 24 hours later, labelled

exosomes (5, 10 or 20 μg/ well) were added to recipient cells. Exosomes uptake was observed and evaluated after 24, 48 and 72 hours via fluorescent microscopy.

2.20 Exogenous protein encapsulation into isolated exosomes

HEK293 derived-exosomes were resuspended with SAP in 1 M Na_2CO_3 pH 11.5 or PBS and incubated 30 min at 37° C. The amount of exosomes used was calculated as protein concentration. A ratio of 1 μg exosomes (EXO): 1.5 μg SAP was used to enhance the exogenous protein encapsulation. pH was then neutralized and the sample filtered by centrifugation through Exosome spin colums 100 KDa MWKO (Merk-millipore) to remove any incorporated protein and washed with NaCl 150 mM to reduce protein aggregation. SAP or exosomes alone were used as negative controls.

2.21 Statistical analysis

All *in vitro* experiments were performed at least in duplicate. Mouse experiments were performed using at least 4 mice per treatment group. When appropriate, statistical significance was determined using a 2-tailed Student's *t* test. For tumor growth analyses, we performed one-way ANOVA statistical analysis. Survival curves were compared using the log rank test. Tests symbols mean: *$p < 0.05$; **$p < 0.01$; ***$p < 0.001$; ns, not significant.

Table 1. List of primers used

Primer	Sequence
CYS-SAP	
CYS-SAP F	5’-atcccatatgtgcggcggcagcggcggcgtgaccagcattaccctgga-3’
SAP R	5’-atccgtcgactttcggcttgccc-3’
SP-RGD-Lamp2b-RFP	
SP F	5’- ataggctagcggtcgccaccatggtgtgcttccgcctct-3’
SP R	5’-atccgcggcaatcgcatgcctcgagtgcataagaccgcacagctc-3’
Lamp2b F	5’-atccgcggcgattgcttttgcggtactagtttggaacttaatttgacagattc-3’
Lamp2b R	5’-atccgtcgactgcagagtctgatatccagcata-3’
RFP/SAP CS/NACS	
RFP-CS F	5’-tgcagtcgactggctttcttggaatggcctcctccgagaacg-3’
RFP- NACS F	5’-tgcagtcgactggcggttctggaatggcctcctccgagaacg-3’
RFP R	5’-agtcgcggccgctacaggaacaggtggtggc-3’
SAP-CS F	5’-tgcagtcgactggctttcttggaatggtcacatcaatcacattag-3’
SAP-NACS F	5’-tgcagtcgactggcggttctggaatggtcacatcaatcacattag-3’
SAP R	5’-atgcggccgcctactttggtttgcccaaatac-3’
CD9/CD81	
CD9 F	5’-ataggctagcgccaccatgccggtcaaaggaggca-3’
CD9 R	5’-atccgtcgactggaccatctcgcggttcctg-3’
CD81 F	5’-ataggctagcgccaccatgggagtggagggctgc-3’
CD81 R	5’-atccgtcgactggtacacggagctgttccgg-3’

3. Results I

This first section of results focuses on the design and production of SAP based recombinant proteins carrying a tumor targeting moiety in their structure. The identification of over-expressed antigens on cancer cells surface allows a highly efficient molecular targeting, which enables the delivery of SAP enzymatic activity specifically to malignant cells.

3.1 uPAR over-expression associates with a stage II muscle invasive bladder cancer and triple negative breast cancer phenotypes

uPAR is known to exert an important role in tumor progression; there are many evidences of the positive correlation between uPAR levels and patient poor prognosis and overall survival [18]. With the aim to verify the clinical relevance of uPAR as a target, we firstly analyzed its gene and protein expression on a panel of bladder and breast cancer cell lines different in staging, grading and invasiveness (Fig. 1). Heterogeneous levels of this receptor were found in all the analyzed cell types: as regards for bladder cancer, a no or poor expression was detected in stage I superficial (RT4) and stage III muscle invasive cells (HT1376, ECV304), while a modest to evident overexpression was found in stage II bladder cancer cell lines RT112 and 5637. On the other hand, among the TNBC cells analyzed, 3 out of 4 (MDA-MB-468, BT549 and SUM149) were highly uPAR positive, in contrast with $HER2^{+}$ SKBR3 breast cancer cell lines.

a.

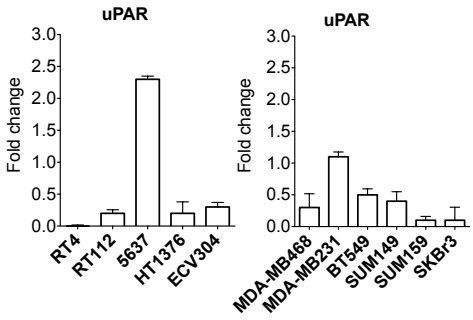

b.

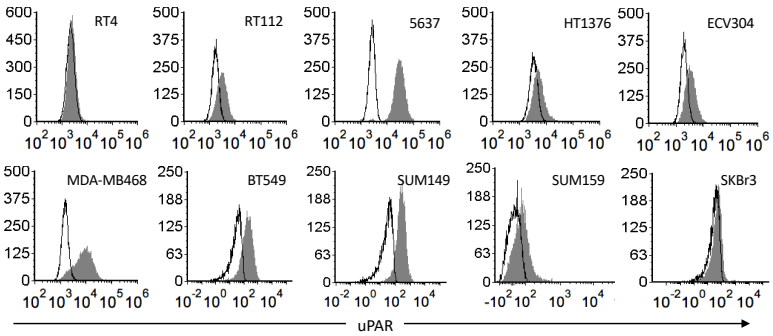

c.

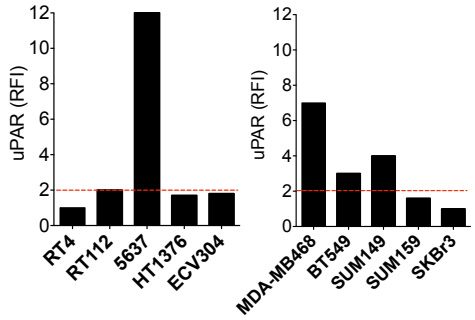

Fig. 1 uPAR espression in bladder and breast cancer cell lines. Bladder and breast cancer cell lines resembling respectively different stages (RT4 -T1 superficial-, RT112 and 5637- T2 muscle invasive-, HT1376 and ECV304 -T3 muscle invasive-) and subtypes (MDA-MB-468, BT549, SUM149, SUM159 -TNBC-, SKBR3 -HER2^{+}-) were analyzed by quantitative PCR (see "Materials and Methods") for uPAR gene expression (a) and by flow cytometry for uPAR protein expression (b and c). uPAR protein expression is shown as histogram plots (b) and Relative Fluorescence Intensity (RFI) (see "Materials and Methods") (c). SKBR3 HER2+ breast cancer cell line was used as subtype control. The dashed line represents the threshold arbitrarily defining positive expression (RFI=2).

3.2 ATF-SAP chimera

After verifying the presence of uPAR on cancer cell lines *in vitro*, we took advantage of a uPAR-directed ATF-SAP chimera as a prototype of a tumor targeting toxin [30, 31]. This fusion protein is composed by SAP fused to the amino-terminal fragment (ATF) of human urokinase-type plasminogen activator (uPA), the natural ligand of uPAR. The insertion of a targeting moiety at the N-terminal of the toxin allows its delivery specifically to uPAR expressing cells, thus limiting potential off-target effects. ATF-SAP coding sequence was cloned into a pPICZ vector for yeast expression and its production and purification was optimized in the methylotrophic yeast *Pichia pastoris* and scaled up in bioreactors [31]. The yeast system was demonstrated to be a suitable platform for the expression of recombinant proteins according to Lombardi et al. [77], allowing protein post-translation modifications, production and secretion of toxic SAP chimera. A catalytically inactive mutant (ATF-SAP KQ) was produced as a control [31].

3.2.1 ATF selectively delivers SAP toxin to uPAR overexpressing bladder and triple negative breast cancer cells

In order to characterize the *in vitro* biological activity of the uPAR targeting chimera, uPAR+ and uPAR- bladder and breast cancer cell lines were incubated with scalar logarithmic concentrations of the toxin (Fig. 2). As expected, ATF-SAP WT efficiency in killing cells was proportional to uPAR levels, impairing cell viability in a dose-dependent manner and in a higher significant extent compared to seed SAP, the untargeted control. In addition, cell death was unambiguously due to the presence of SAP enzymatic activity, as its catalytically inactive mutant ATF-SAP KQ failed to exert any effect. Accordingly, it is worth of noticing that ATF-SAP WT was not able to kill cells expressing low or undetectable uPAR levels (stage I and III bladder cancer and $HER2^+$ breast cancer cell lines), meaning that a higher concentration of chimera is needed to reach an IC_{50}, which results in a loss of receptor specificity.

a.

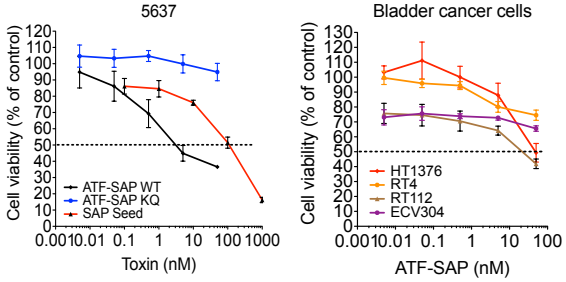

Table 2. ATF-SAP chimeras and SAP activity on bladder cancer cells

		Toxins cytotoxic activity (IC50[a)] in nM):		
Cell line	n[b)]	ATF-SAP WT	ATF-SAP KQ	SAP Seed
5637	3	3.5±2	>1000	100±35
RT4	3	>1000	>1000	150±35
RT112	3	14.5±8	>1000	1000±0
HT1376	3	47.5±3	>1000	150±0
ECV	**3**	>1000	>1000	>1000

[a)] IC50, the half maximal inhibitory concentration (mean±SE); [b)] n, number of independent experiments (each in triplicate).

b.

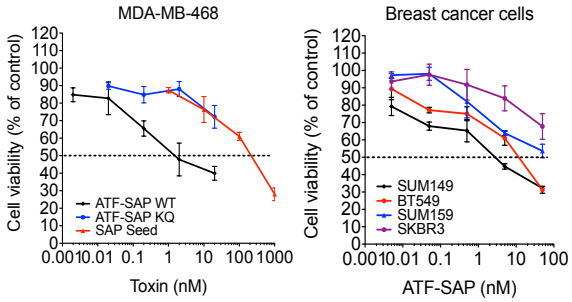

Table 3. ATF-SAP chimeras and SAP activity on breast cancer cells

		Toxins cytotoxic activity (IC50[a)] in nM):		
Cell line	n[b)]	ATF-SAP WT	ATF-SAP KQ	SAP Seed
MDA-MB 468	3	3.2±3	>1000	170±39
BT549	3	13±6	>1000	70±14
SUM149	3	12±11	>1000	125±106
SUM159	3	>1000	>1000	>1000
SKBR3	3	>1000	>1000	825±247

[a)] IC50, the half maximal inhibitory concentration (mean±SE); [b)] n, number of independent experiments (each in triplicate).

Fig. 2 Cytotoxic activity of ATF-SAP on bladder and breast cancer cells. ATF-SAP activity and target specificity were evaluated on RT4, RT112, 5637, HT1376 and ECV304 bladder cancer cell lines (a) and on MDA-MB-468, SUM149, SUM159, BT549 TNBC and HER2+ SKBR3 breast cancer cell lines (b). Cells were incubated for 72h with scalar logarithmic concentrations of the toxin and cell viability was analyzed by MTT assay. The untargeted seed SAP and the catalytically inactive mutant ATF-SAP KQ were used as controls. The IC_{50} from three different experiments is reported as mean ± SE (Table 2 and 3).

On the basis of these results, we can conclude that stage II muscle invasive bladder cancer and TNBC represent good models to test ATF-SAP biological activity; furthermore, ATF targeting domain is absolutely required to increase the toxin selectivity on uPAR+ cells in *in vitro* assays.

3.2.2 ATF-SAP internalization route is cell specific

Next, we investigated the potential off-tumor toxicity of ATF-SAP by exploiting a non-tumoral cell line, such as healthy human skin derived fibroblasts. Due to their implication in physiological wound healing processes, fibroblasts are expected to express uPAR on their surface. In fact, as shown in Fig. 3a, high levels of uPAR were detected on these cells. Therefore, we wondered whether they were also sensitive to the activity of ATF-SAP. Notably, fibroblasts viability resulted unaffected by the toxin (Fig. 3c). To further corroborate their lack of sensitivity to the chimera and to validate bladder cancer as a candidate target for the proposed therapy, we extracted primary bladder-derived fibroblasts from a human bladder biopsy and, after immune-fluorescence characterization for typical fibroblasts markers, analyzed them for uPAR expression (Fig. 3a, b). Similarly to skin fibroblasts, even if a high uPAR positivity could be detected, bladder fibroblasts were spared by ATF-SAP, that resulted completely ineffective (Fig. 3c).
This unexpected behavior was also noticed on MDA-MB 231 breast cancer cell line, which, in spite of displaying a high uPAR expression, were not sensitive to the activity of ATF-SAP (Fig. 3a, c). These data suggest that in some cases uPAR expression is not the sufficient condition to mediate ATF-SAP toxicity.

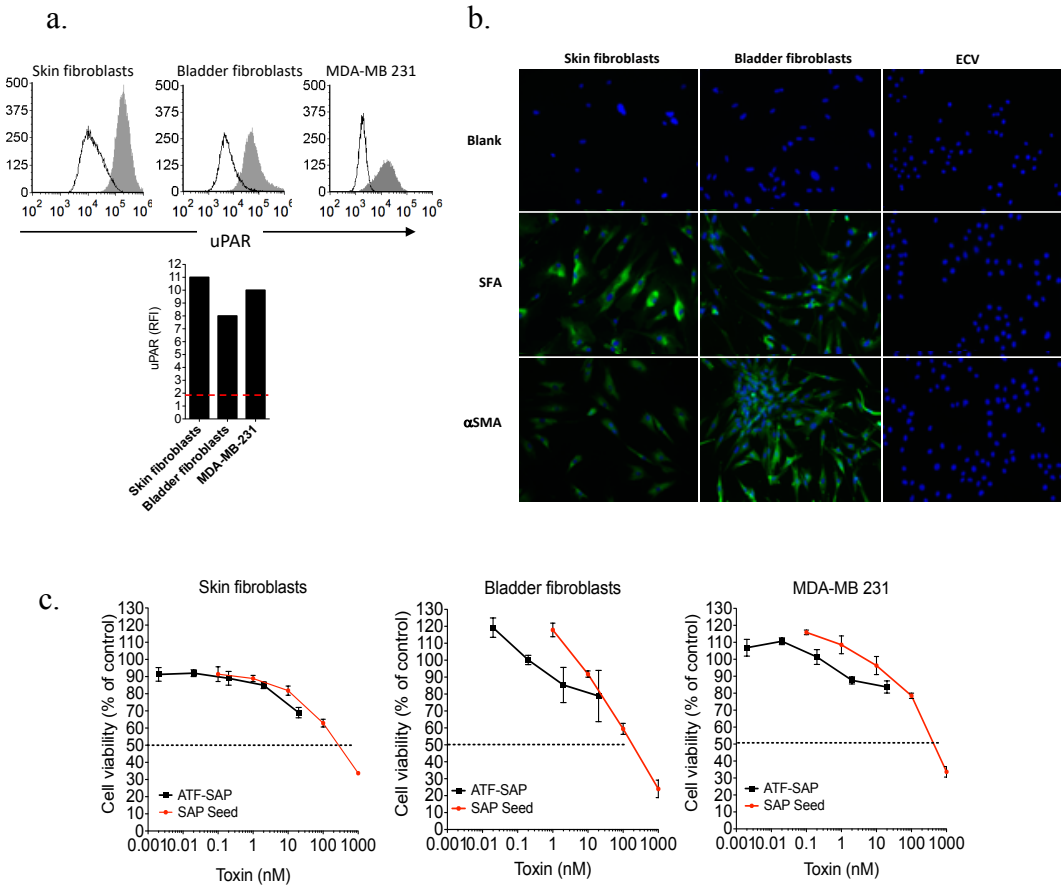

Fig. 3 ATF-SAP activity on fibroblasts and MDA-MB-231 cancer cell line. (a) uPAR expression on skin and bladder-derived fibroblasts as well as breast cancer MDA-MB-231 cell line was analyzed by flow cytometry and expressed as histogram plots (upper panel) and Relative Fluorescence Intensity (RFI) (see "Materials and Methods") (lower panel). The dashed line represents the threshold arbitrarily defining positive expression (RFI=2). b. Molecular profile of skin and bladder-derived fibroblasts. Human skin- and bladder-derived primary fibroblasts were analyzed by immunofluorescence for the expression of Fibroblasts Surface Antigen (SFA) and alpha Smooth Muscle Actin (αSMA). ECV304 epithelial bladder cancer cell line was used as negative control. Nuclei were stained with DAPI (blue). (c) ATF-SAP toxic activity was evaluated after 72 h incubation and compared to the untargeted seed SAP. Results from one representative experiment are shown as mean ± SD. Three independent experiments were performed for each assay.

3.2.3 ATF-SAP internalization does not rely on uPAR natural ligands nor on uPAR cofactor LRP1

Hence, we sought to determine if some other factor implicated in the urokinase plasminogen activation system is also involved in toxin internalization. To this purpose, we analyzed by Real-Time PCR the mRNA levels of LRP-1 (low density lipoprotein receptor related protein 1), known to be important not only in uPAR endocytosis and turnover on cell surface but also for SAP receptor mediated

internalization [51, 52, 55, 77]. Unexpectedly, we could observe LRP1 to be highly expressed by fibroblasts, but not by MDA-MB-231 cells (Fig. 4a). Analogously, we found ATF-SAP sensitive cells to have very low or undetectable LRP1 levels. In order to exclude any post transcriptional regulation of the above-mentioned transcript, we also confirmed this result by measuring LRP1 at a protein level by flow cytometry analysis (Fig. 4b). Such observation suggests that LRP1 seems not to be an essential cofactor for ATF-SAP-bound uPAR internalization.

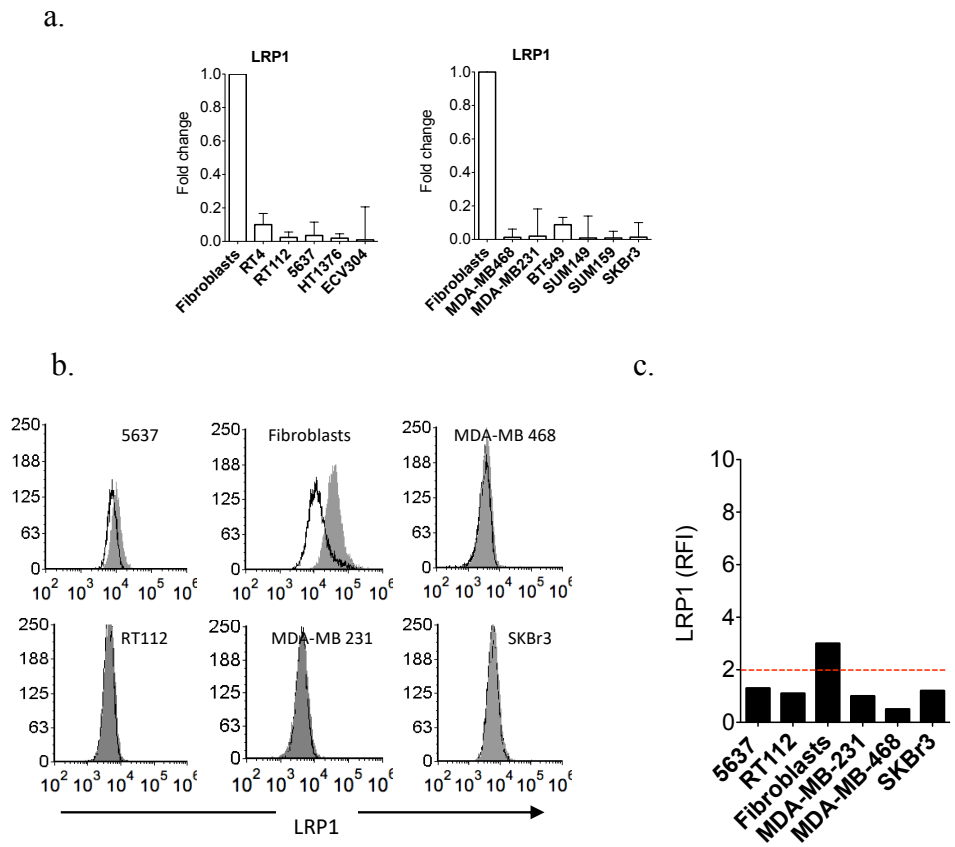

Fig. 4 LRP1 expression in bladder and breast cancer cell lines. Skin fibroblasts, bladder and breast cancer cell lines respectively resembling different stages (RT4 -T1 superficial-, RT112 and 5637- T2 muscle invasive-, HT1376 and ECV304 -T3 muscle invasive-) and subtypes (MDA-MB-468, MDA-MB-231, BT549, SUM149, SUM159 -TNBC-, SKBR3 -HER2^{+}-) were analyzed by qPCR (see "Materials and Methods") for LRP1 gene expression (a) and flow cytometry for LRP1 protein expression (b). LRP1 protein expression is expressed as histogram plots (b, left panel) and RFI (see "Materials and Methods") (b, right panel). The dashed line represents the threshold arbitrarily defining positive expression (RFI = 2).

Then, we investigated if the uPA amount produced by the same cell types is able to sequester its receptor from the ATF-SAP recognition and binding. To achieve this goal, we firstly analyzed its mRNA levels (Fig. 5a), but no differential uPA expression between ATF-SAP responding and not responding cells could be

detected. Moreover, to deeper clarify whether high levels of uPA would compete with ATF-SAP for receptor binding and reduce the toxin uptake, we assessed the ability of ATF-SAP to be internalized in the presence of increasing concentrations of uPA and uPA inhibitor plasminogen activator inhibitor (PAI-1). The latter has been demonstrated to covalently bind and inhibit the proteolytic activity of uPAR-bound uPA, promoting LRP1 association and internalization of the complex [52]. As shown in Fig. 5b, ATF-SAP cytotoxicity remained unchanged, meaning that there is no competition with uPA for receptor binding. Finally, as a proof of concept, aiming at demonstrating that ATF-SAP endocytosis relies on a peculiar uPA:PAI-1-LRP1-independent pathway, we used, for internalization comparison, a SAP-based compound in which SAP is chemically conjugated to the entire pro-uPA ligand (pro-uPA-SAP) [55]. In this setting, both fibroblasts and MDA-MB-231 were efficiently killed by the conjugation product, indicating that uPAR can be efficiently bound and internalized in cells refractory to ATF-SAP (Fig. 5c).

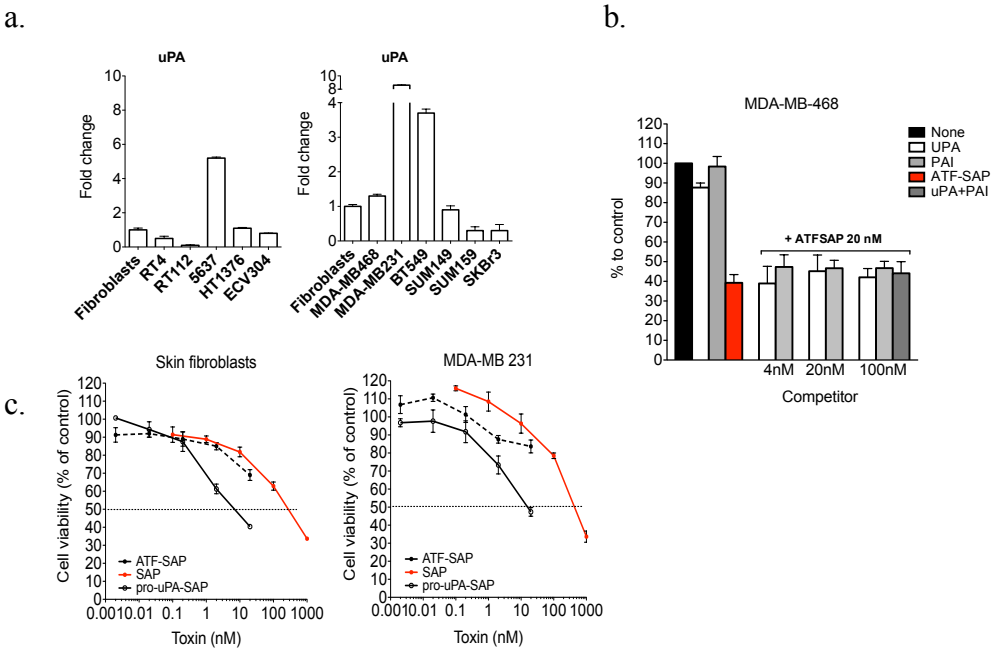

Fig. 5 uPA expression in bladder and breast cancer cell lines. (a) uPA gene expression (see "Materials and Methods") was analyzed in skin fibroblasts, bladder and breast cancer cell lines respectively resembling different stages (RT4 -T1 superficial -, RT112 and 5637 - T2 muscle invasive-, HT1376 and ECV304 - T3 muscle invasive-) and subtypes (MDA-MB-468, MDA-MB-231, BT549, SUM149, SUM159 -TNBC-, SKBR3 -HER2^{+}-). (b) MDA-MB-468 cells were incubated with ATF-SAP 20 nM in the presence of equal or increasing concentrations of uPA or PAI. (c) Comparison of pro-uPA-SAP and ATF-SAP toxic activity on fibroblasts and MDA-MB-231 cells. The effect on cell viability was evaluated after 72h by MTT assay. Seed SAP was used as untargeted control. Results from one representative experiment are shown as mean ± SD. Three independent experiments were performed for each assay.

3.2.4 Evaluation of uPAR expression stability and ATF-SAP activity on stage II bladder cancer cells after implantation in mice

Since tumor propagation via prolonged cell culture generally may promote loss of surface antigens, we investigated if uPAR expression is stably maintained even with multiple serial tumor implantations in mice, in order to predict ATF-SAP efficiency in an *in vivo* environment. To this aim, stage II bladder cancer cells were subcutaneously injected and grown in the flank of NSG mice for two times and, once explanted, analyzed for uPAR expression and ATF-SAP sensitivity. As shown in Fig. 6, a minimal downregulation of receptor was observed and ATF-SAP dose-dependent biological activity was in line with previous results, further supporting the use of stage II bladder cancer cell lines as suitable *in vivo* models to test the chimera pharmacological efficacy.

a.

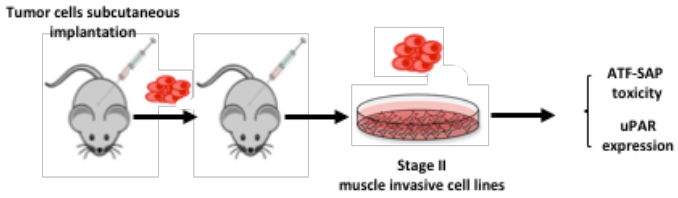

b.

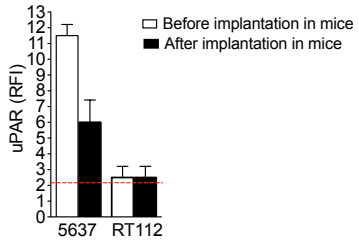

c.

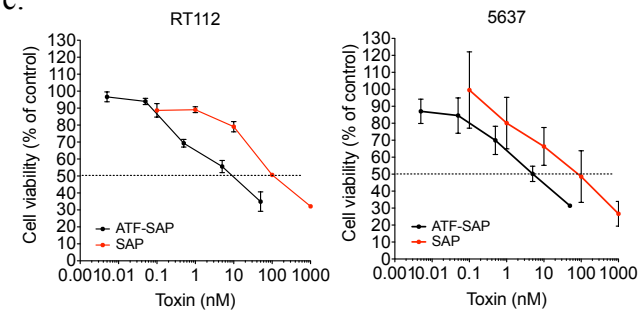

Fig. 6 Cytotoxic activity of ATF-SAP on *ex vivo* bladder cancer cells. (a) Schematic representation of the experimental design. RT112 and 5637 cells were subcutaneously injected in 7-week-old NSG immunocompromised mice serially for two times. (b) After the second implantation, established tumors were minced and tumor cells analyzed for uPAR expression by flow cytometry. Results are shown as RFI (see "Materials and Methods") (left panel). The dashed line represents the threshold arbitrarily defining positive expression (RFI=2). (c) Explanted cells were then incubated for 72h with ATF-SAP and cell viability was evaluated by MTT assay (right panels). Seed SAP was used as untargeted control. Results from one representative experiment are shown as mean ± SD. Three independent experiments were performed.

3.2.5 Development of an αv-integrins targeting SAP- based recombinant protein: RGD-SAP

With the purpose to develop a toxin based-system able to target both cancer cells with epithelial origin and tumor microenvironment, we designed and produced in parallel a recombinant protein in which the effector SAP is fused to the ACDCRGDCFCG peptide, containing an Arginine-glycine-aspartic (RGD) motif. Such peptide can recognize with a certain affinity integrins expressed both on tumor cells and tumor neovasculature, therefore our aim is to extend the application of this targeting strategy to most solid tumors. Owing to the significantly smaller size of the ACDCRGDCFCG peptide compared to ATF, we chose the *E. Coli* bacteria system for RGD-SAP production. As for ATF-SAP, we used recombinant DNA technology to prepare the recombinant product, cloning the sequence into a pET22a plasmid for *E. coli* expression. A non-targeting SAP (CYS-SAP) variant carrying an N-terminal CGGSGG peptide was designed and produced in parallel. Both proteins carry a C-terminal histidine tag, which was exploited to enhance both affinity chromatography purification and endosomal escape of the toxin into recipient cells (Fig. 7).

a.

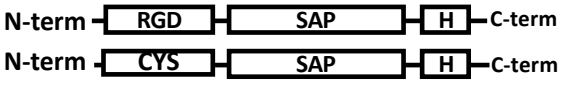

b.

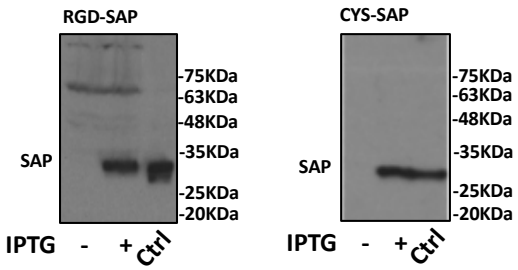

Fig. 7 Designing and optimization of recombinant proteins expression in *E. Coli*. (a) Schematic representation of RGD-SAP and CYS-SAP recombinant proteins. The RGD (ACDCRGDCFCG) targeting and CYS (CGGSGG) -containing non-targeting peptides were inserted at the N-terminus of SAP. A histidine (H)-tag was inserted at the C-terminus to aid in the purification of the recombinant proteins. (b) Proteins production was monitored by western blot with anti-SAP antibody upon IPTG (+) induction of *E. Coli* bacteria; not induced bacteria (-) were used as negative control. SAP protein was used as positive control (Ctrl).

After the optimization of induction, temperature, time and IPTG concentration for the production of the SAP-based proteins, affinity, ion exchange chromatographic steps and dialysis were performed in order to obtain pure products (Fig. 8, 9, 10). As shown by western blot analysis, a single band of 30 kDa could be detected when RGD-SAP was run under both reducing and non-reducing conditions, as expected for monomers, excluding the formation of inter-chain disulfide bonds, owing to the ACDCRGDCFCG domain, and suggesting that this construct does not undergo degradation. In contrast, a double sized product could be detected for CYS-SAP, indicating that inter-chain disulfide bonds are likely formed between the N-terminal cysteines of this recombinant protein (Fig. 10). The final yield of the products was 300 µg per liter of bacterial culture.

a.

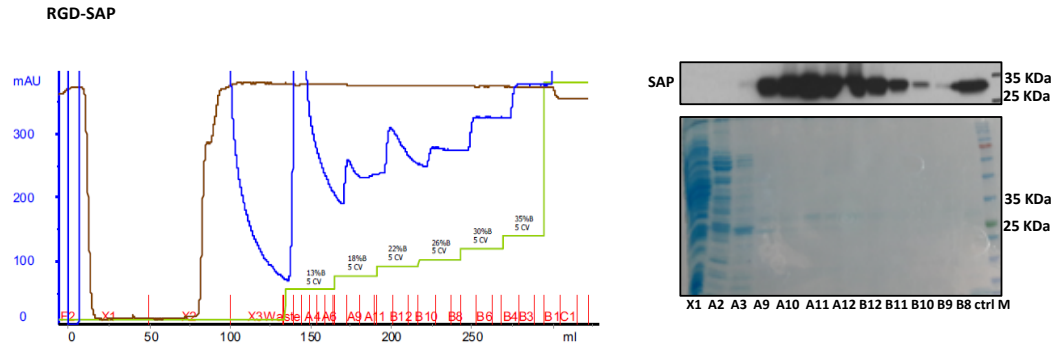

b.

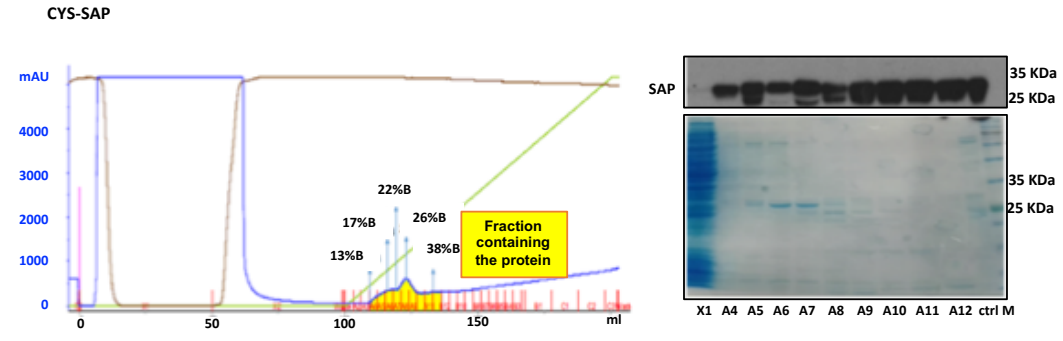

Fig. 8 SAP-recombinant proteins purification by affinity chromatography. RGD-SAP (a) and CYS-SAP (b) recombinant proteins were purified by affinity chromatography using a Ni-NTA resin for His-tagged proteins (left). The green line indicates the increasing levels of imidazole; the blue line indicates the absorbance at 280 nm, which correlates with the presence of proteins. Fraction corresponding to the main elution peak were analyzed by western blot with anti-SAP antibody (upper right) and Coomassie blue staining (lower right) for protein detection and purity determination.

a.

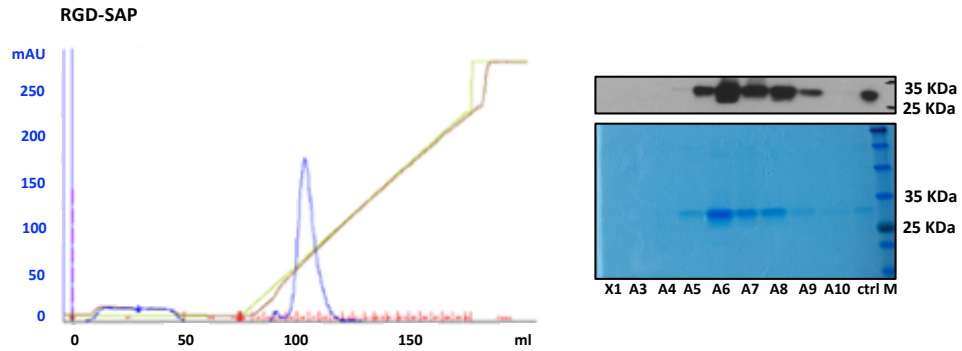

b.

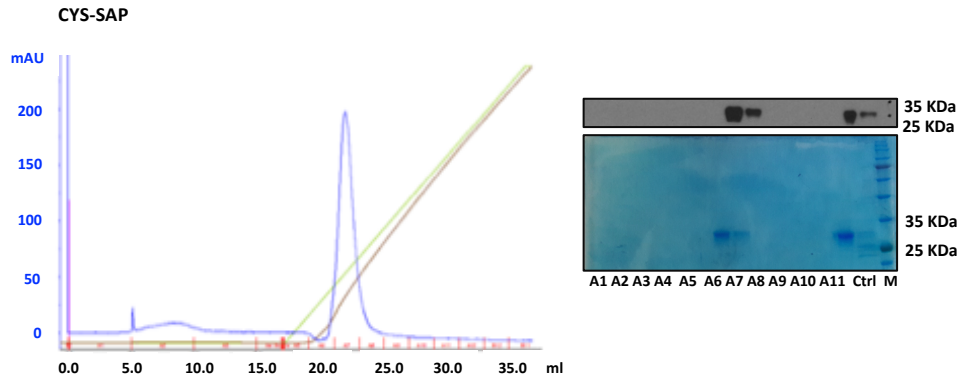

Fig. 9 SAP-based recombinant proteins purification. RGD-SAP (a) and CYS-SAP (b) recombinant proteins derived from positive fractions obtained from affinity chromatography were pooled and further purified by ion exchange chromatography using a Hiprep sp XL column (left). The green line indicates the increasing levels of NaCl; the blue line indicates the absorbance at 280 nm, which correlates with the presence of proteins; The fractions corresponding to the main elution peak were analyzed by western blot with anti-SAP antibody (upper right) and Coomassie blue staining (lower right) for protein detection and purity determination.

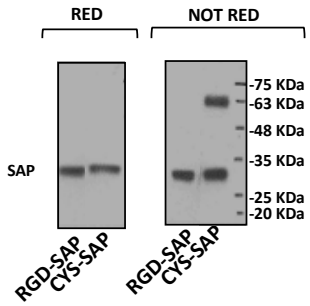

Fig. 10 Sap based recombinant proteins final products after purification steps. Positive fractions from ion exchange chromatography were pooled and dialyzed; products isolation was analyzed by western blot using anti-SAP antibody. SDS-PAGE was performed under reducing (RED, left) and non-reducing (NOT RED, right) conditions in order to evaluate the presence of polymers.

3.2.6 RGD specifically deliver SAP toxin to αv–integrins expressing cells

RGD motif has been demonstrated to specifically recognize and bind αv-integrins (αvβ3, αvβ5 and αvβ6) with different affinities [25]. Besides being overexpressed on the surface of endothelial cells, these integrins are also highly present on a variety of tumor cells [12, 26, 27, 28]. Therefore, with the purpose to identify the best model to validate *in vitro* the targeting efficiency of RGD-SAP, we analyzed different cancer cell lines for αvβ3 and αvβ6 integrins expression by flow cytometry. We detected high αvβ3 levels only on U87 glioblastoma cell lines. In contrast, RT4, RT112 and 5637 bladder and MDA-MB-468 breast cancer cells showed a slight positivity for αvβ6. Remarkably, healthy fibroblasts do not express any of the two integrins of interest (Fig. 11a). Next, to both determine whether RGD-SAP preferentially binds to one particular integrin and to prove its *in vitro* activity, cells were incubated for 72 h with scalar logarithmic concentrations of RGD-SAP or CYS-SAP and the effect on cells viability was evaluated by MTT assay. RGD-SAP activity was proportional to αv-integrins expression levels, in contrast with CYS-SAP, which was around 5-20 folds less active (Fig. 11b). Interestingly, as already demonstrated by Curnis et al. [26], we observed an increase of cytotoxic activity on αvβ3+ cells compared to αvβ6+ cells, meaning that the RGD motif is more specific and preferentially binds the mentioned integrin. As for ATF-SAP, we used fibroblasts as healthy control in order to evaluate any possible off-target effects of the recombinant protein. Strikingly, the effect of RGD-SAP on fibroblasts cell viability was significantly lower and negligible compared to cancer cells, suggesting that a very low concentration treatment could be very specific against cancer and prevent possible off-target effects of the SAP-based protein (Fig. 11b).

a.

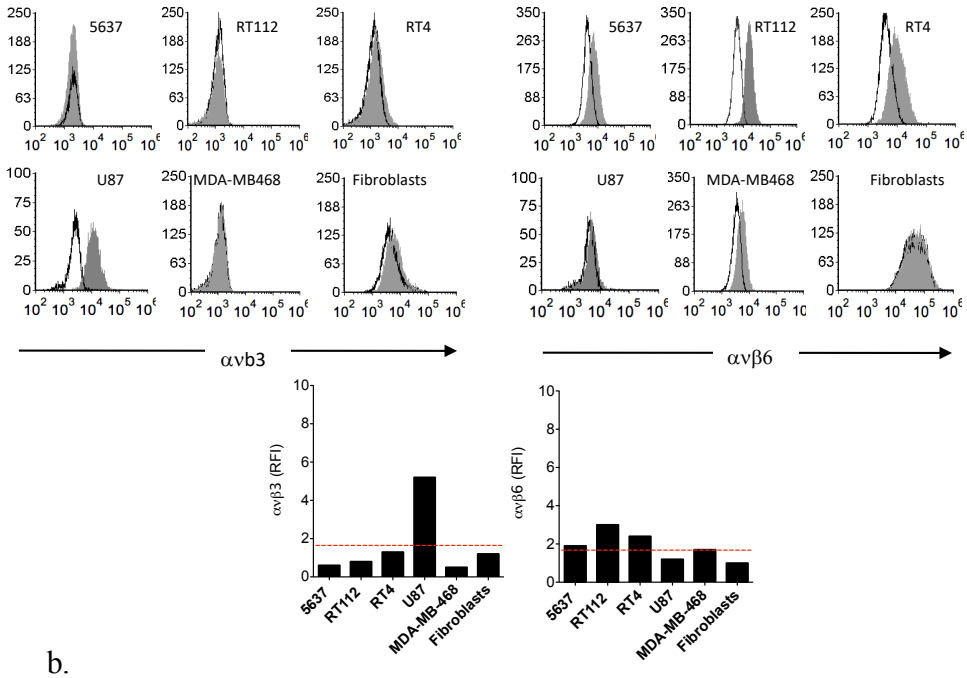

b.

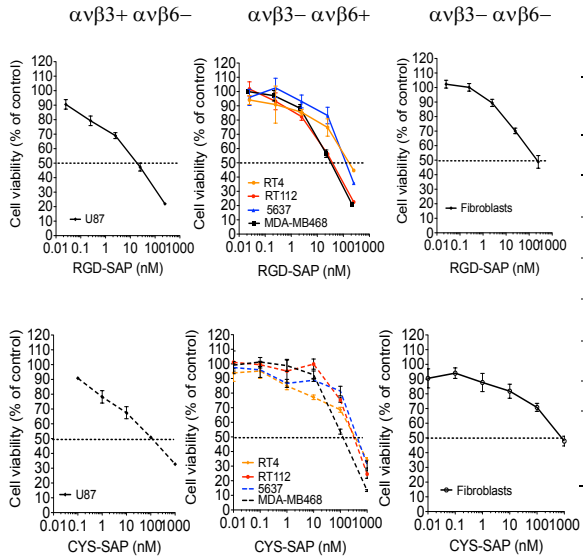

Table 4. SAP-based recombinant proteins *in vitro* activity on cancer cells

		Toxins cytotoxic activity (IC50[a] in nM):	
Cell line	n[b]	RGD-SAP	CYS-SAP
U87	3	22,6±6,4	100±54,4
RT4	3	170±0	750±70,7
RT112	3	66,6±19,2	500±70,7
5637	3	120±52	450±14,2
MDA-MB 468	3	32,5±8,6	187,5±25
Fibroblasts [c]	3	>1000	500

[a] IC50, the half maximal inhibitory concentration (mean±SE); [b] n, number of independent experiments (each in triplicate); [c] Fibroblasts are used as healthy control.

Fig. 11 Integrins expression on cancer cell lines and biological activity evaluation of SAP-based recombinant proteins. (a) 5637, RT112, RT4, U87, MDA-MB-468- epithelial cancer cell lines and fibroblasts were analyzed by flow cytometry for avb3 and avb6 integrins expression. Results are shown as histograms (upper left) or RFI (see "Materials and Methods") (upper right) of a representative experiment. (b) The cytotoxic activity was calculated as cell viability after 72 h incubation with increasing concentrations of the toxins by MTT assay. CYS-SAP was used as untargeted control. The IC_{50} from three different experiments is reported as mean ± SD (c).

To determine if the improved delivery of RGD-SAP compared to CYS-SAP relies on a targeting mechanism, we explored if it could be partially hampered by a competition with the RGD peptide. To this end, cells were treated with RGD-SAP or CYS-SAP in the presence or not of a molar excess of RGD. Noteworthy, the activity of RGD-SAP significantly decreased in the presence of RGD, in a time dependent manner; on the contrary, CYS-SAP activity resulted totally unaffected, suggesting that the RGD moiety is well exposed and the presence of SAP does not sterically interfere with its binding ability and receptor interaction (Fig. 12a).

It is well known that SAP toxin induces cell apoptosis. For corroborating evidence, we investigated the activation of programmed cell death by analyzing the cleavage of caspase 3 in cells treated with RGD-SAP. To this aim, 5637 and MDA-MB-468 epithelial cells, were incubated with RGD-SAP to perform a time-course analysis. DTT, a known apoptosis inducer, was used as a positive control. Cells were lysed and analyzed by western blot after 48 and 72 h. As shown in Fig. 12b, sudden and massive caspase 3 activation was detectable in all samples treated with the toxin. Altogether, these results indicate that fusing the RGD moiety to SAP enhances the delivery of the toxin, proportionally to αv-integrins upregulation by cells. In addition, the cytotoxic activity on cells relies on the uptake and cytosolic release of the toxin, which is able to induce cell apoptosis.

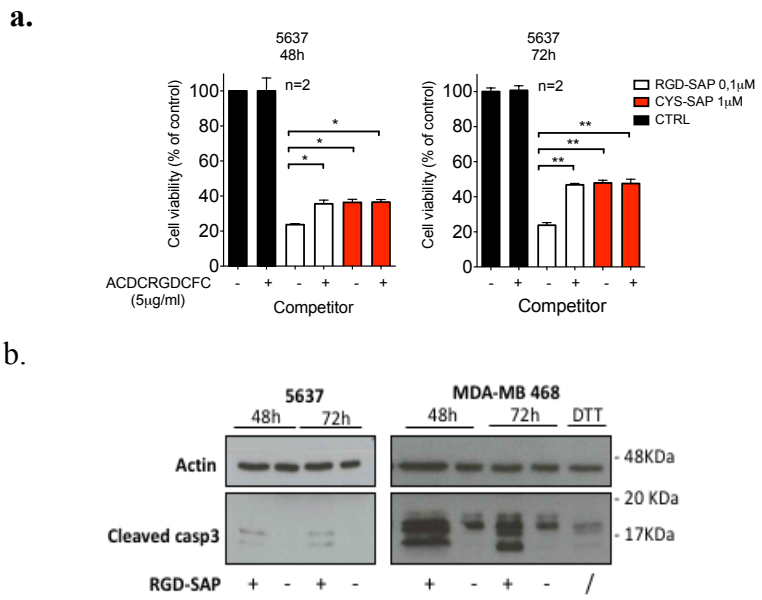

Fig. 12 RGD-SAP target specificity and apoptosis induction. (a) 5637 bladder cancer cells were incubated with RGD-SAP in the presence or absence of a molar excess of RGD peptide. The cell viability was evaluated after 48 and 72 h by MTT assay. CYS-SAP was used as untargeted control. (b) The activation of the apoptosis pathway upon RGD-SAP treatment was evaluated in 5637 and MDA-MB-468 cells by analyzing the intracellular levels of cleaved caspase 3. Cells were incubated with RGD-SAP for 48 and 72h and cell lysates were analyzed by western blot with antibodies against cleaved caspase 3 and beta-actin for protein normalization.

3.2.7 RGD-SAP has *in vivo* potent antitumor activity on a subcutaneous model of syngeneic bladder cancer

To evaluate the *in vivo* efficacy of the two SAP-based recombinant proteins developed, we firstly established a subcutaneous bladder cancer model C57BL/6 female wild type mice, by injecting superficial MB49 urothelial mouse carcinoma cells in the left flank of the animals. This cell line is sensitive to RGD-SAP, as demonstrated in an *in vitro* assay (Fig. 13a). In the first preliminary experiment, five days tumor-bearing mice were treated systemically via tail vein injection with a starting 1 mg/Kg dose of RGD-SAP or CYS-SAP toxins and monitored over time for the progression of disease. The administration was repeated every five days for three times, as shown in the depicted schedule (Fig. 13b). Despite an initial increase of tumor dimensions in all conditions, owing to the high proliferation rate of MB49 cells, treatment with RGD-SAP was able to delay tumor growth soon after the second administration, leading to the complete eradication (n=1) or to a significant reduction of the tumor mass (n=3) (Fig. 13c, d). However, this dosage of RGD-SAP

caused modest weight loss after the last administration and a severe necrotic effect on mice tails (Fig. 13e). CYS-SAP activity on tumor growth was completely null and superimposable with PBS-treated mice, meaning that the therapeutic activity of RGD-SAP was due to the presence of RGD.

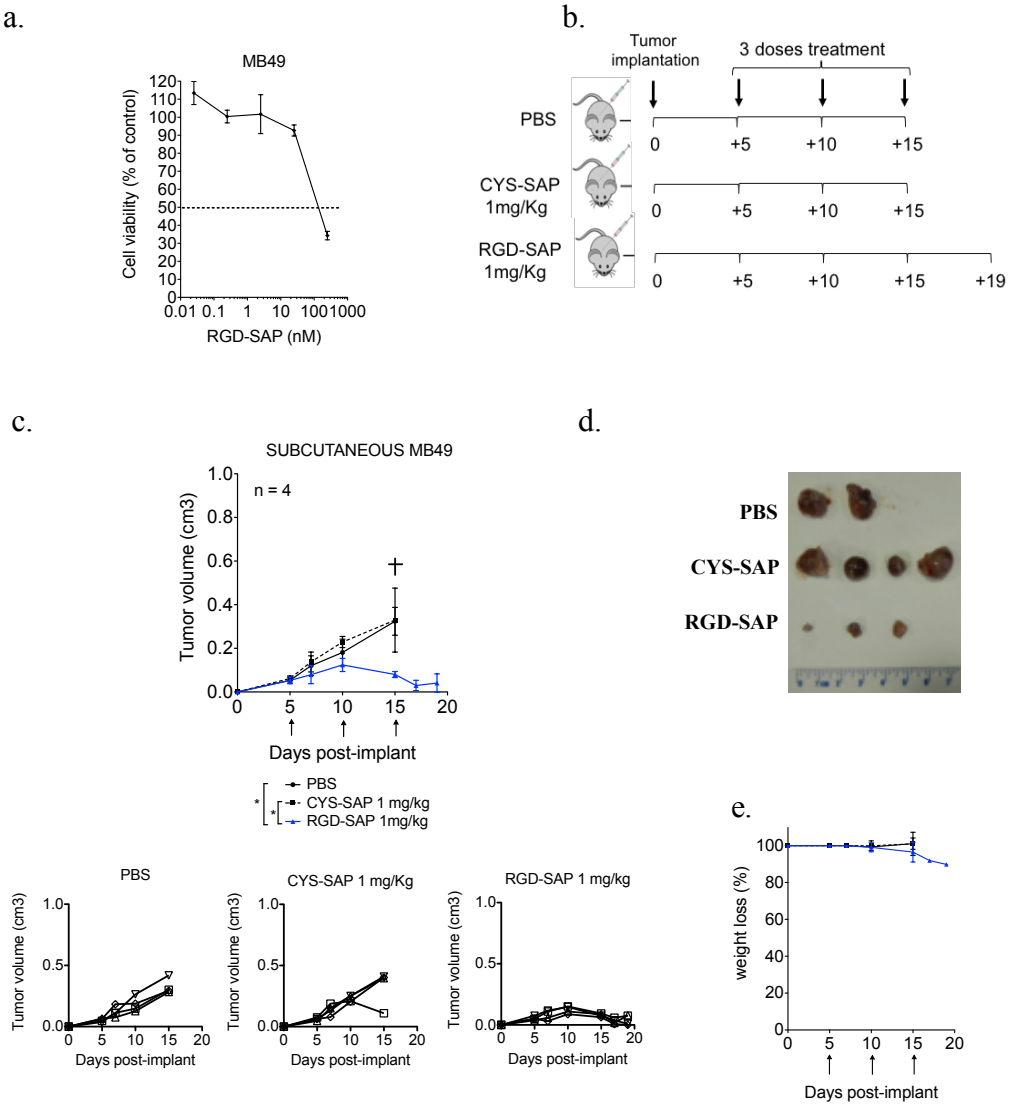

Fig. 13 Effects of RGD-SAP and CYS-SAP on tumor growth in a subcutaneous syngeneic bladder cancer mouse model. (a) RGD-SAP *in vitro* biological activity on MB49 murine bladder cancer cell line. (b) Schematic representation of the experimental design *in vivo*. MB49 cells were subcutaneously implanted in 7-week-old C57 WT female mice. Tumor bearing mice were randomized into 3 experimental groups and treated respectively with PBS, CYS-SAP (1 mg/Kg) or RGD-SAP (1 mg/Kg) via intravenous injection every 5 days after tumor implantation for three times (c). Quantitative analysis of growing tumor volume in mice are shown as mean ± SD from n = 4 mice per condition and as single curves for each individual mouse. Statistical analysis was performed by using 1-way ANOVA (*$p < 0.05$). (d) The mean weight of mice from each treatment group is shown as percentage from initial. (e) Pictures of MB49 subcutaneous tumors explanted after mice sacrifice are shown.

Next, we wanted to define the *in vivo* minimum effective dose of RGD-SAP. To this end, we used three concentrations of RGD-SAP (0.75, 0.5, 0.25 mg/Kg) and maintained the same administration schedule as described above. Although the number of injected MB49 cells was reduced, in order to slow down the growing speed of the mass, tumor reached measurable dimensions in the same time point (5 days) in all the animals. Moreover, similarly to the previous preliminary experiment, a slight increase of the tumors dimensions was observed in all treatment conditions after the first two administration rates. Then, mice treated with 0.75 and 0.5 mg/Kg RGD-SAP underwent a significant delay of tumor growth compared to 0.25 mg/Kg mice, in which a sharp and exponential augment of tumor proliferation was detected, similarly to PBS-treated mice (Fig. 14a). In addition, 0.75 and 0.5 mg/Kg RGD-SAP treatments prolonged animal survival, with no evidence of weight loss, thus confirming the RGD-SAP dose dependent activity (Fig. 14b, c).

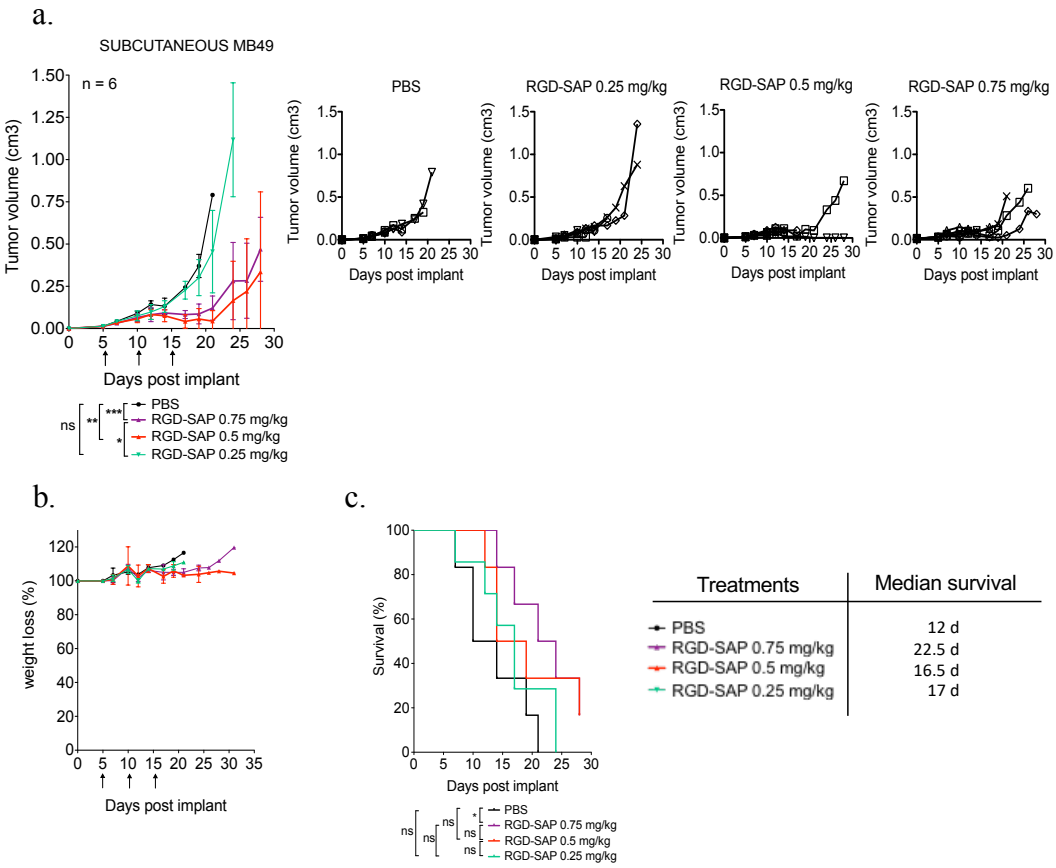

Fig. 14 Dose dependent effects of RGD-SAP on tumor growth in a subcutaneous syngeneic bladder cancer mouse model. (a) MB49 cells were subcutaneously implanted in 7-week-old C57 WT female mice. Tumor bearing mice were randomized into 4 experimental groups (n=6) and treated respectively with PBS or 3 different doses of RGD-SAP (0.75 mg/Kg, 0.5 mg/Kg or 0.25 mg/Kg) via intravenous injection every 5 days. Quantitative analysis of growing tumor volume in mice are shown as mean ± SD from n = 6 mice per condition and as single curves for each individual mouse. Statistical analysis was performed by using 1-way ANOVA (*p < 0.05; **p < 0.01; ***p < 0.001). (b) The mean weight of mice from each treatment group is shown as percentage from initial. (c) Kaplan–Meyer plot of animal survival with median survival time listed in the table. Results from a Mantel–Cox two-sided log-rank test are shown (*p < 0.05) for RGD-SAP 0.75 mg/kg (purple; hazard ratio, 5.2; 95 % CI, 1.2 – 23.1) versus PBS in mice bearing subcutaneous MB49 tumor. Ns: not significant.

Finally, to better understand the effects of the different RGD-SAP doses, we collected blood samples at the end of each experiment and analyzed biochemical parameters linked to liver and kidney toxicity (albumin, alanine transaminase (ALT), aspartate transaminase (AST), creatinine (CHE) and urea). As shown in Fig. 15 the RGD-SAP systemic toxicity is dose dependent: in fact, significant higher values of AST and CHE were measured in mice treated only with 1 mg/Kg RGD-

SAP. In contrast, no significant differences between all the other groups could be detected.

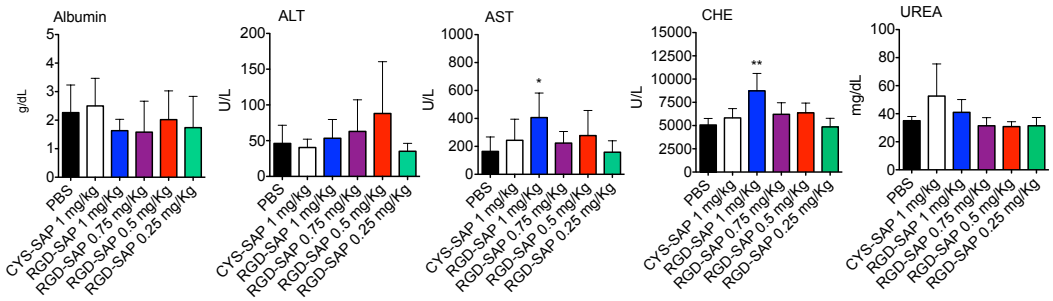

Fig. 15 Comparison of clinical biochemistry parameters in mice treated with different RGD-SAP concentrations. Blood samples were collected from retro-orbital plexus and the concentration of albumin, alanine transaminase (ALT), aspartate transaminase (AST), creatinine (CHE) and urea in the serum were measured. Values are shown as mean ± SD from $n \geq 4$ mice per condition. Results from unpaired Student t test are shown (*$p < 0.05$; **$p < 0.01$).

3.2.8 RGD-SAP pharmacological activity evaluation on an orthotopic mouse model of syngeneic bladder cancer

Thereafter, we sought to determine whether the same results were reproducible on an orthotopic model of urothelial carcinoma. To this aim, we generated Luciferase stably expressing MB49 cells (MB49 luc) and verified the *in vitro* sensitivity to RGD-SAP to be unchanged (data not shown). Thus, luciferase-expressing MB49 were instilled orthotopically into immunocompetent C57 WT mice and the tumor engraftment and progression monitored by *in vivo* bioluminescence imaging (IVIS) (Fig 16). We found successful bladder tumor implantation in all mice within 5-7 days after cells inoculation.

a.

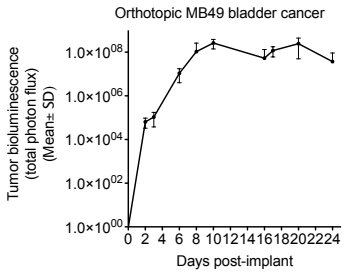

b.

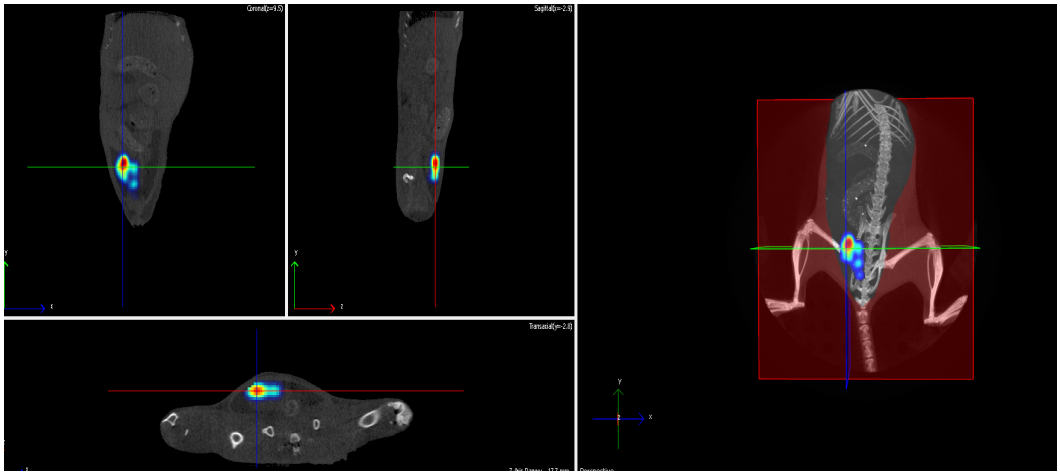

Fig 16 Orthotopic mouse model of a syngeneic bladder cancer. (a) Luciferase-expressing MB49 cells were transurethrally injected into the bladder of 7-week-old C57 WT female mice. Tumor engraftment was monitored via *in vivo* bioluminescence imaging (IVIS). Quantitative analysis of growing tumor volumes are shown as total photon flux (mean ± SD) from n = 4 mice. (b) Computed tomography (CT) images with the corresponding 3D bioluminescence of MB49 bladder tumor implanted in mice are shown**.**

Tumor vascularization was emphasized by bladder ultrasound analysis (Fig. 17).

a. b.

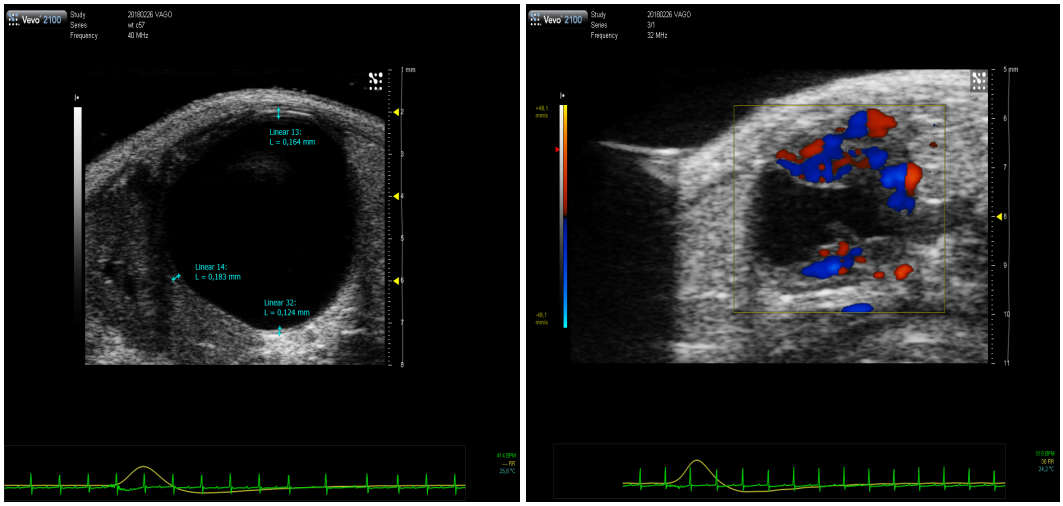

Fig. 17 Orthotopic MB49 bladder cancer vascularization. Representative ultrasound images of mouse bladder before and 15 days after MB49 tumor implantation. Original bladder thickness is measured and reported in the image relative to the healthy control (left). Tumor vascularization is shown as color Doppler mode (right).

Mice bearing orthotopic bladder cancer were then systemically treated via tail vein on days 7, 11 and 16 post-cancer implantation with PBS or RGD-SAP (0.25 and 0.5 mg/kg) (Fig. 18). No significant differences in both tumor growth and overall survival between treated groups and control mice could be distinguished (Fig. 18 b, d).

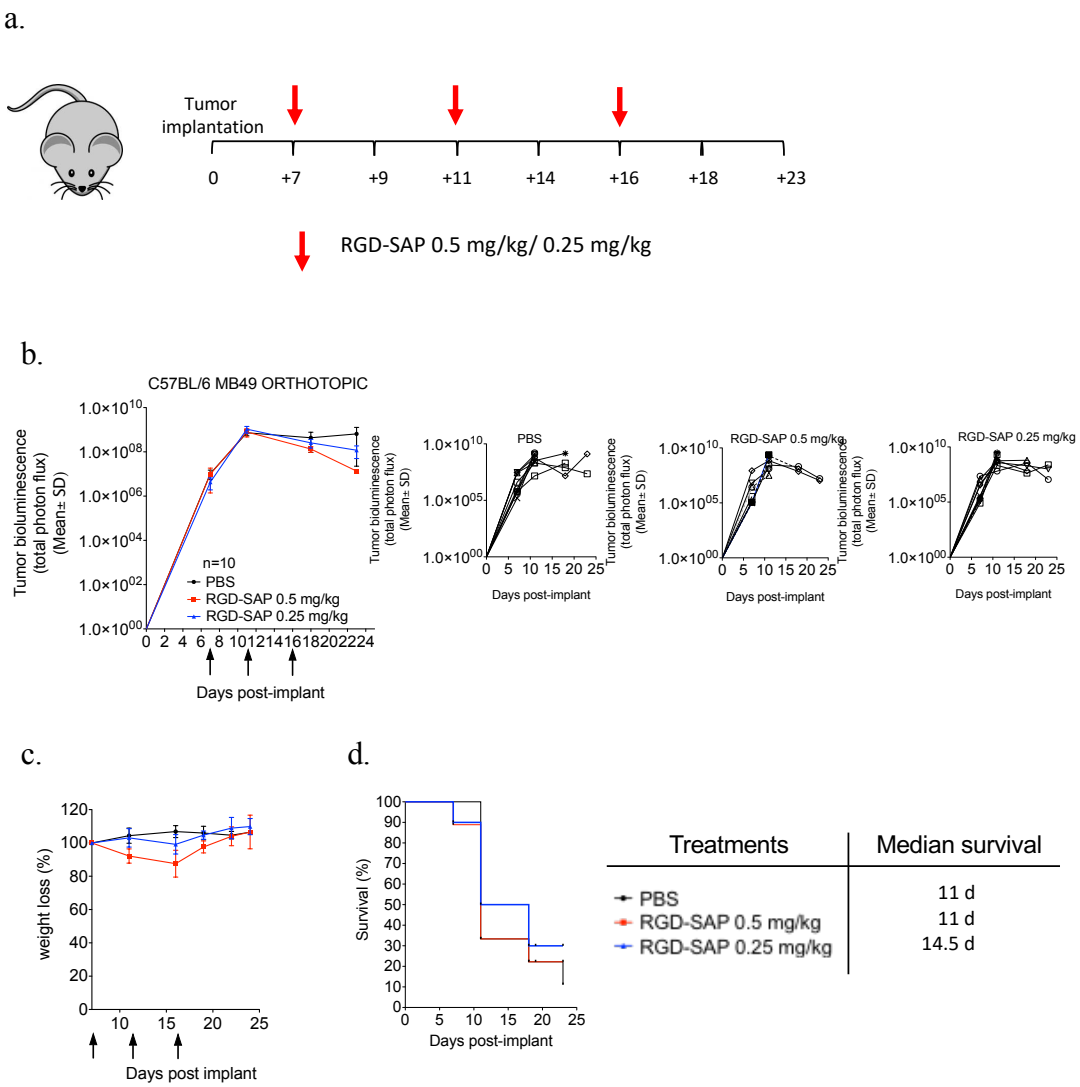

Fig. 18 Effects of RGD-SAP on tumor growth in an orthotopic syngeneic bladder cancer mouse model. (a) Schematic representation of experimental design. Luciferase-expressing MB49 cells were transurethrally injected into the bladder of 7-week-old C57 WT female mice. Tumor engraftment and growth was monitored via in vivo bioluminescence imaging (IVIS). Tumor bearing mice were randomized into 3 experimental groups and treated respectively with PBS, RGD-SAP (0.5 mg/kg) or RGD-SAP (0.25 mg/Kg). (b) Quantitative analysis of growing tumor volume in mice are shown as total photon flux (mean ± SD) from n = 10 mice per condition and from each individual mouse. (c) The mean weight of mice from each treatment group is shown as percentage from initial. (d) Kaplan–Meyer plot of animal survival with median survival time listed in the table.

In order to verify if the lack of response to RGD-SAP is attributable to a high growing rate of the cancer cells, which results into a sudden necrosis area formation and, as a consequence, into an inadequate drug delivery to the tumor, we decided to use Mitomycin (MMC) to control the speed of proliferation of the carcinoma

mass. Mitomycin (MMC) is one of the most used agents for the recurrence prevention of superficial bladder cancer, usually administered intravesically after transurethral resection of cancer lesions. In fact, this administration method, together with its moderate hydrophobicity, result in a less systemic absorption and limited side effects. We first demonstrated that MB49 bladder cancer cells were extremely sensitive to MMC (IC_{50} ~2 μg/ml) (Fig. 19a), then we used our xenograft mouse model to verify if the intravesical administration of MMC might reduce the growth speed of the superficial carcinoma mass and necrosis area formation, allowing the toxin to reach tumor cells and exert its specific toxic effect (Fig. 19). At the time of tumor detection (+7 days after cells infusion into the bladder) all cohorts of mice were treated with MMC through transurethral administration. A second dose of MMC was given after four days. In between, mice received a first systemic regimen of RGD-SAP (0.5 mg/kg) or vehicle (PBS), which was repeated for three times as illustrated in the depicted schedule (Fig. 19b). A slowdown of cancer progression was not revealed by *in vivo* imaging after the instillation of MMC; however, the combination with RGD-SAP seemed to moderately contain the exponential growth and maintain constant the luminescence signal over time (Fig. 19c). Even if no statistically significance compared to the other groups, a slight synergistic effect of RGD-SAP 0.5 mg/kg combined to MMC could also be appreciated on overall survival (Fig. 19e). Furthermore, the treatment resulted to be not toxic at all, as mice did not undergo a drop of body weight (Fig. 19d), nor evident signs of liver or renal toxicity could be detected by serum analysis of albumin, ALT and urea levels (Fig. 20).

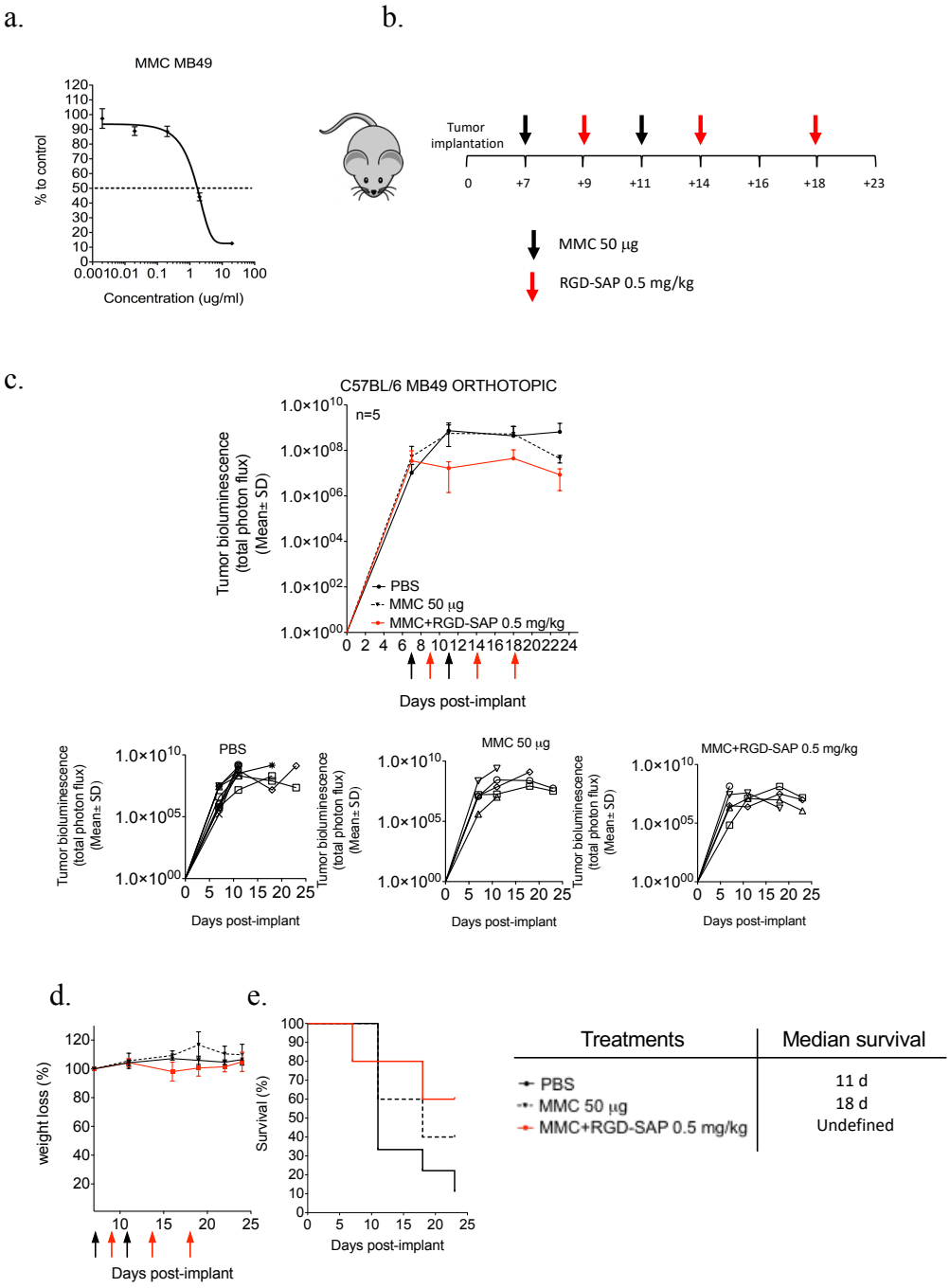

Fig. 19 Effects of MMC and RGD-SAP on tumor growth in an orthotopic syngeneic bladder cancer mouse model. (a) Mitomycin C (MMC) *in vitro* biological activity on MB49 murine bladder cancer cell line. (b) Schematic representation of the experimental design. Luciferase-expressing MB49 cells were transurethrally injected into the bladder of 7-week-old C57 WT female mice. Tumor engraftment was monitored via in vivo bioluminescence imaging (IVIS). Tumor bearing mice were randomized into 3 experimental groups and treated respectively with PBS, MMC (50 µg) or MMC (50 µg) +RGD-SAP (0.5 mg/Kg). (c) Quantitative analysis of growing tumor volume in mice is shown as total photon flux (mean ± SD) from n = 5 mice per condition and from each individual mouse. (d) The mean weight of mice from each treatment group is shown as percentage from initial. (e) Kaplan–Meyer plot of animal survival with median survival time listed in the table.

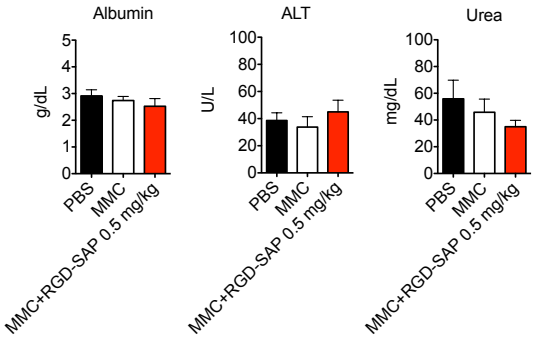

Fig 20. Comparison of clinical biochemistry parameters in mice treated with mitomycin C (MMC) alone or in combination with RGD-SAP. Blood samples were collected from retroorbital plexus and the concentration of albumin, alanine transaminase (ALT) and urea in the serum were measured. Values are shown as mean ± SD from n ≥ 4 per condition.

3.3 ATF-SAP and RGD-SAP antitumor activities synergize in a subcutaneous model of bladder cancer

Intra-tumor-heterogeneity and the acquisition of resistance to drugs represents the main issue to face in cancer treatment. To address this topic, we validated the therapeutic potential of a combined toxin based targeted therapy (ATF-SAP and RGD-SAP) directed against epithelial derived cancer cells and tumor neo-vasculature. We demonstrated that stage II muscle invasive bladder cancer cell lines RT112 and 5637 maintain a stable uPAR expression, even after serial implantation cycles in mice, representing good *in vivo* models. RT112 in particular, even if less uPAR positive compared to 5637, are more sensitive to RGD-SAP *in vitro,* therefore represent an optimal model to appreciate the synergy of the combined treatment. In a first preliminary experiment, RT112 cells were injected in the left flank of immunocompromised nude mice. After verification of tumor engraftment, 10 days tumor-bearing mice were intravenously administered with ATF-SAP and RGD-SAP as single or combination treatments and monitored for toxic effects. In the case of single toxins treatments, we administered a dose equivalent to 0.5 mg/kg every 5 days for three times. On the other hand, the same total concentration of toxins (0.5 mg/kg, with half doses of each) was given for the combination treatment (Fig. 21a). Surprisingly, all groups developed a form of dermatitis after the first toxin administration, therefore we decided to reduce the combo dose to 0.25 mg/kg in total (0.125 mg/kg for each toxin). As shown in Fig. 21b, ATF-SAP and RGD-

SAP alone slightly delayed tumor growth and modestly prolonged animal survival when compared to untreated mice. Nonetheless, when the two toxins were combined, we documented a delated tumor progression similar to controls (ATF-SAP or RGD-SAP alone) but mice survival was significantly improved (Fig. 21b, d). Additionally, no signs of lethargy or weight loss were detected (Fig. 21c). Clearly, these results point to synergistic effects of ATF-SAP and RGD-SAP in reducing bladder tumors growth.

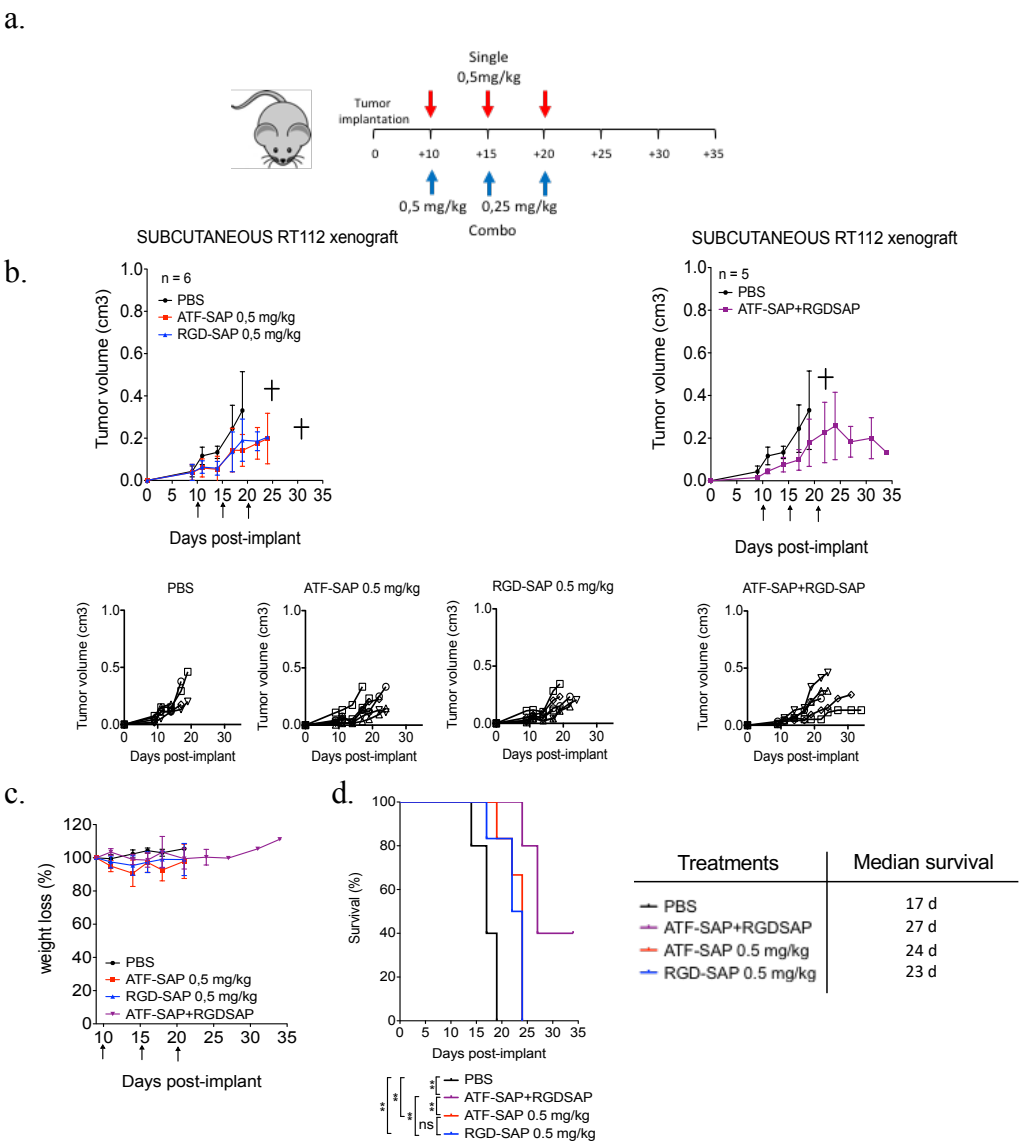

Fig. 21 Effects of SAP-based recombinant fusions single and combination therapy on tumor growth in a subcutaneous xenograft bladder cancer mouse model. (a) Schematic representation of the experimental design. RT112 bladder cancer cells were subcutaneously injected in 7-week-old nude female mice. Tumor bearing mice were randomized into 4 experimental groups and treated respectively with PBS, ATF-SAP (0.5 mg/Kg), RGD-SAP (0.5mg/Kg) or ATF-SAP + RGD-SAP (total first dose 0.5 mg/Kg; total following doses 0.25 mg/kg) via intravenous injection every 5 days after tumor implantation. (b) Quantitative analysis of growing tumor volume in mice treated with single treatments (RGD-SAP or ATF-SAP) (left panel) or combination treatment (RGD-SAP+ATF-SAP) (right panel) are shown as mean ± SD from respectively n = 6 and n = 5 mice per condition and as tumor growth curves for each individual mouse. (c) The mean weight of mice from each treatment group is shown as percentage from initial. (d) Kaplan–Meyer plot of animal survival with median survival time listed in the table. Results from a Mantel–Cox two-sided log-rank test are shown when statistically significant (**$p < 0.01$) for RGD-SAP 0.5 mg/kg (blue; hazard ratio, 11.2; 95 % CI, 1.8 – 69.8) versus PBS, for ATF-SAP 0.5 mg/kg (red; hazard ratio, 19.2; 95% CI, 2.2–165.8) versus PBS, for ATF-SAP+RGD-SAP (purple; hazard ratio, 19.5; 95% CI, 2.8 – 135.9) versus PBS, for RGD-SAP 0.5 mg/kg (blue; hazard ratio, 0.1; 95% CI, 0.1 – 0.5) versus ATF-SAP + RGD-SAP, for ATF-SAP 0.5 mg/kg (red; hazard ratio, 0.08; 95 % CI, 0.1 – 0.5) versus ATF-SAP + RGD-SAP in mice bearing subcutaneous RT112 tumor.

4. Discussion I

The production of recombinant proteins has gained great interest in the biopharmaceutical sector as an increasing amount of protein drugs are currently undergoing preclinical and clinical studies or have been already approved to be on the market. Unlike many drugs, proteins are difficult to synthetize *in vitro* due to their complex structure, which is strictly related to their function. Therefore, host organisms are usually exploited to produce them throughout biotechnological processes. The choice of the most suitable expression host represents a key step in the development of this kind of drugs and depends on both the chemical and biological properties of the recombinant protein of interest. If complex post-translational modifications (glycosylation, phosphorylation, etc.) are required to ensure an accurate folding, very important to guarantee the protein correct function, then a eukaryotic system is usually preferred to bacteria that are not able to provide most of the post-translational modifications. Otherwise, in the case of small peptides that do not require a complex folding upon synthesis, bacteria represent an excellent production system, mostly due to rapid growth, low costs and easy management. From a biological point of view, this aspect is even more relevant for toxins, considering that they can be lethal for production hosts as well. In the present study, we take advantage of ATF-SAP, a recombinant protein in which the toxin SAP is fused to the amino-terminal fragment (ATF) of the urokinase plasminogen activator, uPA [30, 31, 77]. Due to the length and structure of the ATF moiety (a 151 amino acids long peptide, comprising an EGF-like domain or growth factor domain-amino acids 12-32- followed by a kringle domain) ATF-SAP production was set up in *P. Pastoris* yeast, in order to both fulfil a proper folding and minimize the toxicity for the host organism. In fact, in the present eukaryotic organism, the protein can be efficiently segregated into the endoplasmic reticulum and subsequently secreted in the culture medium. Thus, ATF-SAP expression has been optimized in a fermentation process using lab-scale stirred bioreactor to produce discrete batches and demonstrated to be actively cytotoxic on uPAR overexpressing U937 leukemia cells [31]. The choice of uPAR as a target arises from the clinical evidence of a positive correlation between uPAR expression levels

and patient low overall survival in a variety of epithelial and hematological tumors, as it is involved in many steps of tumor progression. Hence, it provides the unique opportunity to tackle with multiple tumors with a single SAP-based product. As a proof-of-concept, a panel of human cell lines resembling bladder and breast cancer was analyzed for uPAR expression in order to identify the best model to test ATF-SAP specificity. We found that high levels of this receptor were mostly confined to cells corresponding to the stage II muscle invasive urothelial bladder cancer lines and TNBC phenotype, which therefore were selected as suitable *in vitro* models, and proved that ATF-SAP is able to recognize and kill uPAR+ cells, proportionally to its expression. As a corollary, cell lines lacking the receptor are not sensitive to the chimera, supporting the hypothesis that the presence of ATF enhances an efficient tumor targeted delivery of SAP activity. In clinical trials, the pharmacological efficiency of current targeted therapies in the treatment of tumors usually associates with toxicities deriving from off-tumor expression of the target. Besides its implication in cancer evolution, uPAR plays a key role in pericellular proteolytic activity, related to tissue remodeling during normal physiological condition, such as wound healing and initiation of angiogenesis [14, 16]. Since fibroblasts are the most involved cell type in the former cited process, we analyzed ATF-SAP activity on a skin fibroblast cell line as well as primary bladder derived fibroblasts, in order to predict any potential *in vivo* side-effect. Even if both types of fibroblasts are highly uPAR expressors, ATF does not determine any increase of the SAP activity on these cells, failing to exert a cytotoxic effect at the given concentrations. Unexpectedly, we also observed ATF-SAP lack of activity on the highly uPAR positive MDA-MB 231 TNBC cell line. The reason for such behavior could be explained by a differential expression of accessory mechanisms/molecules involved in the receptor internalization in highly susceptible tumor cells. To deeper understand this phenomenon, we focused on the principal members of the plasminogen activation system. It is well known that uPAR endocytosis and recycling on the plasma membrane directly relies on different components, among which its natural ligand uPA (responsible for the activation of plasminogen cascade), the plasminogen activator inhibitor-1 (PAI-1) and the alpha2-macroglobulin receptor/low-density lipoprotein receptor-related protein (LRP-1).

When uPA associates with uPAR, it is converted into the active two-chain form, which reacts rapidly with PAI-1, forming a complex that is bound and internalized by LRP1. This route leads to the degradation of the ligand and its inhibitor and to the turnover of the receptor on the cellular surface, allowing the attenuation of proteolytic processes in the extracellular environment [80, 81]. As the activity of the chimera was evident in almost all the uPAR expressing cell lines in our hands, we wondered if there were some differences in the regulation of LRP1 co-receptor or natural ligand uPA compared to fibroblasts and MDA-MB231. Notably, previous studies demonstrated that SAP binds to LRP1 *in vitro*, resulting in its internalization in human monocytes and in fibroblasts, further strengthening the importance of this receptor in this complex system [51]. In 1997, Fabbrini et al. demonstrated that LRP1 is strongly required in ATF-SAP endocytosis. In fact, the observation of toxin resistance in LRP1-deficient cells and competition of anti-LRP1 antibodies to ATF-SAP cytotoxicity, led them to the conclusion that ATF might be necessary for uPAR targeting but internalization is due to the binding of the toxin to LRP1 [50, 55]. Nevertheless, when we analyzed the LRP1 gene expression and protein localization on the plasma membrane, we confirmed its high levels on fibroblasts but not on MDA-MB-231 nor on uPAR+ ATF-SAP sensitive cells, suggesting that the SAP-based chimera internalization does not depend on this co-factor. Similarly, the abundant uPA expression in both responding and non-responding cells and the absence of a competitive activity with ATF-SAP, excluded the implication of the natural ligand in sequestering uPAR, thus reducing its availability on cell surface. It is also worth of noting that ATF-SAP only contains the amino terminal binding domain of uPA, therefore it is not expected to be able to bind PAI-1 and form the complex necessary for the internalization. In fact, no changes in the ATF-SAP toxic activity were detected when PAI was added to the medium. On the other hand, when we used a SAP conjugate carrying the entire pro-uPA zymogen sequence as targeting moiety, the activity of SAP was greatly increased in both fibroblasts and MDA-MB-231 cell lines not responding to ATF-SAP. This observation led us to suppose that different mechanisms might be involved in the internalization of the two SAP-based products. In 2008, Cortese et al. described a novel unusual internalization pathway responsible for constitutive endocytosis of uPAR that

partially ties with micropinocytosis [82]. They observed that this so far unknown endocytosis path does not require the presence of uPA, PAI or LRP1 nor is related to uPAR massive expression on cell surface, as it could be detected either on naturally uPAR expressing cells and on cells transfected to express exogenous uPAR but showing low uPAR levels. Apparently, this micropinocytosis-like mechanism is also clathrin- and lipid rafts- independent and associates to a rapid recycling of the receptor on the cell surface, therefore it might be important in unknown regulations of extracellular functions under particular conditions (i.e. in the absence of ligands or inhibitors). Up to now, macropinocytosis is a still poorly understood mechanism, constitutively induced in some cell types (e.g. dendritic cells and macrophages), but also strictly regulated in cells stimulated with growth factors (such as EGF) [82, 83]. In our study we could well distinguish different condition which might indicate different internalization pathways: uPAR+ LRP1- MDA-MB-468, 5637 and RT112 cells, responsive to ATF-SAP; uPAR+ LRP1- MDA-MB-231 cells, not sensitive to ATF-SAP, but turned in a restored SAP toxicity when pro-uPA-SAP was used; uPAR+ LRP1+ fibroblasts, not sensitive to ATF-SAP but turned in a restored SAP sensitivity when a SAP conjugated to pro-uPA-SAP. Therefore, we propose a model involving two different internalization routes for ATF-SAP chimera or pro-uPA-SAP conjugate: an LRP1 and ligand-independent endocytosis, induced by the ATF binding to uPAR, mainly detected on LRP1 negative cancer cells, but not on MDA-MB231; an LRP1 and ligand-dependent endocytosis, responsible for the pro-uPA-SAP endocytosis observed in LRP1 positive fibroblasts (Fig. 22). The latter could be explained as the need of fibroblasts to activate the plasminogen activation system in physiological conditions (such as wound healing process) and uptake the proteolytic ligands (uPA) in order to attenuate the extracellular process. On the other hand, this scenario does not elucidate the lack of cytotoxicity by ATF-SAP in LRP1 negative MDA-MB-231 cells that, on the contrary, are sensitive to pro-uPA-SAP.

Therefore we conclude that ATF-SAP toxic activity does not rely on the presence of the uPA:PAI ligands or LRP1 internalization cofactor, but it is likely to stimulate a different micropinocytosis-like process that is supposed to faster uPAR turnover on the cell membrane. Whether this kind of micropinocytosis is a cell-specific

mechanism or if there are cofactors involved in the intracellular sorting machinery that might end up in the lysosomal degradation of ATF-SAP are open questions that still require further investigation.

a.

b.

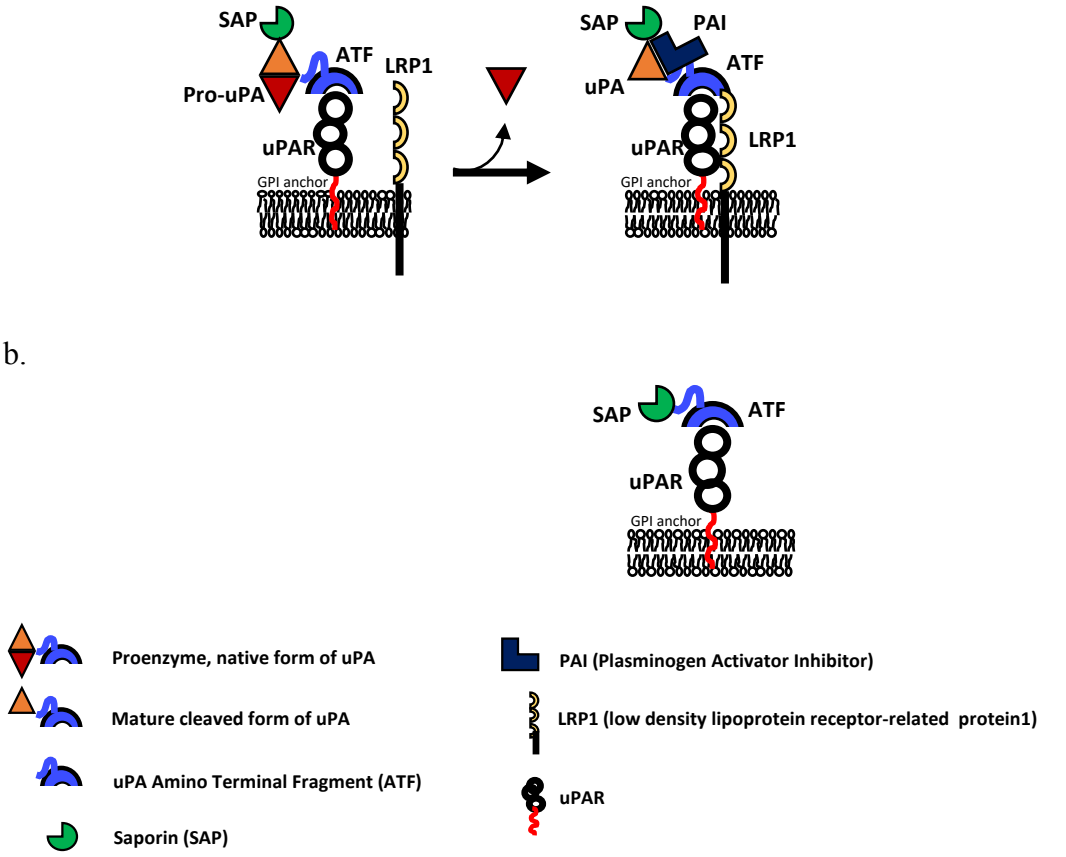

Fig. 22 Schematic representation of internalization pathways proposed for uPAR targeting toxins. a. LRP1-uPA-PAI-dependent endocytosis; b. LRP1-uPA-PAI-indipendent endocytosis.

Intra-tumor heterogeneity represents one of the major obstacles for targeting therapies, together with the ability of tumor cells to suppress effector response by downregulating surface antigens. In order to face this issue, we firstly validated the effect of an *in vivo* environment on the expression of uPAR receptor. RT112 and 5637 stage II resembling bladder cancer cell lines were used as optimal model for this experiment, due to their differential expression of uPAR. We show that after serial implantations in mice, both cell lines maintain uPAR levels and responsiveness to ATF-SAP, further confirming the suitability of this GPI anchored molecule as a target and opening the way to the validation of the chimeric toxin

activity in a preclinical model.

Next, with the aim to expand the spectrum of targets for SAP-based therapeutics, we designed and produced an integrins-targeting recombinant protein, in which SAP is fused to RGD targeting peptide. Integrins represent a class of molecules that are very important in cell adhesion to the extracellular matrix, with multifaceted roles in cancer progression from primary tumor development to metastasis. Their attractiveness in the development of anti-cancer drugs mainly resides in their broad presence on both epithelial and endothelial cells that is restricted to cancer microenvironment. It has already been demonstrated that ACDCRGDCFC-containing fusion proteins (i.e. RGD-TNF) can be efficiently produced in bacteria and provide rapid and stable associations with αv-integrins receptors on both murine and human angiogenic vessels [26, 27, 28]. In fact, unlike ATF, RGD does not need any complex post translational modification other than disulfide bond formation. For this reason, we optimized the production process of RGD-SAP in an *E.coli* system. In this case, as bacteria do not have intracellular compartments and SAP is toxic for bacterial ribosomes too, we employed an IPTG inducible system to limit the dangerous effect of the produced toxin on the host. Therefore, induction time, temperature and amount of inducer were strictly defined allowing the highest yield of protein production with the lowest toxic effect on the producer.

Here we show that, even if it is likely that wrong intra-chain disulfide bonds are formed between the four cysteines present in the peptide structure, when fused to SAP toxin, RGD moiety maintains its ability to recognize and bind αv– integrins expressing epithelial cancer cells proportionally to their levels, enhancing an *in vitro* significant and selective delivery of the SAP moiety, which causes cell death by activating apoptosis program at early time points. Furthermore, competitive binding experiments with an excess of RGD free peptide confirmed that its improved activity is related to a targeting property other than a passive endocytosis. It is worth of noting, however, that we did not measure the αvβ5 component, for this reason we cannot exclude its implication in RGD-SAP activity in all the tested cell lines.

As stated before, our approach is intended to be applied to many cancer subtypes, since the target antigens we chose associate with tumor phenotypes with different

origins. Here, we focused on testing the pharmacological efficacy of SAP-based recombinant proteins in the treatment of bladder cancer. In clinics, bladder cancer therapy is characterized by transurethral resection of cancer lesions (TURBT) or by the removal of the entire organ (radical cystectomy), depending on the tumor stage. Most of the times, a chemoprophylaxis regimen based on chemotherapeutics like platinum complexes is given either before surgery (neoadjuvant chemotherapy) or after surgery (adjuvant chemotherapy) to lower the chance of cancer recurrence [35]. Although the high abundance of molecular antigens [39], targeted therapies still do not represent the first choice for the treatment of advanced urothelial carcinoma. Here we took advantage of a syngeneic and allogeneic bladder cancer mouse models, in order to evaluate: 1- the optimal dosage to achieve a high anti-tumor efficacy and to limit any possible side effect; 2- the clinical outcome when the proposed drugs are used as single or combined therapy. At first, a subcutaneous model of MB49 murine bladder cancer, proven to be responsive to RGD-SAP, was established on small groups of animals to identify, in a preliminary experiment, the minimal effective dose. Interestingly, mice treated with increasing doses of RGD-SAP (0.5, 0.75 and 1 mg/kg) underwent a significant and dose-dependent reduction of tumor growth, while CYS-SAP untargeted control (1 mg/Kg) did not result in any anti-tumor effect, as the tumor development in this group of mice was superimposable with PBS-treated mice. This observation might indicate that, in contrast with CYS-SAP, RGD-SAP is able to reach and actively target the tumor environment, excluding a “passive targeting” mechanism caused by the enhanced permeability and retention (EPR) effect. However, even if the highest dosage used (1 mg/kg) showed an impressive activity, which resulted in tumor debulk in 2 out of 5 mice, it was not associated to a significant prolonged mice survival; furthermore, the analysis of biochemical parameters revealed liver and renal toxicity, evidenced by high aspartate transaminase (AST) and creatinine (CHE) plasma levels. No significant differences could be detected between 0.75 mg/kg and 0.5 mg/kg treatments, which nonetheless had significant effect on tumor growth compared to control without side toxicities. Therefore, we decided to use the lowest doses 0.5 mg/kg and 0.25 mg/kg to investigate the activity and penetration capacity of RGD-SAP in an orthotopic model of bladder cancer. As shown, the intravesical

instillation of MB49 cells leads to the formation of a tumor mass which is well irrorated through neo-angiogenesis vessels (as shown by ultrasound analysis) and superficially proliferates protruding into the bladder lumen. Quite unexpectedly, despite these conditions were apparently ideal to examine RGD-SAP therapeutic efficiency, no influence on tumor growth in terms of light intensity could be appreciated. The reason for this evidence could be attributed to the logarithmic proliferation rate of the tumor mass, which results, in few days, in the formation of an inner necrotic area that causes hematuria and a sudden drop of luminescence signal.

Mitomycin (MMC) is one of the most used agents considered to be effective in the recurrence prevention of superficial bladder cancer [35, 36, 37]. It is usually given via trans-urethral instillation for the treatment of stage I superficial bladder carcinoma and, due to the administration route and its moderate hydrophobicity, it is less absorbed systemically, causing limited side-effects. In this contest, we set up an administration schedule in which the intravesical pretreatment of the established MB49 bladder tumor with MMC was aimed to slowdown the superficial mass growth rate, enabling the formation of new vessels and, thus, an adequate drug delivery to the tumor. Interestingly, upon MMC pretreatment, mice receiving 0.5 mg/kg dose of RGD-SAP incurred in a limited tumor proliferation compared to those administered with MMC only or PBS; this outcome also associated with an increased overall survival (at the end of the experiment -day 23-, 60 % of mice survived upon combined treatment compared to < 40 % in the MMC group and only < 20 % in the PBS group) and welfare of mice in terms of body weight and systemic toxicity (as observed by the biochemical parameters). Notably, *in vitro* experiments did not report a high cytotoxicity of RGD-SAP on MB49 cells (IC50~150 nM); hence, we cannot exclude that the strong *in vivo* activity of RGD-SAP is caused by an active integrin targeting of both epithelial and endothelial cells in our models. Taken together, these results suggest that RGD peptide is able to efficiently deliver SAP to the tumor microenvironment, with potent anti-proliferative effect. Moreover, the lack of a systemic toxicity associated to liver and kidney strongly sustains its specificity, further confirmed by CYS-SAP lack of efficiency; in addition, despite RGD-SAP alone apparently did not lower tumor

progression in a bladder cancer orthotopic model, probably due to the high proliferation rate of MB49 cancer cells, the use of MMC resulted to be a good tool to allow RGD-SAP to reach and exert its toxic function on tumor microenvironment.

Since we found the expression of uPAR and αν-integrins not to entirely overlap on human epithelial cancer cells and since the RGD peptide might be active on murine newformed vessels as well, we used a xenograft subcutaneous model in order to explore if the combination of ATF-SAP and RGD-SAP could induce stronger antitumor effects than single agents. As shown, the combination of the two agents induced not only a delay of tumor proliferation and necrotic area formation into the tumor mass but also substantially improved mice overall survival when compared to single treatments, as the 40 % of mice survived to the end of the experiment (day 35). Therefore, we conclude that the addition of a targeting moiety to SAP structure allows the specific delivery of the toxin to the tumor mass in different models, showing promising results in dealing with cancer heterogeneity. Further investigations will be addressed to elucidate the exact RGD-SAP cellular targets, unravelling the contribution of endothelial cell death in tumor positive response. Furthermore, the influence of immune system activation on the reduction of the tumor mass remains to be explored as well as the effects of proposed combination strategy on different solid tumor mouse models.

5. Results II

5.1 Cells genetic engineering to produce targeting smart prodrug-encapsulating exosomes

The use of nanotechnology as drug delivery system has gained an increasing attention in the last decades. Exosomes, in particular, have been considered promising nanovehicles for the intracellular delivery of drugs, including bioactive proteins. The presence of a lipid bilayer membrane, in fact, ensures the protection of the encapsulated drug from degradation, allowing the achievement of an enhanced bioavailability. We herein explore the possibility to use exosomes as targeted nanocarriers in order to improve SAP delivery to cancer cells and increase its therapeutic outcome. To obtain targeted exosomes, we firstly considered a genetic approach, in which we engineered cells to produce targeted cargo-carrying extracellular vesicles. To this aim, we fused the RGD peptide encoding sequence to the extra-exosomal N-terminus of human Lamp2b cDNA, a typical exosomal marker. The cloning strategy adopted was intended at maintaining the Lamp2b signal peptide (SP) upstream to the coding sequence, because it is essential for the correct Lamp2b sorting into the MVB compartment. In addition, we used an RFP reporter gene fused to the C-terminus of the Lamp2b encoding sequence to allow its orientation towards the intra-exosomal lumen, enabling vesicles tracking (Fig. 23). In order to facilitate the release of the cargo protein in the cytosol of the target cells, a cleavage sequence GFLG (CS) specific for the cellular protease Cathepsin B was then inserted in between the Lamp2b and RFP sequences by PCR amplification. As a control, a non-active cleavage site GGSG (NACS) mutant was prepared.

a.

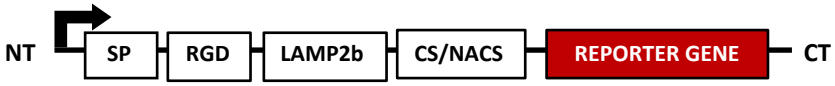

b.

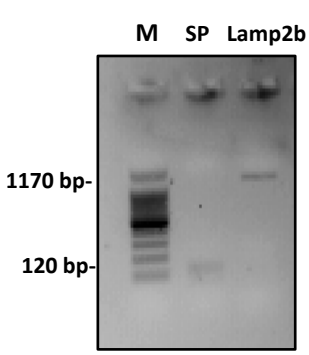

c.

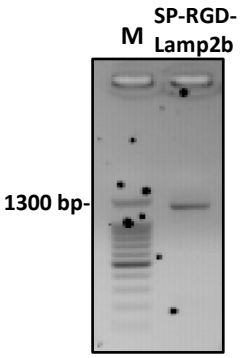

Fig. 23 Schematic representation of the modified Lamp2b protein and preparation of the fusion product. a. NT, N-terminus; SP, signal peptide; RGD, targeting peptide; CS, cleavage site; NACS, non-active cleavage site; CT, C-terminus. b. and c. PCR amplification products of Lamp2b (1170bp) and SP (120bp) sequences form HEK293 cDNA and SP-RGD-Lamp2b (1290bp) fusion sequence were analyzed by agarose gel electrophoresis.

Cathepsin B is a cysteine protease whose massive expression has been reported in several invasive and metastatic cancers [85]. Its presence in cells was monitored by western blot analysis and demonstrated to be high, especially in its mature active form, in HEK293 and 5637 cells while exosomes derived from both cell lines show the presence of Cathepsin B in its native proenzyme non-active form (Fig. 24).

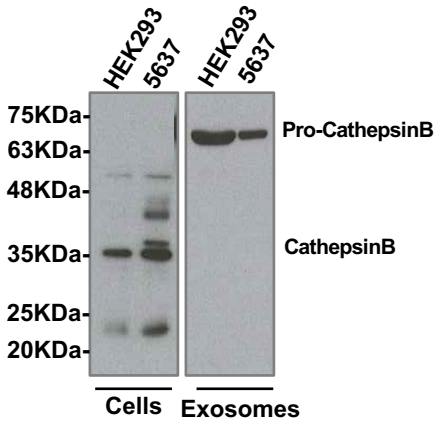

Fig. 24 Cathepsin B western blot of HEK293 and 5637 cell lysates and their corresponding exosomes. Intracellular and exosomal levels of Cathepsin B were analyzed by western blot with an antibody against Cathepsin B, recognizing both the cleaved and the zymogen non-active form.

5.2 Lamp2b-fusion product is horizontally transferred to receiving cells

The correct expression of the two RGD-Lamp2b-RFP constructs (CS and NACS) by cells was then primarily monitored by fuorescence microscopy. 5637 bladder cancer cells were used to this purpose due to their high transfection efficiency (Fig. 25a). However, even if cells appeared punctuated, confirming the correct expression of the protein in the vesicular compartment, we could not detect a high fluorescence signal, most of which was confined to the dead cells, suggesting that the construct might be cytotoxic for parental cells. To verify the correct sorting of the RGD-Lamp2bRFP in the secreted extracellular vesicles and to establish if the targeting peptide was correctly localized on the vesicles surface, we transferred 72h conditioned medium from 5637 parental cells to receiving HUVEC cells. As endothelial cells, in fact, these cells are predicted to express αv–integrins on their surface and be targeted by RGD peptide [6, 21]. As shown in Fig. 24b, a punctuate pattern on HUVEC cells could be distinguished, confirming the transfer via extracellular component secreted into the conditioned medium.

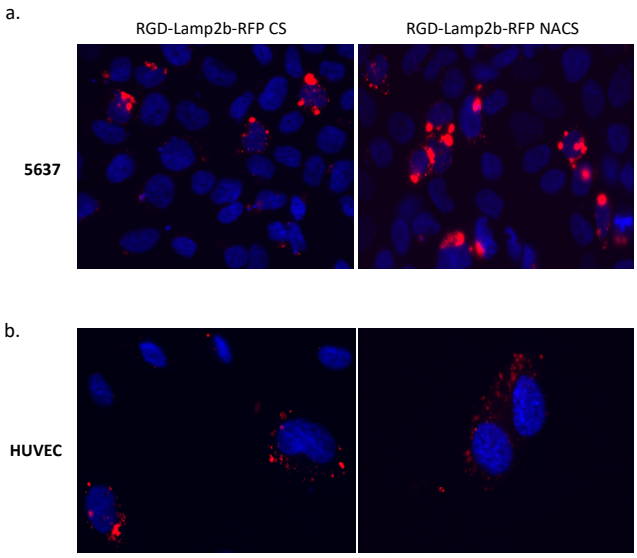

Fig. 25 Lamp2b-RFP recombinant proteins expression and visualization. a. Representative fluorescence microscopy images of 5637 cells 48 h after transient transfection with RGD-Lamp2b-RFP CS/NACS encoding plasmids. b. Representative images of HUVEC cells 24 h after treatment with RGD-Lamp2b-RFP CS/NACS-transfected 5637 conditioned medium. Nuclei were counter stained with DAPI (blue).

5.3 Lamp2b fused, RFP-based smart prodrug expression is not stably maintained overtime

Having demonstrated that the exogenous gene can be correctly expressed and likely conveyed to the extracellular vesicles fraction by parental cells, we sought to determine if the expression level and, thus, the extracellular vesicles enrichment of the exogenous protein could be increased by the production of stably expressing cell clones. Conversely to our expectations, the antibiotic selection resulted in a complete loss of both the exogenous proteins, as confirmed by flow cytometry (Fig. 26). To assess whether the total amount of exogenous protein was relocated to the vesicles membrane, western blot analysis was carried out on cell lysates, purified microvesicles and exosomes fractions. However, as shown in Fig. 26, no signal could be visualized at the molecular weight corresponding to the recombinant protein. The same results were obtained when we replaced the RFP sequence with SAP encoding gene, indicating that a probable degradation of the exogenous protein and adaptation of cells to the antibiotic condition might occur when Lamp2b-fused reporters are used. With the aim to exclude a possible cell type specific degradation of the RGD-Lamp2b constructs, we performed the same experiments on healthy HEK293 cells. As already observed for 5637, neither RGD-Lamp2b-RFP nor RGD-Lamp2b-SAP expression could be observed after antibiotic selection in the cell lysates nor in the purified microvesicles and exosomal fraction.

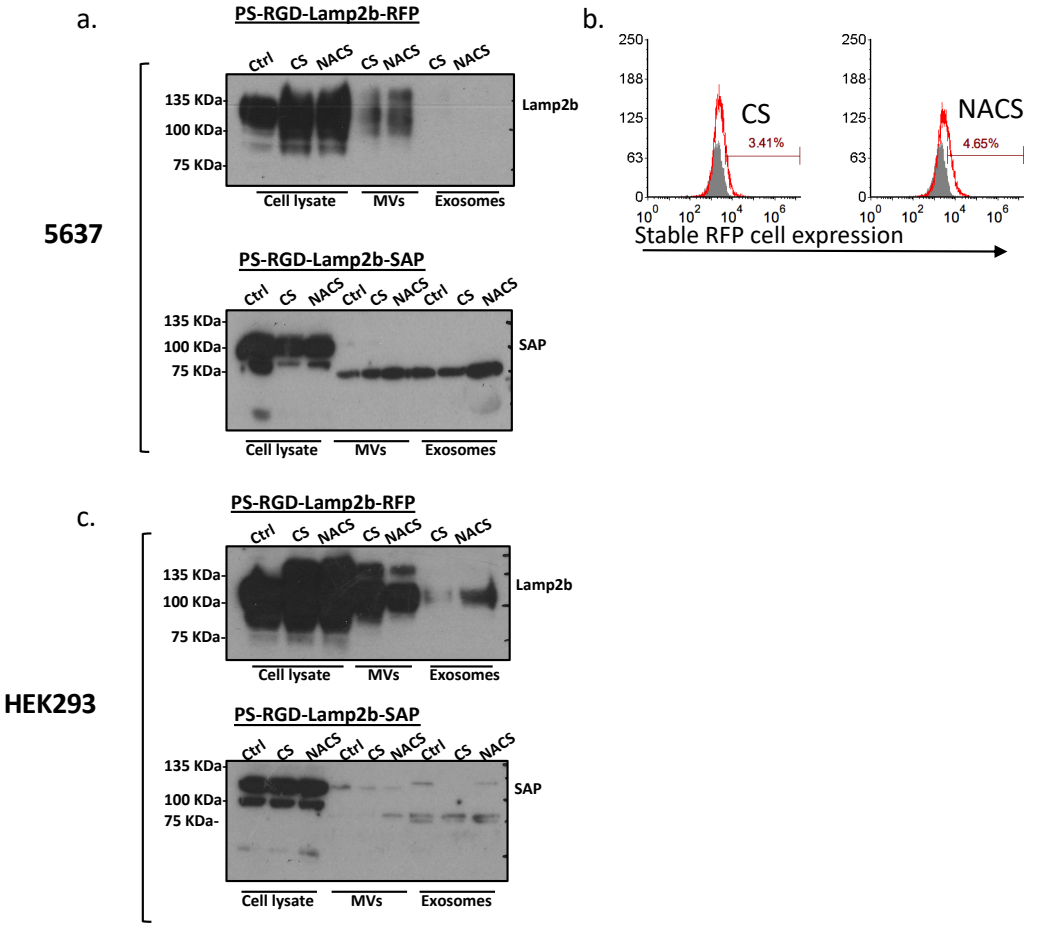

Fig. 26 Exogenous Lamp2bRFP/SAP protein expression in 5637 and HEK cells lysates and extracellular vesicles fraction. a. 5637 and HEK293 cells stably expressing the Lamp2b-based recombinant proteins (RFP-CS/RFP-NACS) were cultured and conditioned media collected for exosomes isolation after 72 hours (left panel). The intracellular, microvesicles (MVs) and exosomal content of the exogenous proteins were analyzed by western blot with anti-Lamp2b antibody to detect RFP fusion or with anti-SAP antibody to detect the expression of SAP. b. 5637 transfected cells were selected with G418 antibiotic for 1 month and analyzed by flow cytometry for Lamp2bRFP-CS/NACS expression; results are shown as representative histograms (right panel).

5.4 Tetraspanins-fused, RFP-based smart prodrugs are massively expressed by cells and transferred to exosomes

Therefore, we wondered whether the loss of expression of the recombinant products was related and confined to Lamp2b marker. To address this question, we cloned the RFP CS or NACS sequence downstream to different specific exosomal markers, tetraspanins CD9 and CD81. Due to their structure and orientation on the exosomal membrane, with both the N- and C-terminus facing the intra vesicle lumen, these tetraspanins cannot be used for a targeting purpose by modifying their termini.

However, as shown in Fig. 27, both 5637 and HEK293 cells efficiently expressed the CD9- and CD81-RFP exogenous proteins, in a significant higher extent compared to Lamp2b-fused RFP. Interestingly, a different expression pattern could be observed between the RFP carrying the active (CS) or non-active (NACS) cleavage site, as a more abundant signal was evident in cells transfected with CD9/CD81-RFP NACS compared to RFP CS-fused tetraspanins, confirming that the active form of Cathepsin B present in both cell types is able to recognize it and release the protein from the membrane constriction. This activity could be also well distinguished in western blot analysis of 5637 cells lysates, in which the quantitative ratio between CD9/CD81-RFP CS and CD9/CD81 alone forms is visibly lower compared to CD9/CD81 RFP NACS and CD9/CD81 alone, highlighting a high protease specificity against the inserted active cleavage site (Fig. 27b). In contrast, we could not observe the same cleavage in healthy HEK293 cell lysates, in which CD9-RFP CS/NACS were not detectable, while CD81-RFP CS/NACS/CD81 alone ratio was comparable. Notably, while HEK 293 cells were able to convey the total CD9 exogenous tetraspanin-fused-RFP to exosomes and partially the CD81 one, 5637 cells appeared to be completely inefficient in transferring the CD9 constructs to exosomes, whereas CD81 exogenous construct was conveyed into exosomes in a minor extent (Fig. 27a).

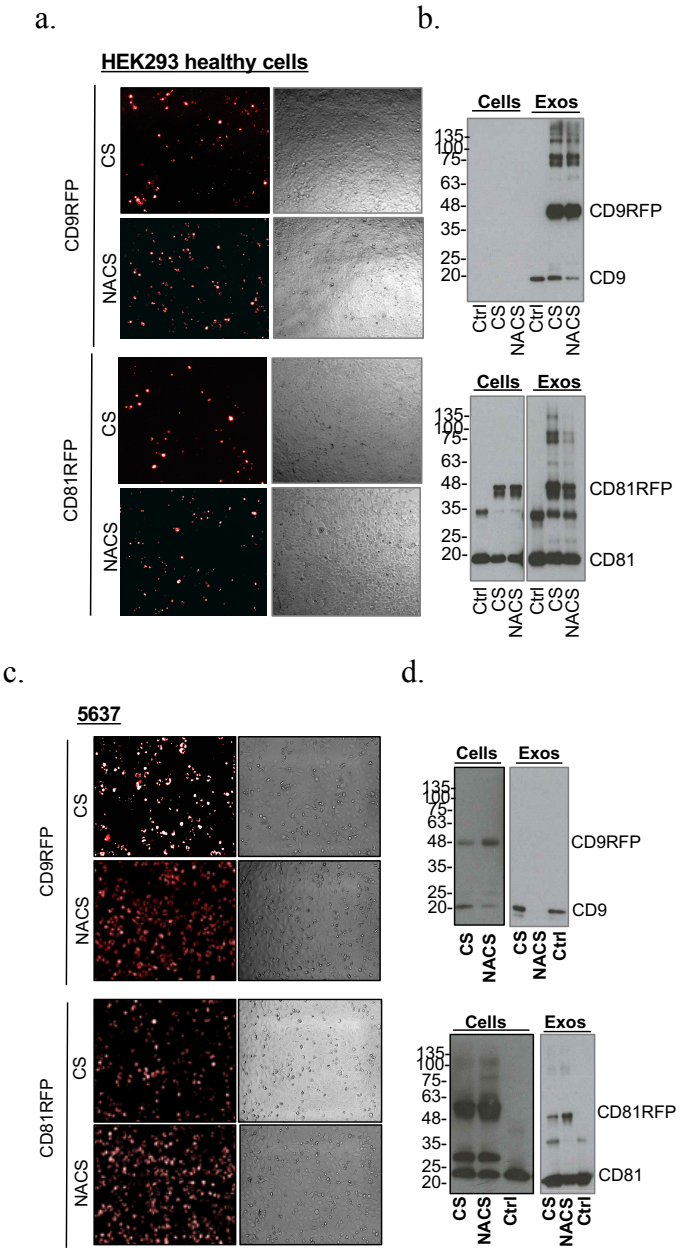

Fig. 27 Exogenous tetraspanin-RFP CS/NACS protein expression in HEK293 and 5637 cells lysates and exosomal fraction. Fluorescence (left panels) and bright field (right panels) microscopy images of HEK293 (a) and 5637 (c) cells stably expressing tetraspanin-RFP (CS/NACS) recombinant proteins. Cells were cultured and conditioned media collected for exosomes isolation after 72 hours. HEK293 (b) and 5637 (d) cellular and exosomal content of the exogenous proteins were analyzed by western blot with anti-CD9 or anti CD81 antibodies (right panels).

6. Discussion II

With the aim to improve our toxin delivery system, we isolated and characterized nano-sized extracellular vesicles, exosomes, and explored *in vitro* their potential as natural drug carriers. One of the major advantages of using cell derived vesicles rather than chemically synthetized liposomes concerns the possibility to completely evade the immune system response [93]. In fact, patient-derived healthy cells can be isolated and cultured *in vitro* with the purpose to both genetically engineer them to produce therapeutic exosomes or induce them to produce exosomes which can be *ex vivo* manipulated. This approach leads to the prospect to produce personalized and well tolerated treatments, as the drug nanocarriers would be recognized as self-molecules by the patient body, achieving an improved circulation time and bioavailability. In this work, we investigated both two different approaches to modify exosomes as drug carriers, a genetic and an *ex vivo* modification of exosomes, and considered the advantages of each method in terms of drug encapsulation efficiency, delivery capacity and targeting. Regarding the former genetic engineering strategy, we used the ACDCRGDCFCG peptide (RGD) encoding gene to decorate exosomes surface, in order to better compare the exosomes-based targeted delivery system to the recombinant RGD-SAP protein. The RGD DNA sequence was cloned at the N-terminus of the Lysosomes-associated membrane protein 2b (Lamp2b), a membrane protein with a single transmembrane domain, already shown to be efficient in displaying targeting moieties on the surface of exosomes [65, 71, 72]. This approach has in fact already been pursued by Tian et al. in 2013 [71], who produced iRGD-Lamp2b fused targeted exosomes and demonstrated their high efficiency in delivering chemotherapeutic drugs to breast tumor-bearing in mice. While the above-mentioned group used electroporation to encapsulate doxorubicin into exosomes, in this work we genetically modified the C-terminus of Lamp2b as well, in order to couple the tumor targeting property to a selectively releasable drug system in the internal lumen of the vesicles. To this aim, we designed a smart-prodrug system, taking advantage of a six amino acids sequence (inserted in between the C-terminus of Lamp2b and an RFP reporter gene resembling a trackable cargo protein)

containing a dipeptide specific for the protease activity of Cathepsin B [84]. Cathepsin B is known to be massively expressed in cancer cells but not in healthy cells, as involved in many steps of cancer progression [85]. In cancer, Cathepsin B is found in lysosomes as well as in vesicles throughout the cytoplasm and at the cell periphery [86, 87]. Smart prodrugs systems based on doxorubicin and other small molecules, targeting the protease activity of Cathepsin B in tumor microenvironment, have already been investigated and demonstrated to be highly efficient in kill metastatic cancer cells sparing normal cell [88, 89, 90]. The aim of these studies was to selectively release the drugs in tumor microenvironment, targeting the secreted Cathepsin B form, which associates to the plasminogen cascade and result in the activation of factors involved in the extracellular matrix degradation and cancer cells invasion. Herein, the present strategy we proposed is directed to avoid the confinement of the cargo protein on exosomes membrane, allowing its release in the cytosol of the receiving cancer cells with a high Cathepsin B expression. The first step in the development of exosomes-based drug delivery systems is the choice of donor cells, which should be able to produce a conspicuous amount of extracellular vesicles lacking immunogenic or tumorigenic components. As a proof of principles, we selected two different kind of tumor cells as exosomes donors, the 5637-bladder cancer cell line and the HEK293 healthy cell line, due to their high transfectability and their capacity to produce exosomes without any special induction condition. Both cell lines were found to be positive to the active cleaved form of Cathepsin B, while exosomes derived from the same cell lines were positive for the zymogen non-active form of the enzyme. The expression of the Lamp2b recombinant proteins was detectable in its punctuated phenotype on both cell types tranfected transiently; furthermore, it could also be well distinguished by microscopy observation on endothelial cells receiving donor cells extracellular vesicles-containing conditioned medium. However, we found that cells underwent a sudden decrease of the signal as soon as they were exposed to an antibiotic clone selection. This behavior was further observed by western blot analysis, where the presence of the RFP-fused Lamp2b at the predicted molecular weight was not detectable neither in the cell nor in the extracellular vesicle fraction (microvesicles and exosomes), indicating that there was not a fluorescent signal intensity problem.

In addition, a time and selection-dependent loss of expression was also detected when the RFP encoding DNA sequence was replaced with the SAP gene, meaning that the probable degradation was not cargo-dependent. This phenomenon could rely on a cell adaptation to the possible citotoxicity of the constructs, that was not related to the presence of the cleavable sequence susceptible to Cathepsin B protease activity and, thus, to the selective degradation of the RFP/SAP moiety. In fact, the same loss of signal was evident in both cells transfected with the construct carrying the active cleavable sequence and its non-active mutant. Consequently, in order to verify such a hypothesis, we cloned the RFP gene carrying the CS or NACS sequences downstream to different exosomal markers (CD9 and CD81). As shown, a high expression of these recombinant proteins could be achieved in both cell types, without any downregulation after antibiotics selection. In addition, the construct was not only delivered to the extracellular vesicles fraction, but also correctly processed by Cathepsin B protease activity, as shown by the differential ratio between the fusion products carrying the CS or NACS. Importantly, we could distinguish two different intracellular sorting paths of recombinant proteins in the cell types we used: while HEK cells were able to direct CD9 fused RFP entirely to the extracellular vesicles fraction, in contrast with CD81 fused RFP constructs that were detectable both in the cell lysates and in exosomes, 5637 cells were able to process both the CD9 and CD81 constructs carrying the Cathepsin B specific cleavage site, but not or minimally sort them into the exosomes. Notably, only the CD9 fused RFP was correctly processed by 5637 cancer cells, whereas CD81 resulted in a series of possible degradation products. This result indicate that 5637 cells represent a good model of cancer recipient cell to test the activity of Cathepsin B specific smart prodrugs, showing a highly specific intracellular activity of the enzyme; on the other hand, HEK293 cells, represent a good model for production of exosomes carrying the Cathepsin B smart prodrug, as the enzymatic activity is not detectable at a cellular level and the recombinant proteins are entirely delivered to the exosomes fraction. Taken together these results suggest that, conversely to what previous studies showed, Lamp2b is not the ideal exosomal marker to produce genetically engineered exosomes, as its expression is unclearly downregulated by cells under antibiotic selection to make stable expressing cells. In contrast,

tetraspanins-based recombinant proteins are able to be massively expressed by cells and conveyed to the extracellular vesicles fraction; furthermore, a Cathepsin B specific smart prodrug system appeared to be a promising strategy in releasing a protein drug specifically to cancer cells when associated to the CD9 tetraspanin. However, even if promising, further investigation are needed to verify both an effective horizontal transfer of cargo proteins from exosomes to cancer cells and, subsequently, to decorate exosomes surface with targeting peptide with a different *ex vivo*, non-genetic method.

7. Results III

7.1 HEK293 derived exosomes as suitable and safe potential nanocarriers

Due to the several difficulties we encountered in genetically engineer cells to produce therapeutic targeted exosomes, we investigated in parallel the possibility of loading SAP into purified exosomes using a different approach based on the use of a chemical method. Since exosomes are nanoscale vesicles that reflect the cell of origin molecular composition, as already highlighted, it is very important to select the proper cell line to produce safe carriers for therapeutic applications. In this contest, we opted for the commercially available HEK293 cells as vesicles donors, as they have been reported to be one of the systems most frequently used to this purpose[15]. A protocol for the isolation and purification of exosomes from HEK293 culture medium, consisting in sequential centrifugation and ultracentrifugation steps and in a 0.22 μm filtration to select nano-sized vesicles was set up and optimized (Fig. 28a). The collected exosomes were homogeneous, with a size distribution picking at 150 nm in diameter as determined by Dynamic Light Scattering (DLS) and Nanoparticle tracking analysis (determined by Nanosight) (Fig. 28d, e). The presence of typical protein markers (Alix, CD9, CD63 and CD81) in the exosomal fraction confirmed the purity of the preparation. (Fig. 28b).

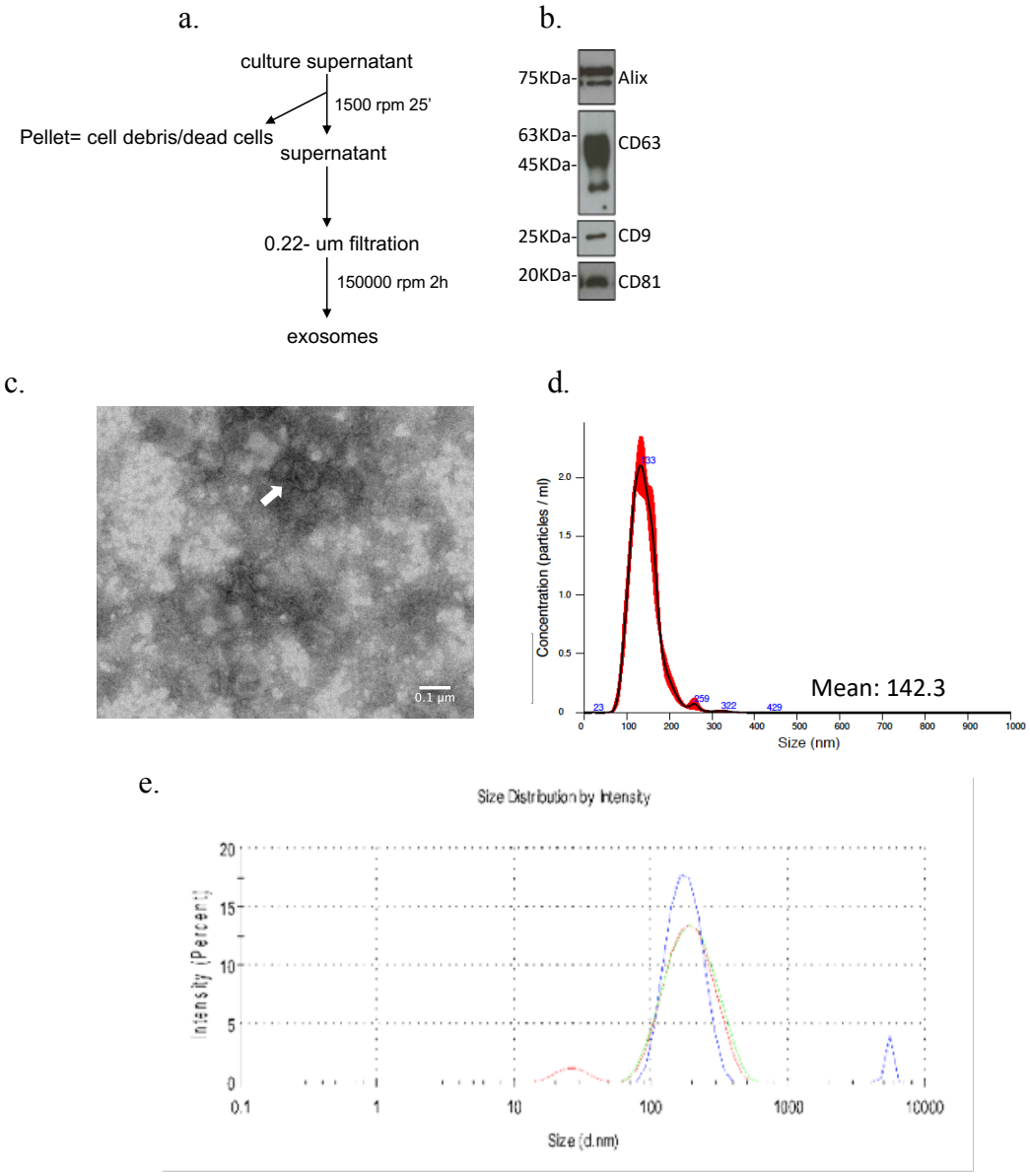

Fig. 28 Isolation and characterization of HEK293 derived exosomes. a. Schematic representation of exosomes isolation procedure. Exosomes were collected from conditioned medium of 72h cultured HEK293 cells by sequential centrifugation and filtration steps. b. Typical exosomal markers were detected by western blot analysis with antibodies specific for Alix, CD63, CD9 and CD81. Transmission electron microscopy (TEM) (c), Nanoparticles tracking analysis (d) and Dynamic light scattering (DLS) analysis (e) were performed to analyze respectively structure and dimensions of the nanovesicles.

Labelling procedures represent the easiest way to follow therapeutic nanoparticles and to elucidate the interaction with target cells, intracellular trafficking pathways and their final fate. To assess whether exosomes can be efficiently captured *in vitro* and trace them once taken up by cells, HEK293-derived purified exosomes were labelled with Vybrant DiO, a lipophylic dye able to intercalate into the vesicle's membrane (Fig. 29). Different concentrations of labelled exosomes were firstly co-incubated with healthy fibroblasts, in order to evaluate the uptake process over time. Fluorescent microscopy analysis revealed that the exosomes uptake was time and concentration-dependent. Exosomes were visible in the form of green clusters in the perinuclear and other subcellular compartments, indicating an efficient internalization of the vesicles, that give cells a punctuate aspect. After 72h of treatment, the detected increase of cell percentage with a diffused cytosolic signal may indicate that exosomal content is likely to be gradually released from the endocytic compartment. Moreover, exosomes uptake resulted to be well tolerated *in vitro* as there were no observable toxic effect to cells (Fig. 29a).

a.

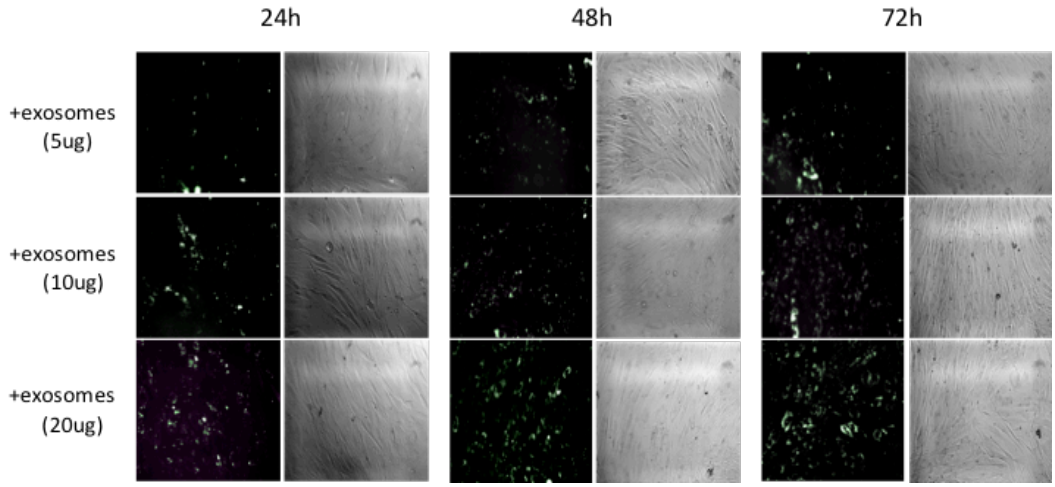

b.

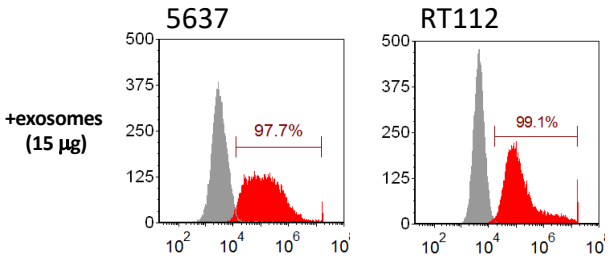

Fig. 29 Exosomes uptake evaluation on heathy and bladder cancer cells a. Healthy skin-derived fibroblasts were treated with increasing concentrations (5, 10, 20 µg) of HEK293-derived exosomes labelled with the lypophilic dye Vybrant DiO. Exosomes uptake was evaluated over time by fluorescence microscopy. **b.** 5637 and RT112 bladder cancer cells were treated with an intermediate concentration (15 µg) of HEK293-derived exosomes labelled with the lypophilic dye Vybrant DiO. Exosomes uptake was evaluated after 24h by flow cytometry analysis. Images from a representative experiment are shown (n=3).

This result was confirmed by using RT112 and 5637 bladder cancer cells, which were co-incubated with labelled HEK-derived exosomes and after 24 hours analyzed by flow cytometry. As shown in Fig. 29b, exosomes could enter almost in the 100 % of cells, supporting the potential use of these vesicles as drug nanocarriers.

7.2 A pH shock exposition enhances SAP incorporation into exosomes preserving vesicles structure and uptake property

So far, different methods have been explored to internalize drugs into extracellular vesicles, among which electroporation, sonication, membrane permeabilization

with detergents, freeze and thaw cycles. However, even if successful, most of them result in a very low drug encapsulation efficiency associated to a strong alteration of the exosomal structure [63]. In the present work, we propose a new technique to load an exogenous protein, SAP, into isolated exosomes, based on the use of an alkaline pH altering buffer, 1 M sodium carbonate pH 11.5 (Na_2CO_3). The rationale of the use of this buffer consists in inducing a membrane reversible perturbation, which allows the insertion of the exogenous protein in the vesicle internal lumen. To verify this principle, exosomes were exposed to a transient pH shock by incubation in the alkaline buffer Na_2CO_3 and the impact of such pH alteration on size and physical structure was analyzed by electron microscopy and Nanoparticle tracking analysis. As shown in Fig. 30, we found that Na_2CO_3 treatment did not affect neither exosomes size nor morphology, which appeared to be perfectly preserved in its round shape and dimensions, peaking at 150 nm.

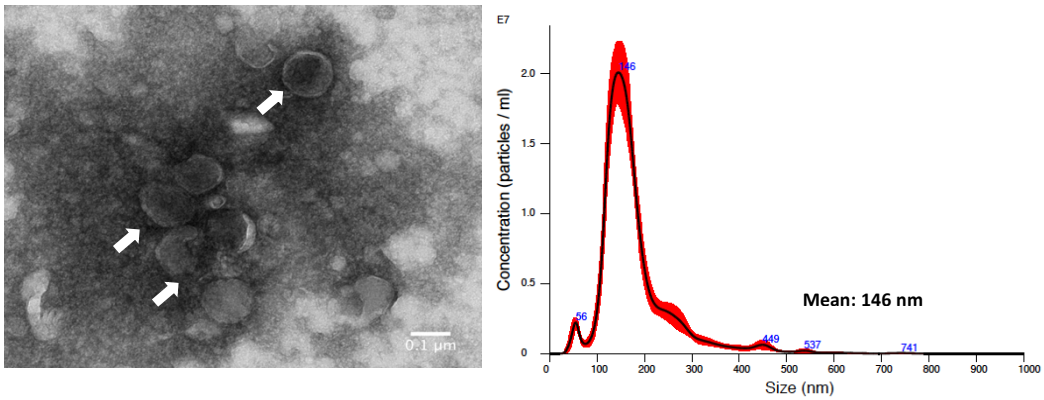

Fig. 30 Evaluation of structural modifications of exosomes after Na_2CO_3 treatment. HEK293 derived exosomes were incubated with alkaline Na_2CO_3 and then neutralized after 30 min. The impact of the treatment on exosomes size and structure was evaluated through electron microscopy (left, scale bar 0.1 µm) and Nanoparticle tracking analysis (right) analysis.

Then, we labelled exosomes with the Vybrant DiO lipophilic fluorescent dye, to compare the cellular uptake efficacy of Na_2CO_3-treated exosomes to PBS-treated exosomes as control. As shown, no significant differences could be observed between the two conditions, further indicating that a short-term pH shock does not alter the capacity the nanovesicles to be captured by cells (Fig. 31).

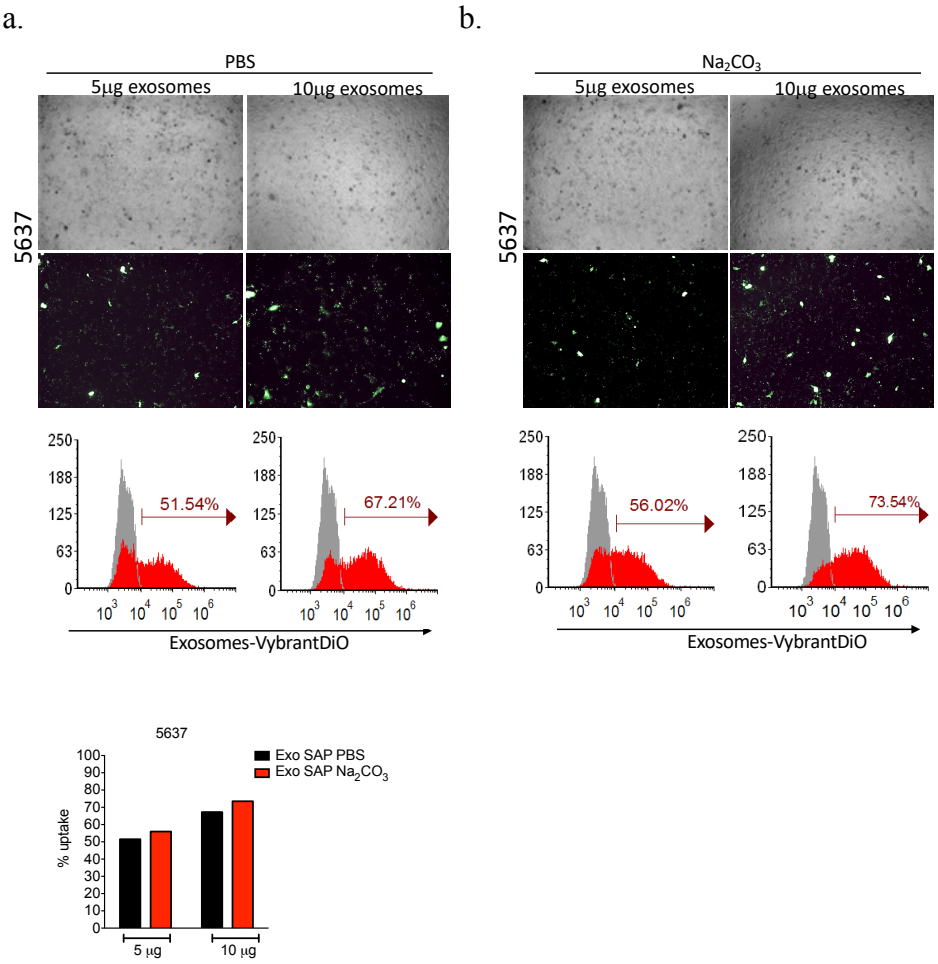

Fig. 31 Chemically treated SAP-encapsulating exosomes uptake. HEK293-derived exosomes were incubated with SAP in the presence of PBS (a) or Na_2CO_3 (b) and stained with Vybrant Dio lipophilic dye. After 24h incubation with 5637 cells, exosomes uptake was evaluated by fluorescent microscopy (upper panel) and flow cytometry analysis and shown as histogram of one representative experiment (lower panel). PBS incubation of exosomes was used as negative control. Different concentrations of exosomes (5 and 10 µg) were used for comparison.

We consequently moved to evaluate the loading capacity of exosomes when incubated with Na_2CO_3. To this aim, exosomes were mixed with SAP in the presence of Na_2CO_3 or PBS as a control. After incubation and pH neutralization, the amount of encapsulated SAP was assayed by western blot analysis (Fig. 32). The presence of Na_2CO_3 resulted in a retention of a conspicuous amount of SAP compared to PBS-treated samples. Importantly, we wondered if the treatment had induced a two-sided transfer of proteins across the exosomal membrane by monitoring the presence of Alix, a soluble exosomal protein. As shown in Fig. 32, Alix was detectable in exosomes treated with PBS, but not in those incubated with

Na_2CO_3, indicating that the treatment results in a parallel loss of material by vesicles.

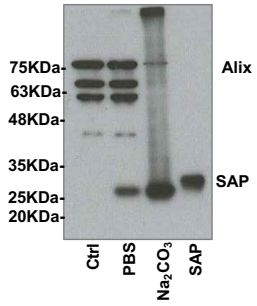

Fig. 32 Evaluation of SAP encapsulation efficiency after Na_2CO_3 treatment. HEK293 derived exosomes were incubated with SAP in the presence of Na_2CO_3 or PBS. SAP encapsulation efficiency and exosomes molecular composition alteration were evaluated after Na_2CO_3 or PBS treatment by western blot analysis by sequentially using the antibody specific for SAP and for the exosomal marker Alix. Untreated exosomes and seed SAP were used as controls.

As a next step, to confirm that SAP was effectively loaded inside the vesicles and exclude any surface aggregation of the toxin, SAP-bearing exosomes were digested with a low concentration of proteinase K to degrade the excess of toxin stuck on the external membrane, thus preserving exosomal content. An almost complete digestion of SAP in exosomes treated with PBS could be achieved as shown by western blot analysis, in contrast with Na_2CO_3 treated exosomes in which SAP was still clearly present, even if at lesser extent compared to the untreated control. In addition, the detection of Flotillin, a protein associated to the inner leaflet of the plasma membrane, confirmed that the protease treatment did not affect the internal molecular composition of the vesicles, but its activity was confined to their surface (Fig. 33).

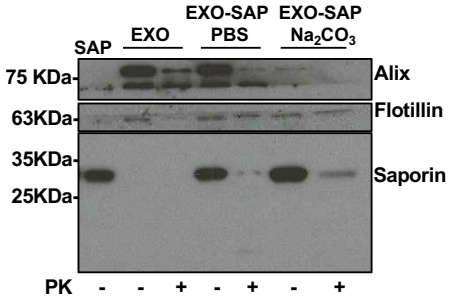

Fig. 33 Evaluation of effective SAP internalization into exosomes after Na_2CO_3 or PBS treatment. HEK293 derived exosomes were incubated with in the presence of Na_2CO_3 or PBS. After pH neutralization, exosomes were treated with Proteinase K, lysed and analyzed by western blot with antibodies specific for SAP, Flotillin and Alix. Untreated exosomes and seed SAP were used as controls.

7.3 Na_2CO_3 treated-SAP-encapsulating exosomes exert a high cytotoxic activity on cancer cells

Hence, we investigated if exosomes loaded with SAP were able to deliver and efficiently release their cargo *in vitro*. To answer this question, stage II bladder cancer cells (5637) were treated for 72 h with increasing concentrations (5, 10, 20 μg) of SAP-bearing exosomes, after Na_2CO_3 or PBS incubation. Strikingly, Na_2CO_3 treated SAP-bearing exosomes affected cell viability in a dose dependent manner and in a significantly more compared to the PBS treatment, demonstrating a good protection and intracellular delivery of SAP (Fig. 34).

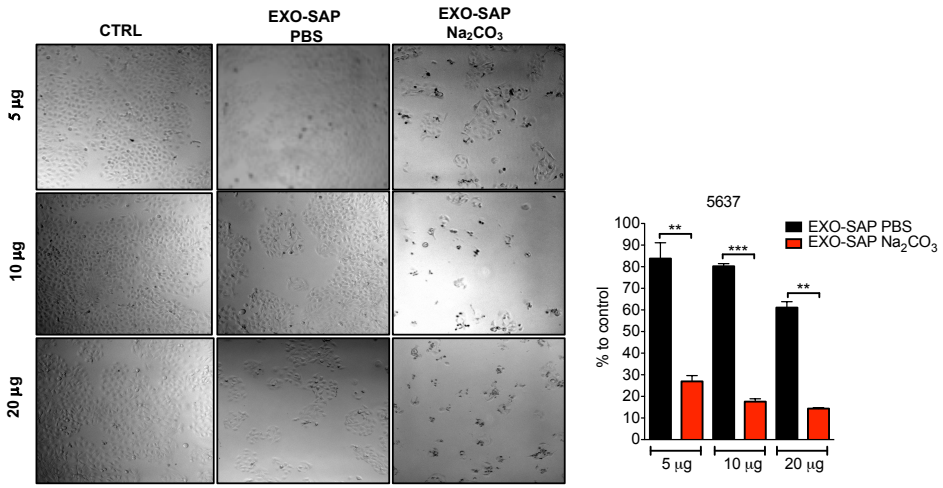

Fig. 34 Chemically treated SAP-loaded exosomes toxic activity. Exosomes were incubated with SAP in the presence of Na_2CO_3 or PBS. 5637 cells were treated for 72 h with increasing concentrations (2, 10 or 20 μg) of SAP-bearing exosomes (EXO-SAP) after Na_2CO_3 (red) or PBS (black) treatments. The toxic activity was evaluated by optical microscopy observation (left) and MTT assay (right). Exosomes incubated with PBS were used as control. Results are shown as mean±SD from three independent experiments.

To achieve a safer SAP protection, limiting the potential toxic effects of the unincorporated fraction, we speculated if the addition of a physiological concentration of NaCl in the process of SAP encapsulation could reduce the week interactions between SAP and exosomal surface. Interestingly, a complete loss of SAP retention was observed in PBS treated exosomes by adding salts in the washing buffer, in contrast to Na_2CO_3 treated exosomes in which SAP was still detectable (Fig. 35b). Notably, the addition of salts also reduced the amount of SAP associated to Na_2CO_3-treated exosomes resulting in a lower cytotoxic activity on cells (IC_{50} >

10 µg SAP-bearing exosomes). However, it is worth of noticing that SAP activity appeared to be increased when loaded into exosomes (estimated to be 100 ng SAP/µg exosomes, therefore 1 µg SAP are contained in 10 µg exosomes), as a conspicuous higher concentration (8 µg) of SAP WT alone was needed to reach an IC_{50} in the same conditions (Fig. 35a). Furthermore, the toxic activity on cancer cells was not influenced by the presence of the buffer nor by the presence of the excess of non-encapsulated SAP as both of them are completely eliminated during the washing procedure with centrifugal filter columns (Fig. 35c, d).

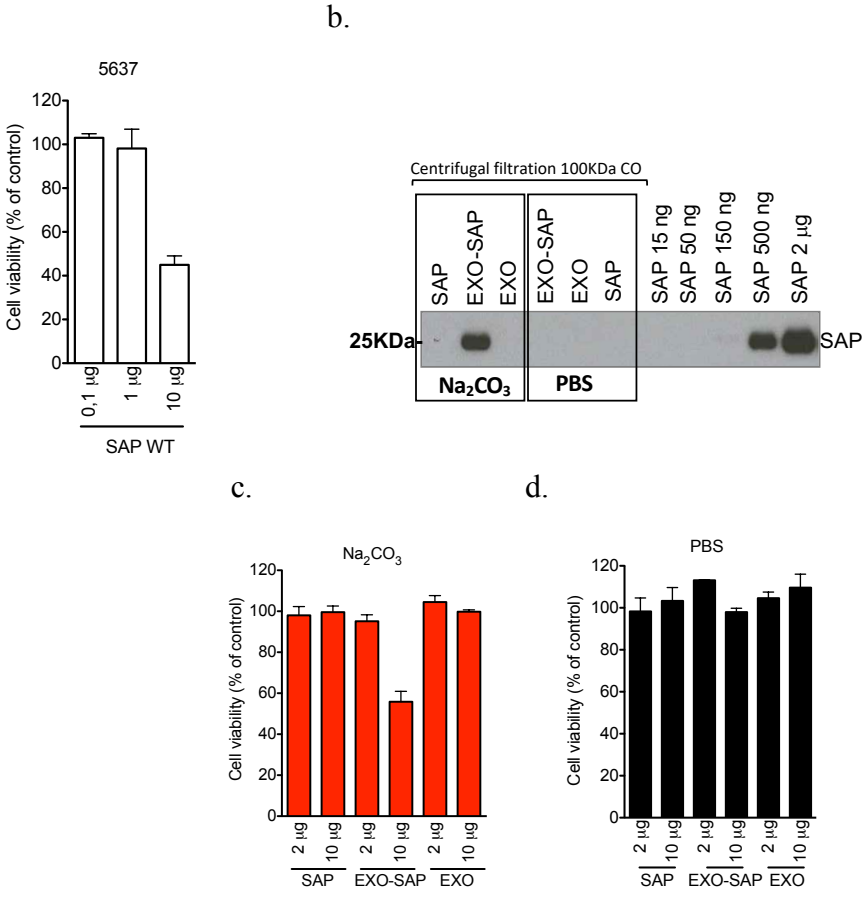

Fig. 35. Elimination of SAP excess from exosomal surface and evaluation of Na_2CO_3 encapsulation efficiency a. 5637 bladder cancer cells were incubated for 72 h with scalar concentrations of SAP WT. The effect on cells viability was evaluated by MTT assay and used as SAP activity control. b. Exosomes were incubated with SAP in the presence of Na_2CO_3 or PBS. 5 µg of exosomes (EXO or EXO-SAP) or SAP alone exposed to Na_2CO_3 or PBS treatment were lysed and analyzed by western blot analysis for SAP detection after purification by filtration. Increasing concentrations of seed SAP were used to as control. c. 5637 bladder cancer cells were treated for 72h with increasing concentrations (2 and 10 µg) of SAP, SAP-bearing exosomes (EXO-SAP) and exosomes alone (EXO) after Na_2CO_3 (red) or PBS (black) treatments. All samples were filtered with 100 KDa MWKO centrifugal devices to remove any unincorporated SAP.

8. Discussion III

In order to overcome the limitations related to the genetic engineering of cells to produce therapeutic exosomes, we investigated in parallel an *ex vitro* method to customize exosomes as drug delivery nanocarriers. To this purpose, we used non-cancerous HEK293 cell derived exosomes, isolated from culture medium through a specifically refined procedure based on sequential centrifugations and filtration and characterized for size and expression of typical exosomal markers. To be an ideal drug delivery system, exosomes should not be toxic on recipient cells. Thus, as a proof of concept, healthy fibroblasts were firstly analyzed for exosomes uptake. We found that these cells were able to capture the vesicles in a concentration and time-dependent manner, but no toxic effects could be detected at any time, further supporting the safety of the proposed strategy. Moreover, when RT112 and 5637 bladder cancer cells where co-incubated with labelled exosomes and analyzed by flow cytometry, we found that 100% of both cell lines were able to uptake the vesicles. Remarkably, the vesicles we used in this study were not subjected to any surface modification. In fact, exosomes can either be captured by macropinocytosis or deliver their biological content through the receptor mediated endocytic pathway [66, 91]. Up to now, many strategies have been developed to load exogenous therapeutic cargoes into purified exosomes, including passive incubation with or without permeabilization agents (i.e. saponin or detergents), sonication or subjection to freeze-thaw cycles [63]. One of the most commonly employed exogenous EV loading approach is electroporation, which has been used by many research groups to incorporate a wide range of molecules, such as siRNA, small molecules, enzymes [63, 64, 65]. Nakase et al. optimized experimental conditions to incorporate SAP into extracellular vesicles using this technique [76]. However, even if successfully able to introduce exogenous molecules into exosomes lumen, all the above-mentioned procedures result in a very low loading efficiency (0.2% in the case of SAP [68]) together with a severe structural alteration of exosomal morphology. In the present study, we took advantage of a highly alkaline buffer Na_2CO_3, to induce a pH shock perturbing the exosomes membrane and induce SAP encapsulation. Na_2CO_3 was first used in 1982 by Fujiki et al. to isolate

intracellular/organellar membranes. They demonstrated that incubation of purified fractions of rat liver endoplasmic reticulum (ER), peroxisomes or mitochondria in Na_2CO_3 100 mM induces a conversion of membranes into membrane sheets, able to retain only integral membrane proteins but not lipid-anchored proteins [93]. The alkaline pH (11.5), in fact, decreases noncovalent protein-protein interactions, releasing weakly attached peripheral membrane proteins without disrupting the integrity of the membranes. In this work, the use of a higher concentration of Na_2CO_3 (1 M) and report the preservation of exosomal structure and exosomal uptake efficiency by receiving cells and a good encapsulation efficiency after the treatment. The higher concentration of salts used supposedly produced a stronger impact on vesicles membrane, creating pores through which an in-and-out bidirectional trafficking allows the gain and loss of molecules by the vesicles, as shown by the loss of Alix signal. Importantly, we excluded SAP aggregation on the surface of vesicles as it was still detectable after protease K treatment, in contrast with the PBS treatment, in which SAP was totally lost after digestion. It is worth of noticing that proteinase K caused a marked reduction of SAP amount even in Na2CO3 treated exosomes. However, a residual amount of the toxin was still clearly present and detectable, probably because confined into the vesicle and protected by the membrane. Furthermore, the presence of flotillin, an integral protein exposed on the internal lumen of vesicles, highlighted the confinement of the protease enzymatic activity on the external surface of vesicles, indicating that the fraction of SAP still visible was protected by exosomal membrane. The difference between Na_2CO_3 treated SAP-bearing exosomes and the PBS control treatment was unambiguously evident in *in vitro* cytotoxic assay, where the formers were able to strongly affect cell viability at very low concentration. Conversely, PBS treated SAP-bearing exosomes did not visibly produce any toxic effect even at the highest concentration used. Eventually, we demonstrated that the use of a physiological concentration of salts (NaCl) in the washing step allows the surface-attached portion of SAP to be released, lowering the weak protein interactions with the vesicle's membrane. We could, thus, evaluate the method incorporation efficiency of SAP to be around 10 %, about 100 times higher compared to the commonly used electroporation (0.1 %).

However, a direct comparison of the two loading methods should be performed in the next future to corroborate the produced data. In conclusion, here we prove that a pH shock is a safe and effective method to functionalize exosomes as drug carriers, preserving their size and structure and allowing a good loading of a therapeutic protein. Nevertheless, to achieve the effective intracellular delivery of EV contents, future experiments will be performed in order to customize exosomal membrane with chemically conjugated targeting moieties, which must enhance a selective and preferential cellular uptake by target cells exploiting a receptor-mediated endocytosis uptake rather than micropinocytosis (Fig. 36).

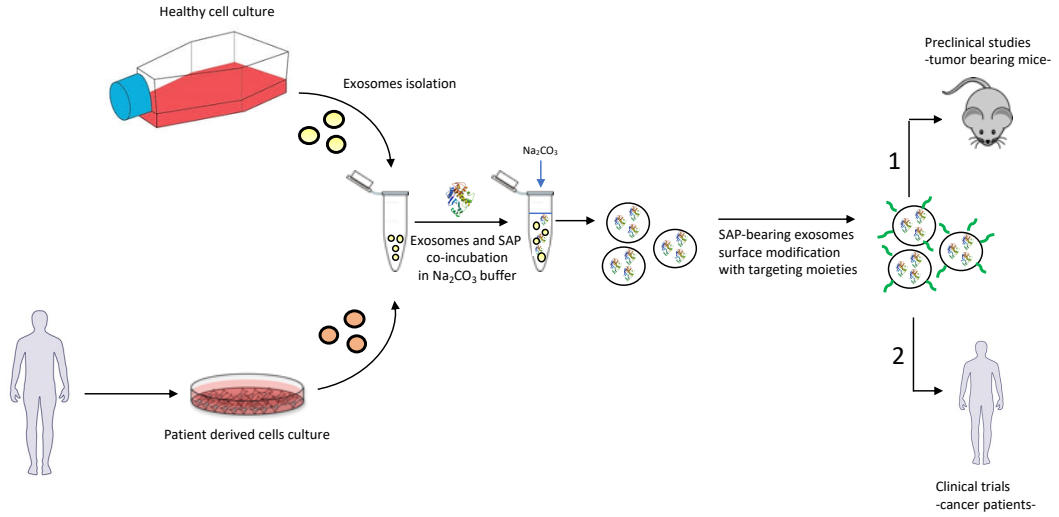

Fig. 36. Graphical outline of the proposed exosomes-based therapeutic strategy: a starting point for future studies. Once isolated from commercially available cultured healthy cells, exosomes can be easily manipulated in order to achieve the incorporation of therapeutic molecules, by a brief exposure to Na_2CO_3 pH altering buffer. Therapeutic exosomes specificity will be improved by decorating their surface with targeting moieties, which will allow the selective recognition and killing of cancer cells in preclinical models of cancer. The future application of the proposed method in human cancer treatment will include the use of patient derived healthy cells to isolate extracellular nanovesicles, in order to develop a personalized therapy.

CONFERENCE PRESENTATIONS ON THIS TOPIC:

- Oral presentation at 12th World Cancer Conference, September 26-28, 2016 London, UK. Presentation title: "**Toxin-based targeted therapeutics for the treatment of solid tumors**".

- Poster presentation at 5th Heidelberg Forum for Young Life Scientists, June 8-9, 2017, Heidelberg, Germany. Title: "**Development of a toxin based dual approach for the treatment of solid tumors**". Zuppone S., Romeo D., Montanari S., Salonia A., Montorsi F., Vago R.

- Poster presentation at 4th Mario Negri PhD students meeting, June 29-30, 2017, Milan, Italy. Title: "**Development of a toxin based dual approach for the treatment of solid tumors**". Zuppone S., Romeo D., Montanari S., Salonia A., Montorsi F., Vago R.

- Poster presentation at 4th Michelangelo Conference. Promises and challenges of developing new drugs in oncology, July 6-7, 2017, Milan, Italy. Title: "**Development of a toxin based dual approach for the treatment of solid tumors**". Zuppone S., Romeo D., Montanari S., Salonia A., Montorsi F., Vago R.

- Poster presentation at ISEV2018 Annual Meeting, May 2-6, 2018, Barcelona, Spain. Title: "**Engineering exosomes as refined drug delivery vehicles**". Zuppone S., Salonia A., Vago R.

Patent in preparation for RGD-SAP recombinant protein.

Bibliography

1. Holohan C, Van Schaeybroeck S, Longley D, Johnston P. Cancer drug resistance: an evolving paradigm. Nature Reviews Cancer. 2013;13(10):714-726.

2. Chames P, Van Regenmortel M, Weiss E, Baty D. Therapeutic antibodies: successes, limitations and hopes for the future. British Journal of Pharmacology. 2009;157(2):220-233.

3. Jain R. Barriers to Drug Delivery in Solid Tumors. Scientific American. 1994;271(1):58-65.

4. Zhang B, Hu Y, Pang Z. Modulating the Tumor Microenvironment to Enhance Tumor Nanomedicine Delivery. Frontiers in Pharmacology. 2017;8.

5. Wong C, Stylianopoulos T, Cui J, Martin J, Chauhan V, Jiang W et al. Multistage nanoparticle delivery system for deep penetration into tumor tissue. Proceedings of the National Academy of Sciences. 2011;108(6):2426-2431.

6. Corti A, Pastorino F, Curnis F, Arap W, Ponzoni M, Pasqualini R. Targeted Drug Delivery and Penetration Into Solid Tumors. Medicinal Research Reviews. 2011;32(5):1078-1091.

7. Hynes R.O. Integrins: Bidirectional, allosteric signaling machines. Cell. 2002;110:673–687. doi: 10.1016/S0092-8674(02)00971-6.

8. Blandin A.F., Renner G., Lehmann M., Lelong-Rebel I., Martin S., Dontenwill M. Beta1 integrins as therapeutic targets to disrupt hallmarks of cancer. Front. Pharmacol. 2015;6:279. doi: 10.3389/fphar.2015.00279.

9. Bianconi D., Unseld M., Prager G.W. Integrins in the spotlight of cancer. Int. J. Mol. Sci. 2016;17:2037 doi: 10.3390/ijms17122037.

10. Kim C, Ye F, Ginsberg M. Regulation of Integrin Activation. Annual Review of Cell and Developmental Biology. 2011;27(1):321-345.

11. Coller B, Shattil S. The GPIIb/IIIa (integrin IIb 3) odyssey: a technology-driven saga of a receptor with twists, turns, and even a bend. Blood. 2008;112(8):3011-3025.

12. Danhier F, Le Breton A, Préat V. RGD-Based Strategies To Target Alpha(v) Beta(3) Integrin in Cancer Therapy and Diagnosis. Molecular Pharmaceutics. 2012;9(11):2961-2973.

13. Raab-Westphal S, Marshall J, Goodman S. Integrins as Therapeutic Targets: Successes and Cancers. Cancers. 2017;9(12):110.

14. Hoeben A. Vascular Endothelial Growth Factor and Angiogenesis. Pharmacological Reviews. 2004;56(4):549-580.

15. Tarui T, Mazar A, Cines D, Takada Y. Urokinase-type Plasminogen Activator Receptor (CD87) Is a Ligand for Integrins and Mediates Cell-Cell Interaction. Journal of Biological Chemistry. 2000;276(6):3983-3990.

16. Breuss J, Uhrin P. VEGF-initiated angiogenesis and the uPA/uPAR system. Cell Adhesion & Migration. 2012;6(6):535-540.

17. LeBeau A, Duriseti S, Murphy S, Pepin F, Hann B, Gray J et al. Targeting uPAR with Antagonistic Recombinant Human Antibodies in Aggressive Breast Cancer. Cancer Research. 2013;73(7):2070-2081.

18. Ulisse S, Baldini E, Sorrenti S, D'Armiento M. The Urokinase Plasminogen Activator System: A Target for Anti-Cancer Therapy. Current Cancer Drug Targets. 2009;9(1):32-71.

19. Neves H, Kwok HF. Recent advances in the field of anti-cancer immunotherapy. BBA Clinical. 2015;3:280–8.

20. Mas-Moruno C, Rechenmacher F, Kessler H. Cilengitide: The First Anti-Angiogenic Small Molecule Drug Candidate. Design, Synthesis and Clinical Evaluation. Anti-Cancer Agents in Medicinal Chemistry. 2010Jan;10(10):753–68.

21. Bretschi M, Cheng C, Witt H, Dimitrakopoulou-Strauss A, Strauss LG, Semmler W, et al. Cilengitide affects tumor compartment, vascularization and microenvironment in experimental bone metastases as shown by longitudinal 18F-FDG PET and gene expression analysis. Journal of Cancer Research and Clinical Oncology. 2012Nov;139(4):573–83.

22. Bäuerle T, Komljenovic D, Merz M, Berger MR, Goodman SL, Semmler W. Cilengitide inhibits progression of experimental breast cancer bone

metastases as imaged noninvasively using VCT, MRI and DCE-MRI in a longitudinal in vivo study. International Journal of Cancer. 2010;128(10):2453–62.

23. Hagen TLT, Seynhaeve AL, Wiel-Ambagtsheer GAD, Bruijn EAD, Tiel STV, Ruegg C, et al. The αVβ3/αVβ5 integrin inhibitor cilengitide augments tumor response to melphalan isolated limb perfusion in a sarcoma model. International Journal of Cancer. 2012May;132(11):2694–704.

24. Ekblom P. Faculty of 1000 evaluation for Increased primary tumor growth in mice null for beta3- or beta3/beta5-integrins or selectins. F1000 - Post-publication peer review of the biomedical literature. 2004.

25. Eskens F, Dumez H, Hoekstra R, Perschl A, Brindley C, Böttcher S, et al. Phase I and pharmacokinetic study of continuous twice weekly intravenous administration of Cilengitide (EMD 121974), a novel inhibitor of the integrins αvβ3 and αvβ5 in patients with advanced solid tumours. European Journal of Cancer. 2003;39(7):917–26.

26. Curnis F, Gasparri A, Sacchi A, Longhi R, Corti A. Coupling Tumor Necrosis Factor-α with αVIntegrin Ligands Improves Its Antineoplastic Activity. Cancer Research. 2004;64(2):565–71.

27. Curnis F, Sacchi A, Longhi R, Colombo B, Gasparri A, Corti A. IsoDGR-Tagged Albumin: A New αvβ3 Selective Carrier for Nanodrug Delivery to Tumors. Small. 2012Dec;9(5):673–8.

28. Temming K, Schiffelers RM, Molema G, Kok RJ. RGD-based strategies for selective delivery of therapeutics and imaging agents to the tumour vasculature. Drug Resistance Updates. 2005;8(6):381–402.

29. Appella E, Blasi F. The Growth Factor Module of Urokinase is the Binding Sequence for Its Receptor. Annals of the New York Academy of Sciences. 1987;511(1 Normal and Ne):192–5.

30. Fabbrini MS, Carpani D, Bello-Rivero I, Soria MR. The amino-terminal fragment of human urokinase directs a recombinant chimeric toxin to target cells: internalization is toxin mediated. The FASEB Journal. 1997;11(13):1169–76.

31. Provenzano AE, Posteri R, Giansanti F, Angelucci F, Flavell SU, Flavell DJ, et al. Optimization of construct design and fermentation strategy for the

production of bioactive ATF-SAP, a saporin based anti-tumoral uPAR-targeted chimera. Microbial Cell Factories. 2016;15(1).

32. Wang M, Löwik DWPM, Miller AD, Thanou M. Targeting the Urokinase Plasminogen Activator Receptor with Synthetic Self-Assembly Nanoparticles. Bioconjugate Chemistry. 2009;20(1):32–40.

33. Drapkin PT, O'Riordan CR, Yi SM, Chiorini JA, Cardella J, Zabner J, et al. Targeting the urokinase plasminogen activator receptor enhances gene transfer to human airway epithelia. Journal of Clinical Investigation. 2000Jan;105(5):589–96.

34. Grossman HB. Chemoprevention of bladder cancer. Urology. 2006;67(3):19–22.

35. Soloway MS. Expectant treatment of small, recurrent, low-grade, noninvasive tumors of the urinary bladder. Urologic Oncology: Seminars and Original Investigations. 2006;24(1):58–61.

36. May M, Helke C, Nitzke T, Vogler H, Hoschke B. Survival Rates after Radical Cystectomy according to Tumor Stage of Bladder Carcinoma at First Presentation. Urologia Internationalis. 2004;72(2):103–11.

37. Woo S, Cho JY. Bladder Cancer. Bladder Cancer. 2018:87–122.

38. Stenehjem D, Tran D, Nkrumah M, Gupta S. PD1/PDL1 inhibitors for the treatment of advanced urothelial bladder cancer. OncoTargets and Therapy. 2018;Volume 11:5973–89.

39. Mohammed AA, El-Tanni H, El-Khatib HM, Mirza AA, Mirza AA, Alturaifi TH. Urinary bladder cancer: biomarkers and target therapy, new era for more attention. Oncology Reviews. 2016;10(2).

40. Hernandez-Aya LF, Gonzalez-Angulo AM. Molecular profile of triple-negative breast cancer. Advances in the Management of Triple Negative Breast Cancer. 2011:38–46.

41. Schmid P. ESMO 2018 presidential symposium—IMpassion130: atezolizumab nab-paclitaxel in triple-negative breast cancer. ESMO Open. 2018;3(6).

42. Tan T, Dent R. Triple-Negative Breast Cancer: Clinical Features. Triple-Negative Breast Cancer. 2017Jan;:23–32.

43. Olaparib for Metastatic Breast Cancer in Patients with a Germline BRCA Mutation. New England Journal of Medicine. 2017;377(17):1700–.

44. Le D, Gelmon KA. Olaparib tablets for the treatment of germ line BRCA-mutated metastatic breast cancer. Expert Review of Clinical Pharmacology. 2018;11(9):833–9.

45. J M, Verma RS. Therapeutic targets and recent advances in protein immunotoxins. Current Opinion in Microbiology. 2012;15(3):300–9.

46. Vago R., Ippoliti R., Fabbrini M.S. Current status & biomedical applications of ribosome inactivating proteins. In: Ng EFFTB (Ed.), Antitumor Potential and Other Emerging Medicinal Properties of Natural Compounds. Springer. 2013; 145-179.

47. Virgilio MD, Lombardi A, Caliandro R, Fabbrini MS. Ribosome-Inactivating Proteins: From Plant Defense to Tumor Attack. Toxins. 2010Oct;2(11):2699–737.

48. Vallera DA. Targeting Urokinase-Type Plasminogen Activator Receptor on Human Glioblastoma Tumors With Diphtheria Toxin Fusion Protein DTAT. CancerSpectrum Knowledge Environment. 2002;94(8):597–606.

49. Rajagopal V, Kreitman RJ. Recombinant Toxins That Bind to the Urokinase Receptor Are Cytotoxic without Requiring Binding to the α2-Macroglobulin Receptor. Journal of Biological Chemistry. 2000Oct;275(11):7566–73.

50. Fabbrini M, Katayama M, Nakase I, Vago R. Plant Ribosome-Inactivating Proteins: Progesses, Challenges and Biotechnological Applications (and a Few Digressions). Toxins. 2017Dec;9(10):314.

51. Cavallaro U, Nykjaer A, Nielsen M, Soria MR. alpha2-Macroglobulin Receptor Mediates Binding and Cytotoxicity of Plant Ribosome-Inactivating Proteins. European Journal of Biochemistry. 1995;232(1):165–71.

52. Conese M. alpha-2 Macroglobulin receptor/Ldl receptor-related protein (Lrp)- dependent internalization of the urokinase receptor. The Journal of Cell Biology. 1995Jan;131(6):1609–22.

53. Fabbrini MS, Rappocciolo E, Carpani D, Solinas M, Valsasina B, Breme U, et al. Characterization of a saporin isoform with lower ribosome-inhibiting activity. Biochemical Journal. 1997;322(3):719–27.

54. Vago R, Marsden CJ, Lord JM, Ippoliti R, Flavell DJ, Flavell S-U, et al. Saporin and ricin A chain follow different intracellular routes to enter the cytosol of intoxicated cells. FEBS Journal. 2005Jul;272(19):4983–95.

55. Ippoliti R. Endocytosis of a chimera between human pro-urokinase and the plant toxin saporin: an unusual internalization mechanism. The FASEB Journal. 2000Jan;14(10):1335–44.

56. Raemdonck K, Braeckmans K, Demeester J, Smedt SCD. Merging the best of both worlds: hybrid lipid-enveloped matrix nanocomposites in drug delivery. Chem Soc Rev. 2014;43(1):444–72.

57. Vago R, Collico V, Zuppone S, Prosperi D, Colombo M. Nanoparticle-mediated delivery of suicide genes in cancer therapy. Pharmacological Research. 2016;111:619–41.

58. Patel GK, Zubair H, Khan MA, Srivastava SK, Ahmad A, Patton MC, et al. Exosomes. Diagnostic and Therapeutic Applications of Exosomes in Cancer. 2018;:261–83.

59. Théry C, Amigorena S, Raposo G, Clayton A. Isolation and Characterization of Exosomes from Cell Culture Supernatants and Biological Fluids. Current Protocols in Cell Biology. 2006;30(1).

60. Batrakova EV, Kim MS. Using exosomes, naturally-equipped nanocarriers, for drug delivery. Journal of Controlled Release. 2015;219:396–405.

61. Vlassov AV, Magdaleno S, Setterquist R, Conrad R. Exosomes: Current knowledge of their composition, biological functions, and diagnostic and therapeutic potentials. Biochimica et Biophysica Acta (BBA) - General Subjects. 2012;1820(7):940–8.

62. Fuhrmann G, Serio A, Mazo M, Nair R, Stevens MM. Active loading into extracellular vesicles significantly improves the cellular uptake and photodynamic effect of porphyrins. Journal of Controlled Release. 2015;205:35–44.

63. Haney MJ, Klyachko NL, Zhaoa YL, Gupta R, Plotnikova EG, He ZJ, et al. Exosomes as drug delivery vehicles for Parkinson's disease therapy. J Control Release 2015; 207: 18–30.

64. Kim MS, Haney MJ, Zhao Y, Mahajan V, Deygen I, Klyachko NL, et al. Development of exosome-encapsulated paclitaxel to overcome MDR in cancer cells. Nanomedicine: Nanotechnology, Biology and Medicine. 2016;12(3):655–64.

65. Alvarez-Erviti L, Seow Y, Yin H, Betts C, Lakhal S, Wood MJA. Delivery of siRNA to the mouse brain by systemic injection of targeted exosomes. Nature Biotechnology. 2011;29(4):341–5.

66. Nakase I, Kobayashi NB, Takatani-Nakase T, Yoshida T. Active macropinocytosis induction by stimulation of epidermal growth factor receptor and oncogenic Ras expression potentiates cellular uptake efficacy of exosomes. Scientific Reports. 2015Mar;5(1).

67. Sato YT, Umezaki K, Sawada S, Mukai S-A, Sasaki Y, Harada N, et al. Engineering hybrid exosomes by membrane fusion with liposomes. Scientific Reports. 2016;6(1).

68. Akishiba M, Takeuchi T, Kawaguchi Y, Sakamoto K, Yu H-H, Nakase I, et al. Cytosolic antibody delivery by lipid-sensitive endosomolytic peptide. Nature Chemistry. 2017;9(8):751–61.

69. Sun D, Zhuang X, Grizzle W, Miller D, Zhang H-G. Abstract 4446: A novel nanoparticle drug delivery system: The anti-inflammatory activity of curcumin is enhanced when encapsulated in exosomes. Cancer Research. 2011;71(8 Supplement):4446–.

70. Pascucci L, Coccè V, Bonomi A, Ami D, Ceccarelli P, Ciusani E, et al. Paclitaxel is incorporated by mesenchymal stromal cells and released in exosomes that inhibit in vitro tumor growth: A new approach for drug delivery. Journal of Controlled Release. 2014;192:262–70.

71. Tian Y, Li S, Song J, Ji T, Zhu M, Anderson GJ, et al. A doxorubicin delivery platform using engineered natural membrane vesicle exosomes for targeted tumor therapy. Biomaterials. 2014;35(7):2383–90.

72. Wang J, Li W, Lu Z, Zhang L, Hu Y, Li Q, et al. The use of RGD-engineered exosomes for enhanced targeting ability and synergistic therapy toward angiogenesis. Nanoscale. 2017;9(40):15598–605.

73. Hung ME, Leonard JN. Stabilization of Exosome-targeting Peptides via Engineered Glycosylation. Journal of Biological Chemistry. 2015May;290(13):8166–72.

74. Lai CP, Mardini O, Ericsson M, Prabhakar S, Maguire CA, Chen JW, et al. Dynamic Biodistribution of Extracellular Vesicles in Vivo Using a Multimodal Imaging Reporter. ACS Nano. 2014Sep;8(1):483–94.

75. Smyth T, Petrova K, Payton NM, Persaud I, Redzic JS, Graner MW, et al. Surface Functionalization of Exosomes Using Click Chemistry. Bioconjugate Chemistry. 2014;25(10):1777–84.

76. Nakase I, Noguchi K, Fujii I, Futaki S. Vectorization of biomacromolecules into cells using extracellular vesicles with enhanced internalization induced by macropinocytosis. Scientific Reports. 2016;6(1).

77. Lombardi A, Bursomanno S, Lopardo T, Traini R, Colombatti M, Ippoliti R, et al. Pichia pastoris as a host for secretion of toxic saporin chimeras. The FASEB Journal. 2010;24(1):253–65.

78. Gonias SL, Gaultier A, Jo M. Regulation of the Urokinase Receptor (uPAR) by LDL Receptor-related Protein-1 (LRP1). Current Pharmaceutical Design. 2011Jan;17(19):1962–9.

79. Lombardi A., Marshall R.S., Savino C., Fabbrini M.S., Ceriotti A. Toxic Plant Proteins. Plant Cell Monographs. 2010; Chapter 4 Lord J.M., Hartley M.R., editors. Vol. 18. Springer-Verlag; Berlin/Heidelberg, Germany: p. 55

80. Rodenburg WK, Kjøller L, Petersen HH, Andreasen AP. Binding of urokinase-type plasminogen activator–plasminogen activator inhibitor-1 complex to the endocytosis receptors α2-macroglobulin receptor/low-density lipoprotein receptor-related protein and very-low-density lipoprotein receptor involves basic residues in the inhibitor. Biochemical Journal 1998;329:55–63. doi:10.1042/bj3290055.

81. Blasi F, Carmeliet P. uPAR: a versatile signalling orchestrator. Nature Reviews Molecular Cell Biology 2002;3:932–43. doi:10.1038/nrm977.

82. Cortese K, Sahores M, Madsen CD, Tacchetti C, Blasi F. Clathrin and LRP-1-Independent Constitutive Endocytosis and Recycling of uPAR. PLoS ONE 2008;3. doi:10.1371/journal.pone.0003730.

83. Nakase I, Kobayashi NB, Takatani-Nakase T, Yoshida T. Active macropinocytosis induction by stimulation of epidermal growth factor receptor and oncogenic Ras expression potentiates cellular uptake efficacy of exosomes. Scientific Reports 2015;5. doi:10.1038/srep10300.

84. Dubowchik GM, Firestone RA. Cathepsin B-sensitive dipeptide prodrugs. 1. A model study of structural requirements for efficient release of doxorubicin. Bioorganic & Medicinal Chemistry Letters 1998;8:3341–6. doi:10.1016/s0960-894x(98)00609-x.

85. Aggarwal N, Sloane BF. Cathepsin B: Multiple roles in cancer. PROTEOMICS - Clinical Applications 2014;8:427–37. doi:10.1002/prca.201300105.

86. Gondi CS, Rao JS. Cathepsin B as a cancer target. Expert Opinion on Therapeutic Targets 2013;17:281–91. doi:10.1517/14728222.2013.740461.

87. Ruan H, Hao S, Young P and Zhang H. Targeting Cathepsin B for Cancer Therapy. Horiz Cancer Res. 2015; 56: 23-40

88. Zhong Y-J, Shao L-H, Li Y. Cathepsin B-cleavable doxorubicin prodrugs for targeted cancer therapy. International Journal of Oncology 2012;42:373–83. doi:10.3892/ijo.2012.1754.

89. Dubowchik GM, Mosure K, Knipe JO, Firestone RA. Cathepsin B-sensitive dipeptide prodrugs. 2. Models of anticancer drugs paclitaxel (Taxol®), mitomycin C and doxorubicin. Bioorganic & Medicinal Chemistry Letters 1998;8:3347–52. doi:10.1016/s0960-894x(98)00610-6.

90. Dubowchik GM, Firestone RA, Padilla L, Willner D, Hofstead SJ, Mosure K, et al. Cathepsin B-Labile Dipeptide Linkers for Lysosomal Release of Doxorubicin from Internalizing Immunoconjugates: Model Studies of Enzymatic Drug Release and Antigen-Specific In Vitro Anticancer Activity. Bioconjugate Chemistry 2002;13:855–69. doi:10.1021/bc025536j.

91. Kooijmans SA, Schiffelers RM, Zarovni N, Vago R. Modulation of tissue tropism and biological activity of exosomes and other extracellular vesicles:

New nanotools for cancer treatment. Pharmacological Research 2016;111:487–500. doi:10.1016/j.phrs.2016.07.006.

92. Fujiki Y. Isolation of intracellular membranes by means of sodium carbonate treatment: application to endoplasmic reticulum. The Journal of Cell Biology 1982;93:97–102. doi:10.1083/jcb.93.1.97.

93. La-Beck NM, Gabizon AA. Nanoparticle interactions with the immune system: clinical implications for liposome-based cancer chemotherapy. Frontiers in Immunology 2017; 8: 416. Doi:10.3389/fimmu.2017.00416.

ACKNOWLIDGMENTS

Firstly, I would like to express my sincere gratitude to my co-tutor Riccardo Vago for his guidance and continuous support during my Ph.D study and related research. His patience, motivation and precious advices helped me in all the time of research.

I thank my labmates, for the stimulating discussions and for all the fun we have had in the last three years. In particular, I am grateful to Chiara Assalini for her invaluable help with the experiments and unwavering support.

I would also like to thank Natasa Zarovni (Exosomics, Siena, Italy), for the help and precious tips and advices essential for the development of the exosomes project.

My sincere thanks also goes to Dr. Claudia Minici and Massimo Degano (Biocrystallography Unit, Dept. of Immunology, Transplantation, and Infectious Diseases, San Raffaele Scientific Institute, Milano, Italy) for the help and suggestions for the recombinant proteins purification, Dr. Paola Branduardi and Stefano Bertagnoli (Università Milano-Bicocca, Dept. of Biotechnology and Biosciences, Milano, Italy) for ATF-SAP production in yeast, Dr. Oronzina Botrugno and Dr. Giovanni Tonon for the help and reagents provided for the generation of MB49 stably expressing luciferase, Dr. Angelo Corti and Dr. Flavio Curnis (Tumor Biology and Vascular Targeting Unit, Division of Experimental Oncology, San Raffaele Scientific Institute, Milano, Italy) for their availability, helpful discussions and reagents provided, Dr. Andrea Salonia (URI, San Raffaele Scientific Institute, Milano, Italy), who gave me access to the laboratory and research facilities, Dr. Fausto Sessa (Dipartimento di Medicina e chirurgia, Università degli Studi dell'Insubria, Varese, Italia) for tutoring and availability.

Last but not least, I would like to thank my family and friends: my parents, my sister Michela, my aunts Lina and Teresa, my uncle Mario, and Simone for their infinite patience and love, supporting me spiritually throughout these years and my life in general. Elettra, Francesca, Eliana and Angela for listening, encouraging, motivating and supporting me during this entire period in the most positive way.